Distribution Agreement

In presenting this thesis or dissertation as a partial fulfillment of the requirements for an advanced degree from Emory University, I hereby grant to Emory University and its agents the non-exclusive license to archive, make accessible, and display my thesis or dissertation in whole or in part in all forms of media, now or hereafter known, including display on the world wide web. I understand that I may select some access restrictions as part of the online submission of this thesis or dissertation. I retain all ownership rights to the copyright of the thesis or dissertation. I also retain the right to use in future works (such as articles or books) all or part of this thesis or dissertation

Signature:

_____ _____

Nianhui Song Date

Single Quantum Dot Electron Transfer Dynamics

By

Nianhui Song
Doctor of Philosophy

Chemistry

_____

Dr. Tianquan Lian, Advisor

_____

Dr. James T. Kindt, Committee Member

_____

Dr. Susanna Widicus Weaver, Committee Member

Accepted:

_____

Lisa A. Tedesco. Ph.D.
Dean of the Graduate School

_____

Date

Single Quantum Dot Electron Transfer Dynamics

By

Nianhui Song

B.S., University of Science and Technology of China, P.R. China, 2008

Advisor: Tianquan Lian, Ph.D.

An abstract of
A dissertation submitted to the Faculty of the
James T. Laney School of Graduate Studies of Emory University
in partial fulfillment of the requirements for the degree of
Doctor of Philosophy
in Chemistry
2013

Abstract

Single Quantum Dot Electron Transfer Dynamics

By Nianhui Song

The understanding of interfacial charge transfer dynamics from single quantum dots (QDs) is essential to the full utilization of their outstanding spectroscopic properties for solar cell applications. In this dissertation, we investigated three different types of QD-X systems, in which X represents: (1) molecular charge acceptors which are adsorbed on QD surface, (2) transparent conduction films which are widely used in QD based optoelectronic devices, and (3) redox electrolytes used in quantum dot-sensitized solar cells.

For the first system, time-resolved single QD spectroscopy is utilized to study the electron transfer dynamics from single QDs to fullerene molecules and the hole transfer dynamics from single QDs to phenothiazine molecules. It was found that both electron and hole transfer processes can reduce the fluorescence lifetime of QDs. Also, in these self-assembly complexes, a distribution in the ratio of adsorbates to QDs was observed and was attributed to the origin of static and dynamic heterogeneities in charge transfer properties. The distribution is found to be governed by Poisson Statistics. Differing from electron transfer which could introduce more off-states in single QD fluorescence, we found that hole transfer process from single QDs to phenothiazine molecules has little effect on the statistics of the off-states, which is often believed to be positively charged QDs with a valence band hole. Instead, it increases the probability of weakly emissive or “grey” states.

In the second system, by comparing ensemble averaged fluorescence decay and transient absorption kinetics, we show that for QDs on SnO_2, the exciton is quenched by electron transfer from the QD to SnO_2. At QD-ATO interface, much faster exciton quenching rates are observed and attributed to fast Auger recombination in charged QDs formed by Fermi level equilibration between the QD and n-doped ATO. Single QDs on SnO_2 and ATO shows similar blinking dynamics with correlated fluctuation of emission intensities and lifetimes. Compared to QDs on SnO_2, QDs on ATO films show larger variation of average exciton quenching rates, which is attributed to a broad distribution of the number of charges and nature of charging sites on the QD surface.

In the third system, with ensemble averaged steady-state and time-resolved absorption and emission spectroscopy, we show that QDs in the presence of sulfide electrolyte are charged due to redox active surface midgap states. As a result, excitons in such QDs decay much faster via Auger recombination involving the additional charges. Such charging induced fast Auger recombination can compete with excition dissociation by interfacial electron transfer, which may be a hereto overlooked reason for low efficiency in many quantum dot-sensitized solar cells (QDSSCs). Using single QD fluorescence spectroscopy, we investigated the evolution of QD properties during the charging process as a function of charging time and the heterogeneity of charging degree among different QDs. Due to the efficient recombination of surface electrons with the hole in the core of QDs, off-states in charged QDs are significantly suppressed. We also found that with longer charging time, both the average decay rates and the width of rate distributions become bigger which is attributed to the different charging degree and charging sites in different QDs.

Single Quantum Dot Electron Transfer Dynamics

By

Nianhui Song

B.S., University of Science and Technology of China, P.R. China, 2008

Advisor: Tianquan Lian, Ph.D.

A dissertation submitted to the Faculty of the
James T. Laney School of Graduate Studies of Emory University
in partial fulfillment of the requirements for the degree of
Doctor of Philosophy
in Chemistry
2013

ACKNOWLEDGEMENT

First, I would like to express my deepest thank to my advisor, Professor Tianquan Lian, for his guidance and support throughout my graduate career. His wide knowledge and critical thinking have been of great value to me. I also wish to extend my sincere thanks to my graduate committee members, Dr. James T. Kindt and Dr. Susanna Widicus Weaver, for their insightful questions and helpful comments during my graduate career.

I would like to thank my lab fellows for their support and friendship. In particular, I would like to thank Dr. Shengye Jin for introducing me to the single molecular fluorescence project and providing guidance in my earlier graduate years. Dr. Zhen Liu, whom I've been working with in the past two years, has provided me extensive training and help on the AFM system and insightful discussions on the experiment results and phenomena. Dr. Jier Huang, Dr. Zhuangqun Huang and Dr. Chantelle Anfuso all happily welcomed me to the group and have made themselves available to offer help and suggestions whenever needed. I am also grateful for the help from my other group members, Ye Yang, Haimin Zhu, Kaifeng Wu, Nannan Han, Dr. Zheyuan Chen.

Last but not least, I would like to thank my entire family for their support over the years. My mother and parents in-law have given me encouragement and support when I had difficult times and especially in taking care of my son. My husband, Haiming Zhu, has given me understanding and support by encouraging me throughout the graduate career. My lovely son, Bruce, has provided me with endless happiness.

Table of Contents

List of Figures

Chapter 1

Chapter 2

Chapter 3

Chapter 4

Chapter 5

Chapter 6

List of Tables

Chapter 3

Chapter 4

Chapter 5

Chapter 6

Chapter 1 Introduction

1.1 Theory of Fluorescence

1.1.1 General Introduction

The concept "luminescence" was brought up as "*luminescenz*" by the physicist and science historian Eilhardt Wiedemann in 1888 to describe "all those phenomena of light which are not solely conditioned by the rise in temperature". Then, luminescence has been generalized as a process where photons are emitted from electronically excited species. Fluorescence is one particular case of luminescence. The mode of excitation is the absorption of a photon, which promotes the absorbing species into an electronic excited state.

When a molecule is excited by absorbing a photon, in addition to emitting a photon, it has many other pathways to return to the ground state, such as: internal conversion (direct return to the ground state without emission of fluorescence), intersystem crossing (usually followed by emission of phosphorescence), intramolecular charge transfer, and conformational change. The Perrin-Jablonski diagram, shown in Figure 1.1, is convenient for visualizing these possible processes. High frequency photons can be used to excite the molecules in ground state (S_0) into a higher electronic state. The excited molecules will then relax to the first electronic excited state (S_1) by vibrational relaxation. At this stage, fluorescence can happen if the molecule in S_1 relaxes to S_0 by emitting a photon. In some cases, the system can transfer to a triplet state (T_1) through an intersystem crossing process, followed by phosphorescence or vibrational relaxation. If the molecule undergoes the internal conversion process which is usually followed by a vibrational relaxation process, no

photon will be emitted. Both the intersystem crossing process and internal conversion process will result in the absence of fluorescence emission, thus they are all called non-radiative decay processes.

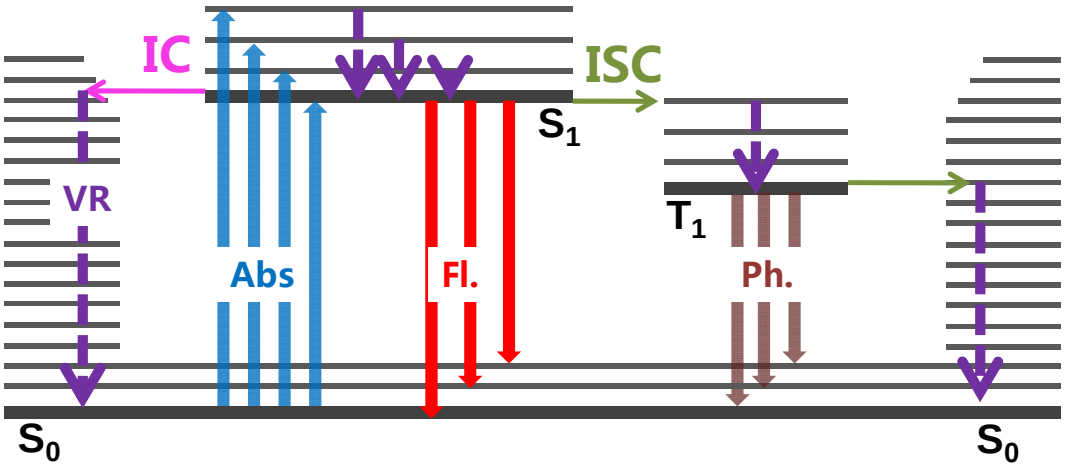

Label	Name	Characteristic Time
Abs.	Absorption	10^{-15}s
VR	Vibrational Relaxation	10^{-12}~10^{-10}s
IC	Internal Conversion	10^{-11}~10^{-9}s
ISC	Intersystem Crossing	10^{-10}~10^{-4}s
Fl	Fluorescence	10^{-10}~10^{-7}s
Ph	Phosphorescence	10^{-5}~1s

Figure 1.1 The Perrin-Jablonski diagram of a chromophore and list of characteristic time of corresponding processes.

1.1.2 Lifetime and Quantum Yield

Let us consider a simplest case in a dilute solution of a fluorescent species A whose concentration is *[A]*. A pulse laser at time *0* brings a certain amount of A to its S_1 excited state by photon absorption. These excited species A^* then return to S_0, either by a fluorescence process with rate k_r, or by a non-radiative process with rate

k_{nr}. As in classical chemical kinetics, the concentration of A^* will decay according to equation 1.1:

$$-\frac{d[A^*]}{dt} = (k_r + k_{nr})[A^*] \quad (1.1)$$

By solving this equation, the time dependence of concentration of A^* can be obtained:

$$[A^*] = [A^*]_0 \exp\left(-\frac{t}{\tau}\right) \quad (1.2)$$

Where τ is the lifetime of excited state S_1:

$$\tau = \frac{1}{k_r + k_{nr}} \quad (1.3)$$

The amount of photons emitted per unit time per unit volume of solution according to the reaction, $A^* \rightarrow A$ + photon, i_F at time t after excitation is proportional to the concentration of A^* at that time:

$$i_F = k_r[A^*] = k_r[A^*]_0 \exp\left(-\frac{t}{\tau}\right) \quad (1.4)$$

The fluorescence quantum yield Φ_F is the fraction of excited molecules that return to the ground state S_0 by emitting fluorescence photons:

$$\Phi_F = \frac{k_r}{k_r + k_{nr}} = k_r\tau \quad (1.4)$$

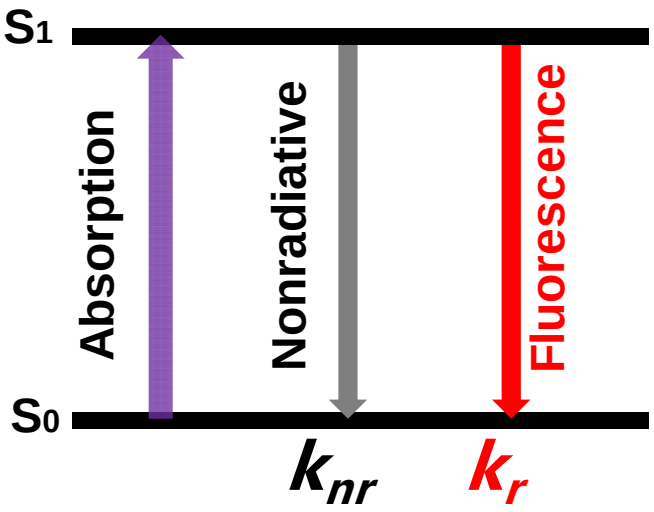

Figure 1.2 Schematic diagram of absorption and de-excitation processes in a two-level system.

1.1.3 Fluorescence Quenching Processes

If the molecule in the excited state can interact with other molecules, other relaxation processes can also happen, such as, electron transfer, proton transfer, energy transfer, excimer or exciplex formation. As illustrated in Figure 1.3, due to the existence of quenching species, the excited state of A can react with Q to produce some "product" with a rate denoted as k_q, which will relax to the ground state through a non-radiative pathway. This quenching process competes with the intrinsic relaxation pathways within A*, which includes both the fluorescence decay and non-radiative decay. The intrinsic decay rate of an isolated A* is the sum of the fluorescence decay rate and non-radiative decay rate: $k_0 = k_r + k_{nr}$.

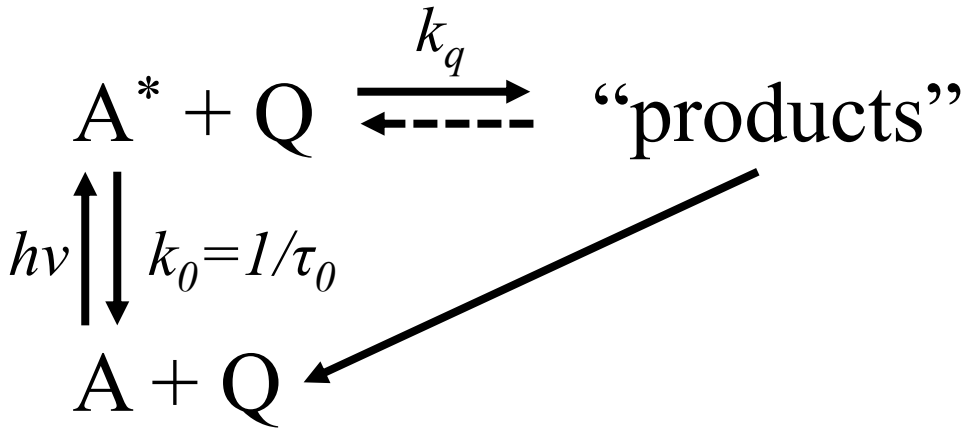

Figure 1.3 Schematic diagram of reaction pathways of A* with the presence of quenching species Q.

In this case, one could easily get the reaction rate equation for A^*:

$$-\frac{d[A^*]}{dt} = (k_0 + k_q)[A^*] \quad (1.5)$$

As a result, the lifetime of S_1 now becomes:

$$\tau' = \frac{1}{k_0 + k_q} \quad (1.6)$$

The quantum yield is reduced to:

$$\Phi_F' = \frac{k_r}{k_0 + k_q} = k_r \tau' \quad (1.7)$$

In most of our studies, the quenching process is a charge transfer process, which could either be an electron transfer or a hole transfer process.

Either pulse fluorometers or phase-modulation fluorometers can be used to determine the lifetimes and all the rate components of the excited states. The former is

used in our lab and it is based on the time-correlated single-photon counting (TCSPC) method which will be discussed in detail in Chapter 2. Briefly, by building up the histogram of all the delay times between each emission photon and corresponding excitation pulse, the fluorescence decay profile can be constructed, which is described by equation 1.4.

1.1.4 Fluorescence of Semiconductor Nanocrystals

Semiconductor nanocrystals or quantum dots (QDs) have been a subject of intense interest and extensive research in the last two decades. Due to many outstanding properties, they are considered as promising alternatives to molecular chromophore in various applications ranging from biological application such as bioimging and biotracker,[1,2] to optoelectronic devices such as light emitting diodes (LED)[3,4], photodetectors[5,6] and solar cells.[7,8] For example, their enhanced photostability enables longer detecting time in biological imaging. Moreover, the longer fluorescence lifetime of QDs opens the opportunity to study quenching processes such as electron transfer from QDs. QDs also have high absorption cross section over a broad spectral range, and size dependent optical properties, which offers great opportunity to both fundamental studies and practical applications.

The origin of QD fluorescence comes from the recombination of the electron and hole pairs which are generated by a photon absorption process. In QDs, a band gap exists, i.e. a forbidden zone between a full valence band (VB) and an empty conduction band (CB). Upon excitation, an electron is pumped from the VB to CB, leaving a hole in the VB, followed by ultrafast intraband relaxation to the lowest energy state. The electron and hole can recombine by emission of one photon (fluorescence) or through non-radiative recombinations. The lifetime and quantum

yield analysis of molecular emitters is applicable to QDs and we will continue use the same denotations in the following discussions.

Fluorescence intermittence or blinking is one of the fundamental properties of quantum dots. Under continuous illumination, single QDs tend to shut off their fluorescence emission and turn it on after some time duration.[9-34] Many models have been proposed to explain the mechanism of blinking and the observed power law statistics of "on-off" times in single QD fluorescence. The off-states have been attributed to photoinduced charging of QDs by Auger ionization and/or electron transfer to trap states in QDs or the surrounding matrix.[9-11,13,25,28,33,34] The probability densities of the on- and off- times obey a power-law distribution with an exponent of ~ 1.5,[10,13,35,36] and this dependence can be explained by models that assume diffusion controlled electron transfer (ET).[10,28,32,33,36-38]

1.2 Single Quantum Dot Fluorescence Spectroscopy

Single particle detection is firstly established by the pioneering work of Moerner and Kador in 1989 on doped crystals.[39] Compared with bulk measurements, in which the properties of individual particles are hidden in ensemble averages, single-QD level detection provides new insights into physical, chemical and biological phenomena. Single QD fluorescence spectroscopy is believed to be one of the best ways to study single QD photophysical processes, such as intersystem crossing[40], energy transfer[41], excitonic interaction[42].

1.2.1 Confocal Fluorescence Microscopy

Fluorescence confocal microscopes, invented in the mid-1950s, are widely used in the detection of single molecules. In a confocal microscope, as shown in Figure 1.4, a

focused spot of light scans the specimen. The fluorescence emitted by the specimen is separated from the incident beam by a dichroic mirror and is focused by the objective lens through a pinhole aperture to a detector. Fluorescence from out-of-focus planes above and below the specimen is reduced due to a smaller pinhole size compared with the beam size. Due to this special design, a confocal microscope is well suited for detecting fluorescence signal from a single emitter because of its excellent spatial resolution and signal-to-noise ratio.

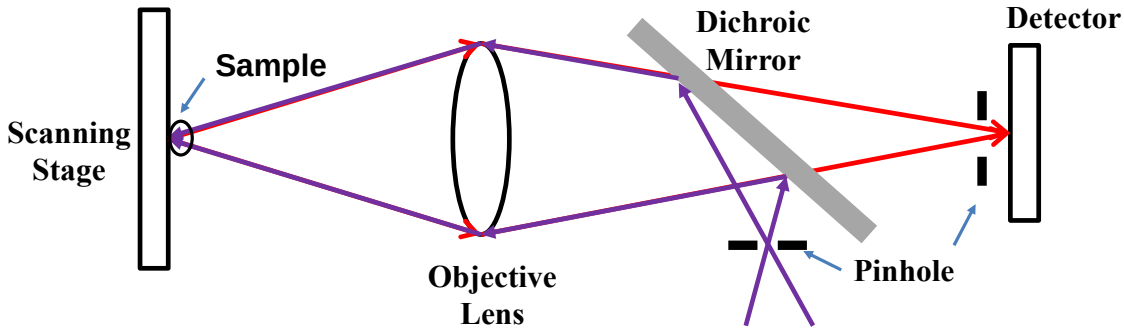

Figure 1.4 Principle of confocal microscope.

1.2.2 Time-Resolved Single Quantum Dot Spectroscopy

Time resolution in single QD spectroscopy is also desirable in many fundamental studies: to investigate the charge transfer dynamics from single QD to adjacent charge acceptors[43-45], to measure the Förster resonant energy transfer (FRET) [46] rate between two proximal fluorophores which are coupled by Coulomb interaction[47], and so on. By integrating a confocal microscope with time-resolved techniques, such as TCSPC, time-resolved single QD spectroscopy can be conducted, using which, one will be able to study the fluorescence dynamics on a single particle level. Detailed discussion of the working principle will be provided in Chapter 2.

1.3 Photo Induced Interfacial Charge Transfer from Single Quantum Dots

1.3.1 Interfacial Charge Transfer from QDs to Molecular Adsorbates

Interfacial charge transfer (IFCT) process plays important roles in many chemical and biological processes. Specifically, IFCT between molecular adsorbates and QDs has been a subject of intense research interest in recent years[48-64]. Understanding dynamics of charge transfer from or to quantum dots is essential to their potential application in many photovoltaic devices such as solar cells.[7,65-67] Interest in this topic has been intensified by reports of multiexciton generation (MEG),[68-70] which provides a potential approach to improve the efficiency of QD-based solar cells. However, to utilize the MEG process in devices, excitons have to be separated before the ultrafast exciton-exciton annihilation process, which is on the tens to hundreds of picoseconds time scale.[71,72] Charge transfer to adsorbed molecular electron and hole acceptors has been proposed as a potential approach to separate multiexcitons. Ultrafast dissociation of excitons in CdS and CdSe QDs by electron transfer [50-64] or hole transfer to molecular acceptors has been reported.[73-77] These early reports show multiexponential electron transfer kinetics, indicating a heterogeneous distribution of electron transfer rates. The inherent complication in ensemble averaged spectroscopy is the loss of spectral information originating from such heterogeneities.

Single molecule experiments, however, can reveal information which is hidden in ensemble averaged bulk measurements, including static and dynamic heterogeneity. In our study, time-resolved single QD spectroscopy is utilized to investigate the electron transfer dynamics from single QDs to fullerene molecules and hole transfer dynamics from single QDs to phenothiazine molecules. Detailed discussion can be found in Chapter 3 and Chapter 4, respectively.

1.3.2 Interfacial Charge Transfer from QDs to Semiconductor Nanoparticles

Interaction between QDs and transparent conducting films have been studied extensively because it is essential to the application of QDs in QDs based optoelectronic devices.[3,4,7,78-87] Despite those reports, it remains unclear how QDs interact with TCF and how TCF affects the excited state dynamics of deposited QDs. Such understanding is essential to the application of QDs since the excited state dynamics plays a key role in determining photo-electric conversion performance and efficiency as well as the interpretation of spectroelectrochemistry results regarding the photophysical properties of QDs.

In previous reports, shorter exciton lifetime and suppressed fluorescence blinking in single QDs on ITO films were observed.[21,85] However, the origin of the observations were debated to be charging of QDs by ITO or energy transfer from QDs to ITO films. Based on only fluorescence measurements, it is difficult to differentiate those excited state quenching pathways (electron transfer, hole transfer, energy transfer and Auger process) since they contribute to fluorescence intensity and kinetics in similar ways.

In this work, by combing transient absorption spectroscopy and single QD fluorescence spectroscopy and comparing QDs on glass, nanoporous SnO_2 and ATO films, we studied the exciton dynamics in charged QDs deposited on ATO films and the heterogeneity in exciton decay rates which is attributed to a wide distribution of charging degrees and sites for different QDs on ATO. Blinking dynamics for single QDs on SnO_2 and ATO films were also investigated and negligible influence of surface charging on blinking behavior was observed. Details of this work are reported in Chapter 5.

1.3.3 Charging of Quantum Dots by Sulfide Electrolyte

Interest in QDSSCs as an alternative to molecular dyes in sensitized solar cells[50,88-90] has been intensified due to the possibility of multiexciton and hot carrier extraction from QDs, which potentially can improve the device efficiency.[68-70] However, the highest solar energy conversion efficiency of QDSSCs has reached only ~ 5% using CdS/CdSe co-sensitized TiO_2,[91,92] significantly inferior to that of dye-sensitized solar cell (DSSC) analogue (~ 12%).[93-95] The reason for the rather low efficiencies of QDSSCs is still yet to be understood.[90,96-98]

Redox electrolytes are widely used in QDSSCs to reduce and stabilize QDs, however, the effect of redox electrolyte on the photophysical properties of QDs including optical properties and carrier dynamics has not been fully studied, which is critical to the performance assessment and device design of QDSSCs.[99] Nowadays, the sulfide/polysulfide redox couple (-0.45 V *vs.* NHE[100]) still remains as the favorite choice due to appealing device efficiency and durability.[90,99] Recently, it has been reported by Kamat's group that both emission quenching and faster fluorescence decay for CdSe QDs in the presence of Na_2S could be attributed to valance band hole transfer process from photo excited QDs to sulfide.[99] Because fluorescence is sensitive to all possible exciton decay process and any carrier depopulation processes (including electron/hole transfer/trapping, Auger recombination) contribute to fluorescence quenching/decay, it is still not clear how the presence of sulfide electrolyte affects the photophysical properties of QDs including optical properties and carrier dynamics.

In our work, we employed both steady state and time resolved absorption and fluorescence spectroscopy to investigate the effect of sulfide on CdSe based QDs.

Ensemble experiments suggested that in the presence of sulfide electrolyte, QDs actually are charged, and charging induced fast Auger recombination process dictates the carrier lifetime of QDs. The hole transfer from QDs to sulfide was also observed but with a much slower rate compared with the charging induced Auger recombination process. In addition, using single QD fluorescence spectroscopy, we investigate the evolution of QDs properties during the charging process as a function of charging time and the heterogeneity of charging degrees among different QDs, which are not accessible by ensemble-averaged measurements. Detailed discussion can be found in Chapter 6.

1.4 Summary

In summary, the interfacial charge transfer dynamics from single QDs have been investigated using time-resolved single QD fluorescence spectroscopy. With the ability to detect fluorescence on a single QD level, static and dynamic heterogeneities are revealed which are usually hidden in ensemble average measurements. In our study of charge transfer from single QDs to molecular adsorbates, the self-assembly induced ratio distribution was proved and has been attributed to the origin of static and dynamic heterogeneities in charge transfer properties. By combing ensemble averaged transient absorption spectroscopy with time-resolved fluorescence spectroscopy, we found that QDs can be charged by transparent conducting film (n-type ATO) and sulfide electrolyte which are widely used in quantum dot-sensitized solar cells.

The rest of this thesis will be organized as follows: Chapter 2 summarizes the experimental techniques and procedures, including the preparation and characterization of quantum dot-quencher complex samples and semiconductor

nanocrystalline thin films. Chapter 3 introduces the electron transfer dynamics from quantum dots to C_{60} molecules. Chapter 4 reports the study of hole transfer dynamics from quantum dots to PTZ molecules. Chapter 5 discusses the quenching mechanism for excited quantum dots on Sb doped SnO_2 films by combining transient absorption spectroscopy and single QD fluorescence spectroscopy. Finally, in Chapter 6, we will summarize the studies of charging of quantum dots by sulfide electrolyte.

Reference

(1) Bruchez Jr, M.; Moronne, M.; Gin, P.; Weiss, S.; Alivisatos, A. *Science* **1998**, *281*, 2013.

(2) Chan, W. C. W.; Nie, S. M. *Science* **1998**, *281*, 2016.

(3) Colvin, V. L.; Schlamp, M. C.; Alivisatos, A. P. *Nature* **1994**, *370*, 354.

(4) Coe, S.; Woo, W.-K.; Bawendi, M.; Bulovic, V. *Nature* **2002**, *420*, 800.

(5) Sukhovatkin, V.; Hinds, S.; Brzozowski, L.; Sargent, E. H. *Science* **2009**, *324*, 1542.

(6) Konstantatos, G.; Howard, I.; Fischer, A.; Hoogland, S.; Clifford, J.; Klem, E.; Levina, L.; Sargent, E. H. *Nature* **2006**, *442*, 180.

(7) Huynh, W. U.; Dittmer, J. J.; Alivisatos, A. P. *Science* **2002**, *295*, 2425.

(8) Robel, I.; Subramanian, V.; Kuno, M.; Kamat, P. V. *J. Am. Chem. Soc.* **2006**, *128*, 2385.

(9) Nirmal, M.; Dabbousi, B. O.; Bawendi, M. G.; Macklin, J. J.; Trautman, J. K.; Harris, T. D.; Brus, L. E. *Nature* **1996**, *383*, 802.

(10) Shimizu, K. T.; Neuhauser, R. G.; Leatherdale, C. A.; Empedocles, S. A.; Woo, W. K.; Bawendi, M. G. *Phys. Rev. B* **2001**, *63*, 205316/1.

(11) Krauss, T. D.; O'Brien, S.; Brus, L. E. *Journal of Physical Chemistry B* **2001**, *105*, 1725.

(12) Empedocles, S.; Bawendi, M. *Acc. Chem. Res.* **1999**, *32*, 389.

(13) Shimizu, K. T.; Woo, W. K.; Fisher, B. R.; Eisler, H. J.; Bawendi, M. G. *Physical Review Letters* **2002**, *89*, 117401/1.

(14) Chen, Y.; Vela, J.; Htoon, H.; Casson, J. L.; Werder, D. J.; Bussian, D. A.; Klimov, V. I.; Hollingsworth, J. A. *J. Am. Chem. Soc.* **2008**, *130*, 5026.

(15) Mahler, B.; Spinicelli, P.; Buil, S.; Quelin, X.; Hermier, J.-P.; Dubertret, B. *Nature Materials* **2008**, *7*, 659.

(16) Hohng, S.; Ha, T. *Journal of the American Chemical Society* **2004**, *126*, 1324.

(17) Wang, X.; Ren, X.; Kahen, K.; Hahn, M. A.; Rajeswaran, M.; Maccagnano-Zacher, S.; Silcox, J.; Cragg, G. E.; Efros, A. L.; Krauss, T. D. *Nat.* **2009**, *459*, 686.

(18) Odoi, M. Y.; Hammer, N. I.; Early, K. T.; McCarthy, K. D.; Tangirala, R.; Emrick, T.; Barnes, M. D. *Nano Letters* **2007**, *7*, 2769.

(19) Hammer, N. I.; Early, K. T.; Sill, K.; Odoi, M. Y.; Emrick, T.; Barnes, M. D. *J. Phys. Chem. B* **2006**, *110*, 14167.

(20) Ray, K.; Badugu, R.; Lakowicz, J. R. *Journal of the American Chemical Society* **2006**, *128*, 8998.

(21) Jin, S.; Song, N.; Lian, T. *Acs Nano* **2010**, *4*, 1545.

(22) Fomenko, V.; Nesbitt, D. J. *Nano Lett.* **2008**, *8*, 287.

(23) Issac, A.; Jin, S.; Lian, T. *J. Am. Chem. Soc.* **2008**, *130*, 11280.

(24) Jin, S.; Lian, T. *Nano Letters* **2009**, *9*, 2448.

(25) Efros, A. L.; Rosen, M. *Physical Review Letters* **1997**, *78*, 1110.

(26) Fisher, B. R.; Eisler, H.-J.; Stott, N. E.; Bawendi, M. G. *J. Phys. Chem. B* **2004**, *108*, 143.

(27) Issac, A.; von Borczyskowski, C.; Cichos, F. *Phys.l Rev. B* **2005**, *71*, 161302/1.

(28) Kuno, M.; Fromm, D. P.; Johnson, S. T.; Gallagher, A.; Nesbitt, D. J. *Phys. Rev. B:* **2003**, *67*, 125304/1.

(29) Montiel, D.; Yang, H. *J. Phys. Chem. A* **2008**, *112*, 9352.

(30) Peterson, J. J.; Nesbitt, D. J. *Nano Lett.* **2009**, *9*, 338.

(31) Schlegel, G.; Bohnenberger, J.; Potapova, I.; Mews, A. *Phys. Rev. Lett..* **2002**, *88*, 137401.

(32) Tang, J.; Marcus, R. A. *J. Chem. Phys.* **2006**, *125*, 044703/1.

(33) Verberk, R.; van Oijen, A. M.; Orrit, M. *Phys. Rev. B* **2002**, *66*, 233202/1.

(34) Zhang, K.; Chang, H.; Fu, A.; Alivisatos, A. P.; Yang, H. *Nano Letters* **2006**, *6*, 843.

(35) Kuno, M.; Fromm, D. P.; Hamann, H. F.; Gallagher, A.; Nesbitt, D. J. *J. Chem. Phys.* **2001**, *115*, 1028.

(36) Tang, J.; Marcus, R. A. *J. Chem. Phys.* **2005**, *123*, 204511/1.

(37) Tang, J.; Marcus, R. A. *Phys. Rev. Lett.* **2005**, *95*, 107401/1.

(38) Tang, J.; Marcus, R. A. *J. Chem. Phys.* **2005**, *123*, 054704/1.

(39) Moerner, W. E.; Kador, L. *Phys Rev Lett* **1989**, *62*, 2535.

(40) Xie, X. S. *Accounts Chem Res* **1996**, *29*, 598.

(41) VandenBout, D. A.; Yip, W. T.; Hu, D. H.; Fu, D. K.; Swager, T. M.; Barbara, P. F. *Science* **1997**, *277*, 1074.

(42) Ying, L. M.; Xie, X. S. *Journal of Physical Chemistry B* **1998**, *102*, 10399.

(43) Jin, S.; Hsiang, J. C.; Zhu, H.; Song, N.; Dickson, R. M.; Lian, T. *Chem Sci* **2010**, *1*, 519.

(44) Jin, S. Y.; Lian, T. Q. *Nano Lett* **2009**, *9*, 2448.

(45) Song, N. H.; Zhu, H. M.; Jin, S. Y.; Zhan, W.; Lian, T. Q. *Acs Nano* **2011**, *5*, 613.

(46) Förster, T. *Annalen der Physik* **1948**, *437*, 55.

(47) Ha, T. *Methods* **2001**, *25*, 78.

(48) Nozik, A. J.; Memming, R. *J Phys Chem-Us* **1996**, *100*, 13061.

(49) Kamat, P. V. *Prog React Kinet* **1994**, *19*, 277.

(50) Kamat, P. V.; Tvrdy, K.; Baker, D. R.; Radich, J. G. *Chem. Rev.* **2010**, *110*, 6664.

(51) Kamat, P. *J. Phys. Chem. C* **2008**, *112*, 18737.

(52) Tisdale, W. A.; Williams, K. J.; Timp, B. A.; Norris, D. J.; Aydil, E. S.; Zhu, X.-Y. *Science (Washington, DC, United States)* **2010**, *328*, 1543.

(53) Boulesbaa, A.; Issac, A.; Stockwell, D.; Huang, Z.; Huang, J.; Guo, J.; Lian, T. *J. Am. Chem, Soc.* **2007**, *129*, 15132.

(54) Huang, J.; Stockwell, D.; Huang, Z.; Mohler, D. L.; Lian, T. *J. Am. Chem. Soc.* **2008**, *130*, 5632.

(55) Rossetti, R.; Beck, S. M.; Brus, L. E. *J. Am. Chem. Soc.* **1984**, *106*, 980.

(56) Rossetti, R.; Brus, L. E. *J. Phys. Chem.* **1986**, *90*, 558.

(57) Ramsden, J. J.; Gratzel, M. *Chem. Phys. Lett.* **1986**, *132*, 269.

(58) Henglein, A. *Pure & Appl. Chem.* **1984**, *56*, 1215.

(59) Logunov, S.; Green, T.; Marguet, S.; El-Sayed, M. A. *J. Phys. Chem. A* **1998**, *102*, 5652.

(60) Burda, C.; Green, T. C.; Link, S.; El-Sayed, M. A. *J. Phys. Chem. B* **1999**, *103*, 1783.

(61) Kamat, P. V.; Dimitrijevic, N. M.; Fessenden, R. W. *Journal of Physical Chemistry* **1987**, *91*, 396.

(62) Blackburn, J. L.; Selmarten, D. C.; Nozik, A. J. *J. Phys. Chem. B* **2003**, *107*, 14154.

(63) Robel, I.; Kuno, M.; Kamat, P. V. *J. Am. Chem. Soc.* **2007**, *129*, 4136.

(64) Spanhel, l.; Weller, H.; Henglein, A. *J. Am. Chem. Soc.* **1987**, *109*, 6632.

(65) Pattantyus-Abraham, A. G.; Kramer, I. J.; Barkhouse, A. R.; Wang, X.; Konstantatos, G.; Debnath, R.; Levina, L.; Raabe, I.; Nazeeruddin, M. K.; Gratzel, M.; Sargent, E. H. *Acs Nano* **2010**, *4*, 3374.

(66) Sambur, J. B.; Novet, T.; Parkinson, B. A. *Science (Washington, DC, United States)* **2010**, *330*, 63.

(67) Robel, I.; Subramanian, V.; Kuno, M.; Kamat, P. V. *J. Am. Chem. Soc.* **2006**, *128*, 2385.

(68) Sambur, J. B.; Novet, T.; Parkinson, B. A. *Science* **2010**, *330*, 63.

(69) Semonin, O. E.; Luther, J. M.; Choi, S.; Chen, H.-Y.; Gao, J.; Nozik, A. J.; Beard, M. C. *Science* **2011**, *334*, 1530.

(70) Tisdale, W. A.; Williams, K. J.; Timp, B. A.; Norris, D. J.; Aydil, E. S.; Zhu, X.-Y. *Science* **2010**, *328*, 1543.

(71) Klimov, V. I. *Annu Rev Phys Chem* **2007**, *58*, 635.

(72) Nozik, A. J. *Annu Rev Phys Chem* **2001**, *52*, 193.

(73) Huang, J.; Huang, Z.; Jin, S.; Lian, T. *J. Phys. Chem. C* **2008**, *112*, 19734.

(74) Sharma, S. N.; Pillai, Z. S.; Kamat, P. V. *J. Phys. Chem. B* **2003**, *107*, 10088.

(75) Landes, C. F.; Burda, C.; Braun, M.; El-Sayed, M. A. *J. Phys. Chem. B.* **2001**, *105*, 2981.

(76) Landes, C. F.; Braun, M.; El-Sayed, M. A. *J. Phys. Chem. B* **2001**, *105*, 10554.

(77) Guyot-Sionnest, P. *Structure and Bonding (Berlin, Germany)* **2005**, *118*, 59.

(78) Greenham, N. C.; Peng, X.; Alivisatos, A. P. *Phys. Rev. B* **1996**, *54*, 17628.

(79) Klem, E. J. D.; MacNeil, D. D.; Levina, L.; Sargent, E. H. *Adv. Mater. (Weinheim, Ger.)* **2008**, *20*, 3433.

(80) Leschkies, K. S.; Beatty, T. J.; Kang, M. S.; Norris, D. J.; Aydil, E. S. *ACS Nano* **2009**, *3*, 3638.

(81) Pattantyus-Abraham, A. G.; Kramer, I. J.; Barkhouse, A. R.; Wang, X.; Konstantatos, G.; Debnath, R.; Levina, L.; Raabe, I.; Nazeeruddin, M. K.; Grätzel, M.; Sargent, E. H. *ACS Nano* **2010**, *4*, 3374.

(82) Rivest, J. B.; Swisher, S. L.; Fong, L.-K.; Zheng, H.; Alivisatos, A. P. *ACS Nano* **2011**, *5*, 3811.

(83) Jha, P. P.; Guyot-Sionnest, P. *J. Phys. Chem. C* **2007**, *111*, 15440.

(84) Jha, P. P.; Guyot-Sionnest, P. *ACS Nano* **2009**, *3*, 1011.

(85) Jha, P. P.; Guyot-Sionnest, P. *J. Phys. Chem. C* **2010**, *114*, 21138.

(86) White, M. A.; Weaver, A. L.; Beaulac, R. m.; Gamelin, D. R. *ACS Nano* **2011**, *5*, 4158.

(87) Galland, C.; Ghosh, Y.; Steinbruck, A.; Sykora, M.; Hollingsworth, J. A.; Klimov, V. I.; Htoon, H. *Nature* **2011**, *479*, 203.

(88) Nozik, A. J.; Beard, M. C.; Luther, J. M.; Law, M.; Ellingson, R. J.; Johnson, J. C. *Chem. Rev.* **2010**, *110*, 6873.

(89) Debnath, R.; Bakr, O.; Sargent, E. H. *Energy Environ. Sci.* **2011**, *4*, 4870.

(90) Kamat, P. V. *Acc. Chem. Res.* **2012**, *45*, 1906.

(91) Santra, P. K.; Kamat, P. V. *J. Am. Chem. Soc.* **2012**, *134*, 2508.

(92) Yu, X.-Y.; Liao, J.-Y.; Qiu, K.-Q.; Kuang, D.-B.; Su, C.-Y. *ACS Nano* **2011**, *5*, 9494.

(93) Yella, A.; Lee, H.-W.; Tsao, H. N.; Yi, C.; Chandiran, A. K.; Nazeeruddin, M. K.; Diau, E. W.-G.; Yeh, C.-Y.; Zakeeruddin, S. M.; Grätzel, M. *Science* **2011**, *334*, 629.

(94) Bessho, T.; Zakeeruddin, S. M.; Yeh, C.-Y.; Diau, E. W.-G.; Grätzel, M. *Angew. Chem. Int. Ed.* **2010**, *49*, 6646.

(95) Chen, C.-Y.; Wang, M.; Li, J.-Y.; Pootrakulchote, N.; Alibabaei, L.; Ngoc-le, C.-h.; Decoppet, J.-D.; Tsai, J.-H.; Grätzel, C.; Wu, C.-G.; Zakeeruddin, S. M.; Grätzel, M. *ACS Nano* **2009**, *3*, 3103.

(96) Hodes, G. *J. Phys. Chem. C* **2008**, *112*, 17778.

(97) Mora-Seró, I. n.; Giménez, S.; Fabregat-Santiago, F.; Gómez, R.; Shen, Q.; Toyoda, T.; Bisquert, J. *Acc. Chem. Res.* **2009**, *42*, 1848.

(98) Lee, H. J.; Yum, J.-H.; Leventis, H. C.; Zakeeruddin, S. M.; Haque, S. A.; Chen, P.; Seok, S. I.; Grätzel, M.; Nazeeruddin, M. K. *J. Phys. Chem. C* **2008**, *112*, 11600.

(99) Chakrapani, V.; Baker, D.; Kamat, P. V. *J. Am. Chem. Soc.* **2011**, *133*, 9607.

(100) Tachibana, Y.; Akiyama, H. Y.; Ohtsuka, Y.; Torimoto, T.; Kuwabata, S. *Chem. Lett.* **2007**, *36*, 88.

Chapter 2 Experimental Setup and Sample Preparation

2.1 Time-Resolved Single Quantum Dot Fluorescence Spectroscopy

2.1.1 Principle of Time-Correlated Single Photon Counting

The time-correlated single photon counting (TCSPC) technique is based on Poisson statistics of photon detection, which requires that the time differences between adjacent detected photons are much longer than their excitation pulse period. In single QD fluorescence detection, the total number and emission rate of photons from a single emitter are very low and limited which makes TCSPC preferable in our experimental setup.

Figure 2.1 illustrates how the TCSPC works in the fluorescence decay curve measurement.[1] Two times of each emitted photon (red line in Figure 2.1b) are recorded by TCSPC: the delay time (Δ), as indicated in Figure 2.1b, between the emitted photon and the excitation pulse (green line in Figure 2.1b); and the chronological time (t), which is the arrival time of each emitted photon since the start of each detection. The fluorescence decay profile can be constructed from the histogram of measured delay times, as shown in Figure 2.1a. The chorological times are binned properly to construct the time trace of fluorescence intensity, as plotted in Figure 2.1c. In our experiment, a 50 ms bin is usually used for fluorescence trajectories.

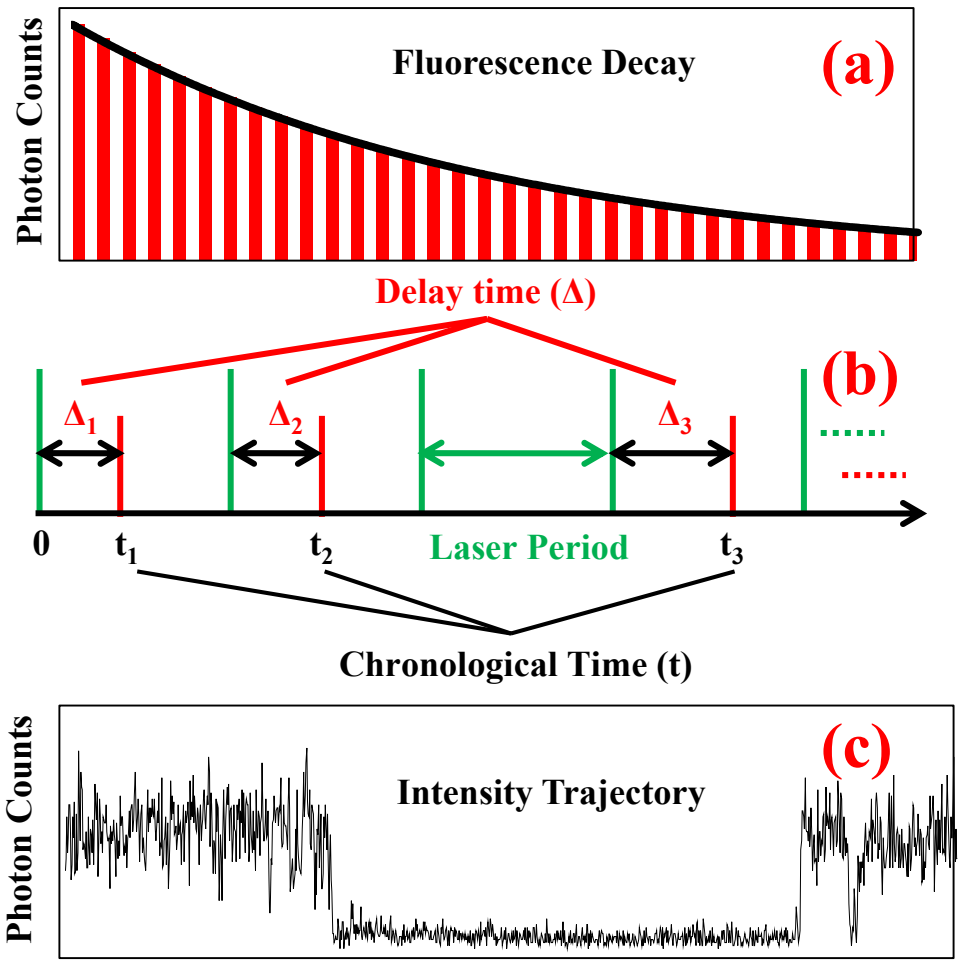

Figure 2.1 Photon counting method of TCSPC technique (b) Photon counting module monitors the time interval between laser pulse and detected photon (delay time). The outputs of a TCSPC measurement are (a) histogram of delay times and (c) fluorescence intensity trajectory (number of photons per integration time).

A schematic diagram of the basic components of TCSPC is shown in Figure 2.2. A brief description is discussed below:

A mode-locked laser outputs the pulsed excitation light which is focused on the sample. Fluorescence from the sample is collected by an objective lens and is detected by a single photon counter detector. The detector outputs an electrical pulse to signal the arrival of a photon to a photon counting board (Becker & Hickl GmbH, SPC-600)

which is installed in a PC. The excitation reference time is supplied by a fast photodiode detecting the pulsed laser light inside the laser. The time difference between the excitation reference time and the time registered by the signal from the detector is the delay time in Figure 2.1. The delay time measurement is carried out by using the emission signal as a trigger for "start" and using the reference signal from excitation laser as a trigger for "stop", shown in Figure 2.2. This reversed "start-stop" method is un-conventional, but it can save a lot of memory and speed up the signal processing because, within this method, the periods without photon emission can be "ignored" to save computational resources.

Those start and stop signals pass through the Constant Fraction Discriminator (CFD) to get rid of timing jitter [2] and are fed to Time-to-Amplitude Converter (TAC). The TAC converts the time difference between the start and stop signals into voltage which is linearly related to the time difference. The voltage of TAC is read by Analog-Digital Converter (ADC) and written in the memory banks. The ADC resolution is 12 bit that there can be 4096 (=2^{12}) channels in the TAC window.

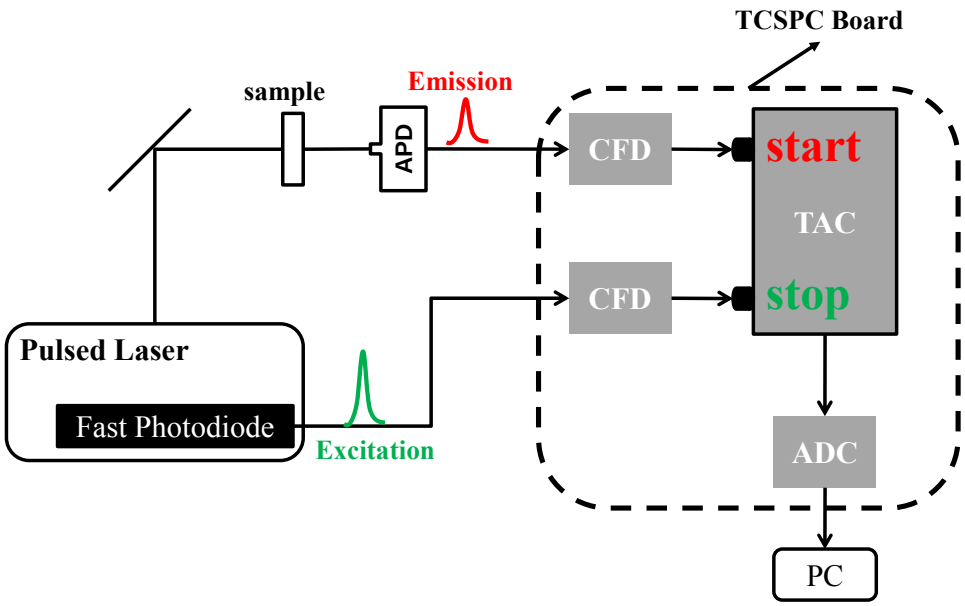

Figure 2.2 Schematic diagram of the basic components of reversed start-stop mode TCSPC system. CFD (Constant Fraction Discriminator), TAC (Time-to-Amplitude Converter), and ADC (Analog-Digital Converter) are integrated in a TCSPC PC board.

2.1.2 Time-Resolved Single QD Fluorescence Detection

Single QD fluorescence detection is carried out with a home-built scanning confocal microscope. A schematic diagram is shown in Figure 2.3. The excitation source is provided by femtosecond laser pulses (~ 100 fs) with a repetition rate of 80 MHz which are generated with a mode-locked Ti:Sapphire laser (Tsunami oscillator pumped by 10 W Millennia Pro, Spectra-Physics). The output light has a wavelength range from 700 to 1000 nm. A pulse picker (Conoptics, USA) is used to reduce the repetition rate by a proper factor according to the experiment requirement. The laser frequency is doubled by a BBO crystal using second harmonic generation. The excitation beam (~ 200 nW) is then focused through an objective (100× N.A 1.4, oil immersion, Olympus) down to a diffraction-limited spot on the sample, which was spin coated onto the glass cover slip and placed on a piezo scanner (Asylum Research). The resulting epi-fluorescence from the sample was detected by a single photon counting avalanche photodiode (APD, Perkin Elmer SPCM-AQRH-16). The APD output was analyzed by a time-correlated single photon counting (TCSPC) board (Becker&Hickel SPC 600). The instrument response function for the fluorescence lifetime measurement had a full-width-at-half-maximum of ~ 500 ps. The concentration of QDs used in single QD study is typically ~ 10 pM. A raster scan fluorescence image of a single QD is shown in Figure 2.4, indicating spatially well-separated single particles.

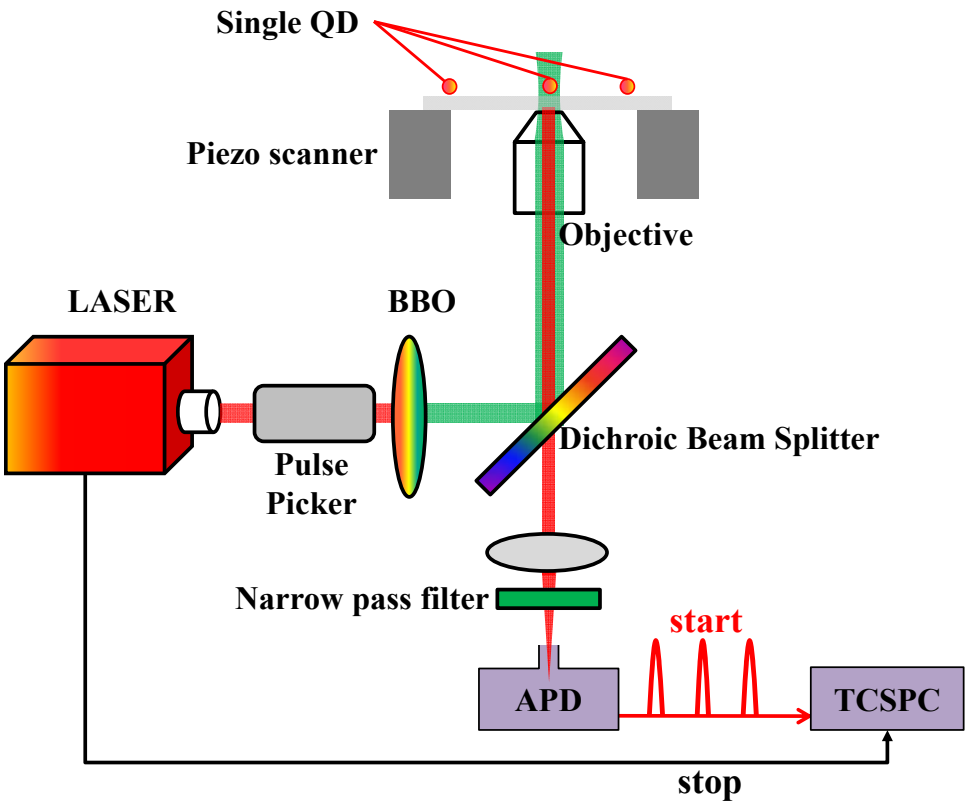

Figure 2.3 Confocal microscope setup attached with TCSPC module.

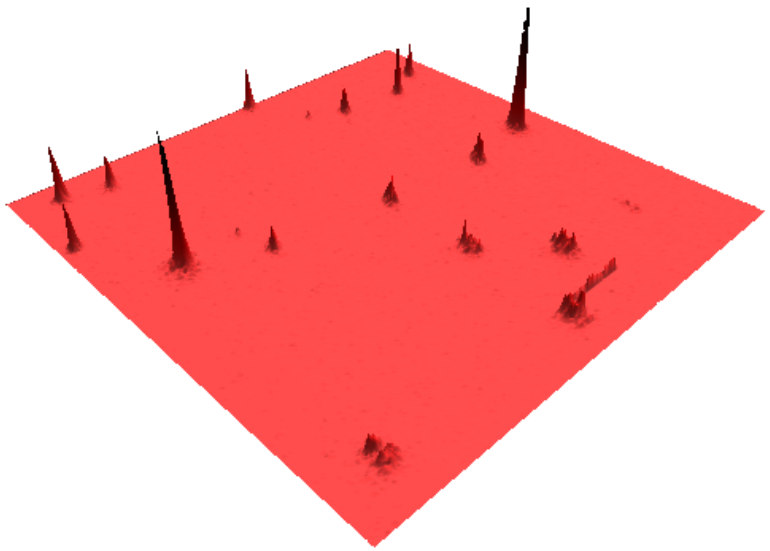

Figure 2.4 A raster scan fluorescence image of single QD on a glass cover slip.

2.2 Sample Preparation

2.2.1 Preparation of QD-C_{60} Complexes

In this study, water soluble CdSe/CdS_{2ML}/$CdZnS_{1ML}$/ZnS_{1ML} core/shell QDs were obtained from Ocean NanoTech, LLC, USA. The first exciton peak of this QD is at 585 nm. The UV-VIS spectrum of the QD is shown with the pink curve in Figure 2.5. A monomalonic derivative of fullerene (C_{60}) was prepared by the Bingel cyclopropanation[3,4] reaction as previously detailed.[5] The C_{60} molecules have been functionalized with carboxylic groups which can bind with QDs. A molecular structure of C_{60} is shown in the insert of Figure 2.5. The mixture of C_{60} powder and QD water solution were sonicated to facilitate chemical bonding between QD and C_{60}. Undissolved C_{60} powder was removed by a follow up filtration process. The ratio between C_{60} and QD was controlled by the sonication time. UV-VIS spectra of QD-C_{60} complex solution are plotted in Figure 2.5. The blue, red, and green curves represent QD-C_{60} complexes solutions with sonication times of 10, 30, and 60 minutes, respectively.

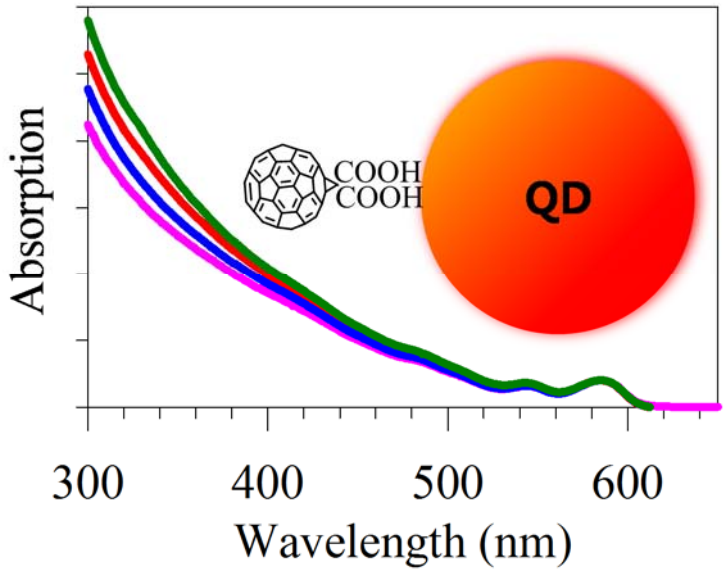

Figure 2.5 UV-VIS spectra of free QD (pink curve) and QD-C_{60} complexes with different sonication times: 10 mins (blue curve), 30 mins (red curve), and 60 minutes (green curve). The insert figure is a cartoon of QD-C_{60} complex with one C_{60} adsorbed.

2.2.2 Preparation of QD-PTZ Complexes

The QDs used in this study are CdSe/CdS_{3ML}/$CdZnS_{2ML}$/ZnS_{2ML} core/multishell QD powders obtained from Ocean NanoTech, LLC, USA which have the first exciton absorption peak at 605 nm (capped by octadecylamin ligand). Phenothiazine, the molecular structure of which is shown in the Figure 2.6a, was purchased from Sigma-Aldrich, USA. Three QD-PTZ samples, A, B and C, were prepared for an ensemble averaged experiment and the PTZ-to-QD ratios were controlled by adding different amount of PTZ to QD solutions (in heptane). The mixtures were kept in the dark for 30 minutes before experiments. Absorption spectra of these samples are plotted in Figure 2.6 (b). For single QD studies, the QD-PTZ complex samples (1, 2, and 3) were prepared in the same manner, with a much lower concentration of QDs (~ 10 pM). The solutions were spin coated on glass cover-slips for single QD studies.

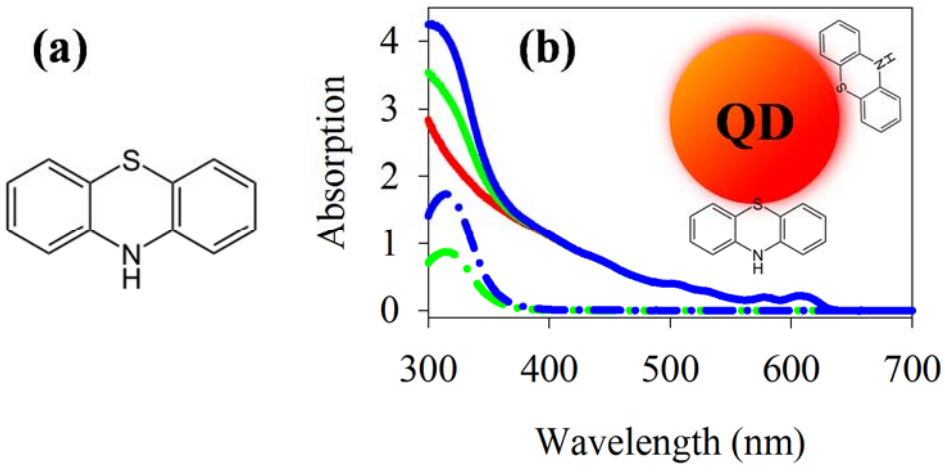

Figure 2.6 (a) the chemical structure of the phenothiazine molecule. (b) UV-VIS spectra of free QD solution (red solid line) and QD-PTZ complexes with different PTZ-to-QD ratios: low ratio (green solid line), and high ratio (blue solid line). UV-VIS spectra of PTZ are obtained by subtracting spectrum of free QD from the spectra of QD-PTZ complexes: the green dotted line is for the low ratio sample and the blue dotted line is for the high ratio sample. The insert figure is a cartoon of QD-PTZ complex with two PTZ molecules adsorbed.

2.2.3 Preparation of SnO_2 and ATO Films

Colloidal ATO was synthesized according to a published procedure.[6,7] Briefly, 30 g (~ 85 mmol) of $SnCl_4 \cdot 5H_2O$ (98%, from Aldrich) was dissolved in 500 mL of H_2O (Millipore, 18.3 MΩ/cm), to which a solution of $SbCl_3$ (98%, from Aldrich) dissolved in 20 mL of HCl (37 wt %) was added drop wise in an ice bath under rapid stirring. The doping level was controlled by the amount of $SbCl_3$ solution added, and two samples with Sb/Sn molar ratios of 0:1 and 0.1:1 (referred to as SnO_2 and 10% ATO, respectively) were prepared. The resulting clear colorless solution was stirred for 30 min before aqueous ammonia (25%) was added to adjust the pH to 3.5-4.0 and was allowed to settle overnight in the dark. The precipitate was washed at least three times with water and re-suspended in water. The suspension was adjusted to pH 9.5-10, stirred vigorously overnight, and dialyzed against 10 L of aqueous ammonia at pH 10 to produce clear ATO colloidal solution. The ATO colloidal solution was refluxed for 4 h. This colloid (120 mL) was poured into an autoclave and heated at 150 °C for 1 h and at 270 °C for 16 h. The colloid was then concentrated to 60 mL. Five milliliters of the solution and 2 drops of TritonX-100 (from Aldrich) were mixed and stirred for 1 day. The resulting solution was cast onto sapphire windows, dried in air, and then

baked at 400 °C for 1 h in an oven to produce nanoporous crystalline thin films. A detailed characterization of the ATO films prepared in our laboratory by X-ray diffraction, scanning electron microscopy and FTIR were described in a previous publication.[6,7]

2.2.4 Preparation of QD-SnO_2 and QD-ATO Complexes

Water-soluble CdSe/CdS_{3ML}ZnCdS_{2ML}ZnS_{2ML} core/shell QDs with the first exciton peak at 585 nm, purchased from Ocean NanoTech, LLC, USA, were spin coated on SnO_2 and ATO films to prepare the QD-SnO_2 and QD-ATO complexes. The samples were washed by water to remove weakly adsorbed QDs. The concentration of the QD solution is 10 pM for single QD detection and ~ 0.1 μM for averaged ensemble fluorescence measurements. QDs were believed to attach on the TiO_2 nanoparticle surfaces through the carboxylic functional groups. An AFM height image in Figure 2.7 shows the single QD spin coated on an ATO nanoparticle film.

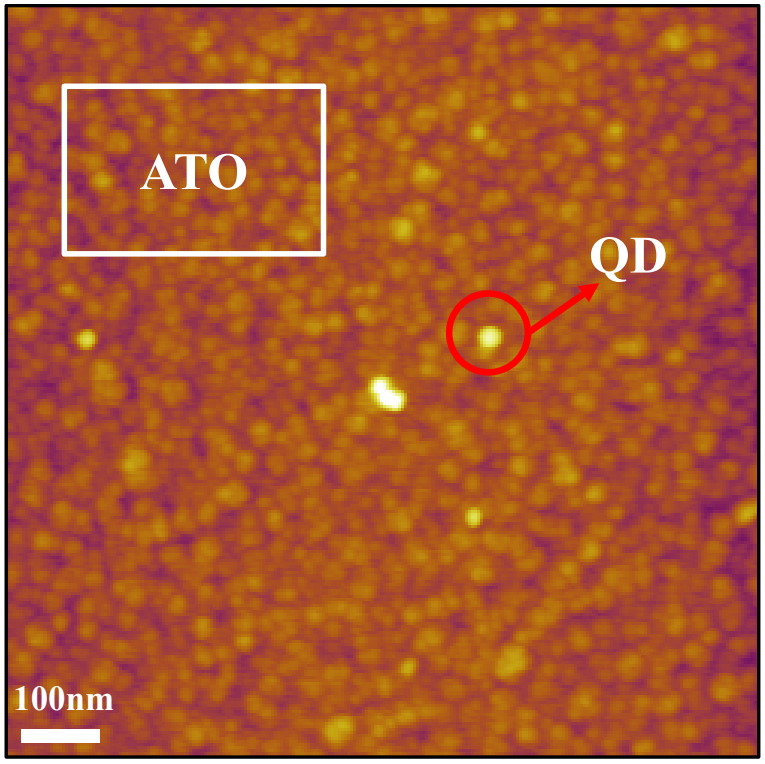

Figure 2.7 AFM image of QD on ATO films. The red circle marks the position of single QD ($CdSe/CdS_{3ML}ZnCdS_{2ML}ZnS_{2ML}$).

2.2.5 Preparation of Charged QD

Water-soluble $CdSe/CdS_{3ML}ZnCdS_{2ML}ZnS_{2ML}$ core/shell QDs with a lowest energy exciton peak at 608 nm were obtained from Ocean NanoTech, LLC, USA. QD-S^{2-} solution samples for fluorescence measurement were prepared by mixing QDs solution (10^{-6} M) with Na_2S solution (0.01 M) in the dark. To account for the possible effect of solution pH on QD exciton dynamics, we also prepared a reference QD solution by mixing QDs (10^{-6} M) with NaOH (pH = 11.5) without adding Na_2S. The solutions were spin coated on cover glass slides, which dried in air before experiments. The concentration of the QD-S^{2-} solution is 10 pM for single QD detection and ~ 0.1 μM for averaged ensemble fluorescence measurements. A schematic diagram showing QD-S^{2-} solution is plotted in Figure 2.8.

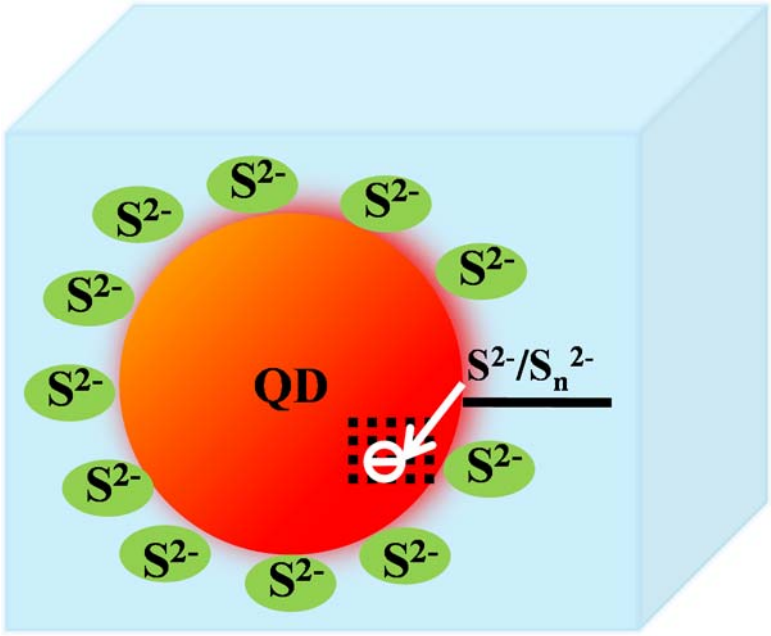

Figure 2.8 Schematic diagram showing QD-S^{2-} complexes in solution

2.2.6 Preparation of QD-TiO_2 and QD-ZrO_2 Complexes

Preparation of TiO_2 Colloid and Thin Films[8,9]

250 mL of water and 80 mL of acetic acid were added to a 1000 mL round bottom flask and cooled to 0 °C. A mixture of 10 mL of 2-propanol and 37 mL of Ti (IV) isopropoxide (Aldrich, 97%) was dropped slowly to the water/acetic acid bulk solution over a 30-40 min period under vigorous stirring and dry N_2 purge. After stirring overnight, the transparent colloid was poured into a 1000 mL beaker and heated in an 80 °C hot water bath for 3-4 h under vigorous stirring. The colloid was autoclaved at 230 °C for 12 h, and then stirred for 4 days. The colloidal solution was spin coated on glass cover slips and then sintered at 550 °C for 2.5 h in air to form nanocrystalline thin films.

Preparation of ZrO_2 Colloid and Thin Films[8,9]

ZrO_2 nanoparticles were obtained from Degussa Corporation. ZrO_2 powder (2 g) was ground in a mortar with distilled water (4 mL), acetylacetone (10 μL) and 5 drops of Triton X-100 to break up the aggregate into a dispersed paste. The paste was washed several times with water. A final diluted ZrO_2 nanoparticle water solution (~ 0.01 g/mL) was spin coated on glass cover slips. The films were then sintered at 550 °C for 2.5 h in air.

To prepare the QD-TiO_2 and QD-ZrO_2 complexes, QD solution with and without Na_2S were spin coated on those semiconductor films.

Reference

(1) Felekyan, S.; Kuhnemuth, R.; Kudryavtsev, V.; Sandhagen, C.; Becker, W.; Seidel, C. A. M. *Rev Sci Instrum* **2005**, *76*.

(2) Knight, A. E. W.; Selinger, B. K. *Aust J Chem* **1973**, *26*, 1.

(3) Bingel, C. *Chem Ber-Recl* **1993**, *126*, 1957.

(4) Lamparth, I.; Hirsch, A. *J Chem Soc Chem Comm* **1994**, 1727.

(5) Zhan, W.; Jiang, K. *Langmuir* **2008**, *24*, 13258.

(6) Guo, J. C.; She, C. X.; Lian, T. Q. *The Journal of Physical Chemistry B* **2005**, *109*, 7095.

(7) Guo, J. C.; She, C. X.; Lian, T. Q. *The Journal of Physical Chemistry C* **2008**, *112*, 4761.

(8) Ai, X.; Anderson, N.; Guo, J. C.; Kowalik, J.; Tolbert, L. M.; Lian, T. Q. *Journal of Physical Chemistry B* **2006**, *110*, 25496.

(9) She, C. X.; Guo, J. C.; Lian, T. Q. *Journal of Physical Chemistry B* **2007**, *111*, 6903.

Chapter 3 Electron Transfer from Quantum Dot to C_{60} Molecule

3.1 Introduction

QD-based nanostructures have been proposed to be useful in many aspects, such as biological imaging and detection,[1-3] light emitting diodes,[4-6] and solar cells.[7-9] Förster resonance energy transfer from QDs to molecular acceptors has been carefully investigated due to its potential application in biological sensing.[3,10-13] Study of charge transfer from QDs to acceptors[8,14-27] has intensified recently with the proposal of the highly controversial multi-exciton generation (MEG) processes in some QDs.[28-31] The QD-molecular acceptor complexes used for both energy and charge transfer applications are usually prepared by linking the molecule to the QD by replacing or reacting with the capping ligands on the QD surface.[1-3,10-16,32] This assembly process produces QDs with a distribution of acceptors on the surface.[33] In other nanoparticle-molecule or nanoparticle-nanoparticle complexes, similar heterogeneities should also exist. Understanding the nature of this distribution is essential for the study of the properties of QD-based nanostructures.

Due to the limited surface area and finite solubility of QDs, the number of adsorbed molecules on the surface of QDs is usually small. Thus the distribution is often assumed to be Poisson. The number of absorbed molecules on one QD is different from the other, which generates a static distribution among QDs. In addition, the number of molecular adsorbates fluctuates with time because of the dynamic adsorption process. The distribution property is difficult to be determined by

ensemble averaged techniques, such as fluorescence decay and transient absorption spectroscopy.

Single particle fluorescence spectroscopy has been proven to be a useful technique for directly studying these distributions.[33-37] The ability of collecting fluorescence signals from single particles enables researchers to study each particle independently, which is essential to determining the statistical distribution of number of adsorbates on QD.

In this chapter, we discuss our study of electron transfer (ET) from single QDs to adsorbed Fullerene (C_{60}) molecules, which are chosen as a model system to represent QD-molecule and QD-nanoparticle complexes. Fluorescence decay of single QD-C_{60} complexes is directly probed, and the distribution of electron transfer rates is deduced. Static distribution and dynamic fluctuation in the ET dynamics in theses complexes are observed, and the fluctuation degree increases with average ET rate. We propose a model to account for these distributions and suggest they are caused by the Poisson statistics of the number of adsorbed C_{60} on QDs in these self-assembled nanostructures.

3.2 Results and Discussions

3.2.1 Ensemble-Averaged Electron Transfer Dynamics

In this study, water soluble CdSe/CdS_{2ML}/$CdZnS_{1ML}$/ZnS_{1ML} core/shell QDs, with the first exciton peak absorption at 585 nm, were used due to their higher quantum yield and better stability in air compared with core only QDs. Four samples were prepared for ensemble-averaged fluorescence decay experiments according to the procedure in Chapter 2: free QDs (sample A) and QD-C_{60} complexes with different

C_{60}-to-QD ratios (samples B, C, and D). The UV-VIS spectra of these samples are plotted in Figure 3.1a. These spectra show the same first exciton peak absorption at 585 nm and increased C_{60} absorption (broad feature at < 500 nm) from sample A to D, suggesting a constant QD concentration and increasing C_{60}-to-QD ratio from samples A (free QD without C_{60}) to D. The exact adsorbed C_{60}-to-QD ratios cannot be determined from the absorption spectra due to the unknown extinction coefficient of the QD and non-negligible solubility of C_{60} in water. For the ensemble averaged fluorescence decay measurement, the solutions were spin coated on thin glass cover slips and dried in air. The QD fluorescence from 540 nm to 625 nm was collected after the excitation of the sample at 500 nm. Ensemble averaged fluorescence decays of these samples are shown in Figure 3.1b. It is clear that faster exciton decay was observed in QD-C_{60} complexes compared to the free QDs and the exciton quenching rate increases with the C_{60}-to-QD ratio.

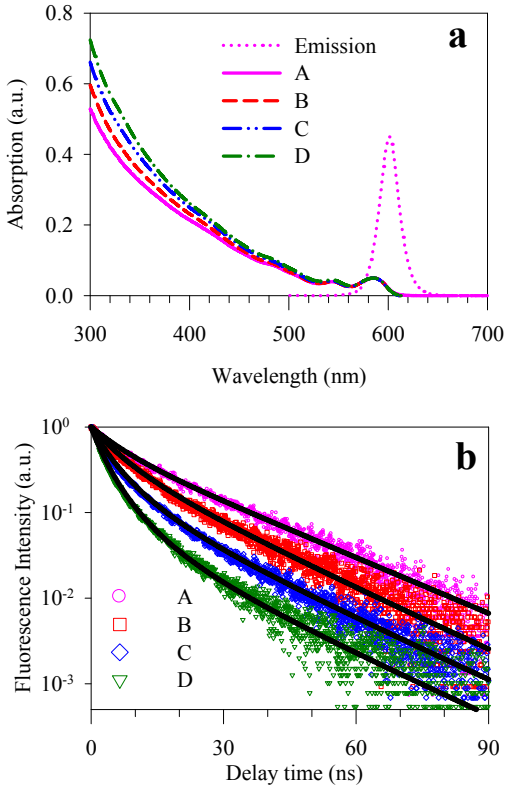

Figure 3.1 a) UV-VIS absorption spectra (lines) and b) ensemble-averaged fluorescence decays (open symbols) of QD-C_{60} complexes from samples A (pink, free QDs), B (red), C (blue) and D (green). The emission spectrum of free QDs is plotted in a dotted line in figure a). Solid lines in b) are best fits according to the Poisson distribution model described in the main text.

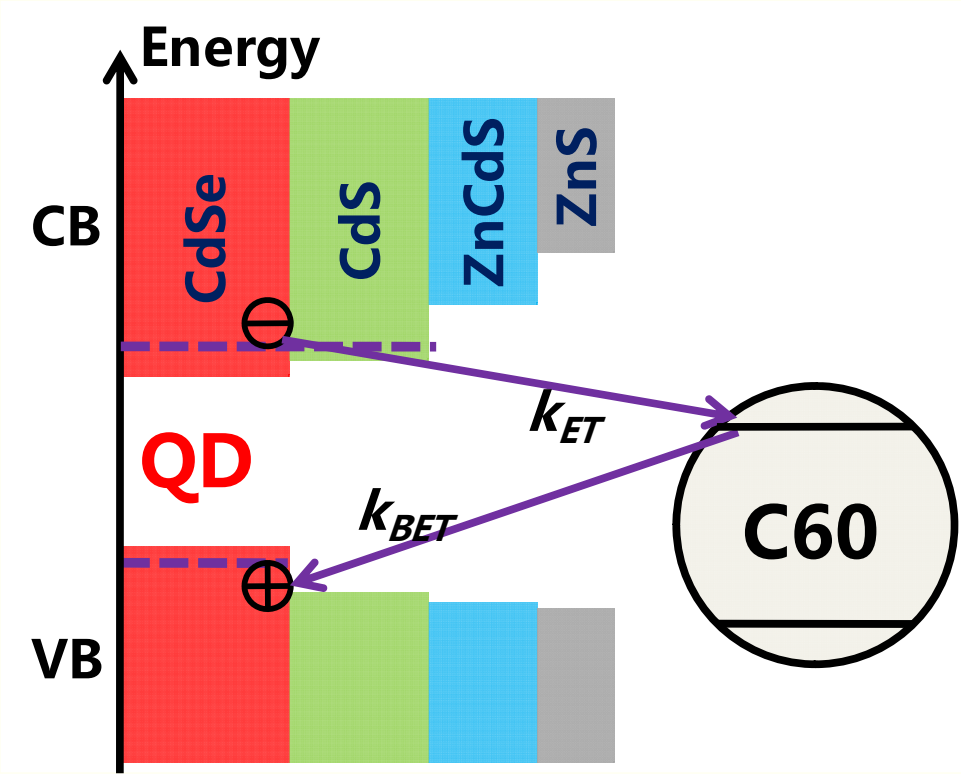

Figure 3.2 Energetic diagrams of the QD-C_{60} complex and possible charge transfer processes: ET from the QD conduction band (CB) to C_{60} LUMO followed by the back ET process.

The relative positions of the conduction (CB) and valence (VB) bands in QD and the highest occupied (HOMO) and lowest unoccupied (LUMO) molecular orbitals of C_{60} are shown in Figure 3.2, from which possible reasons for the observed exciton quenching in QD-C_{60} complexes are discussed. The conduction and valence band levels of QDs can be estimated to be -3.84 and -5.77 V (relative to vacuum) from its

first exciton peak position, according to the method reported in previous works.[38-40] The LUMO and HOMO levels of C_{60} molecules were reported to be -4.30 and -6.60 V, respectively.[41,42] Hole transfer from QDs to C_{60} is energetically forbidden in this system. Energy transfer is not possible either because of the lack of spectral overlap of the QD emission with C_{60} absorption. Electron transfer from the QD conduction band to the LUMO of C_{60} is energetically allowed and has been reported in previous works.[43-46]

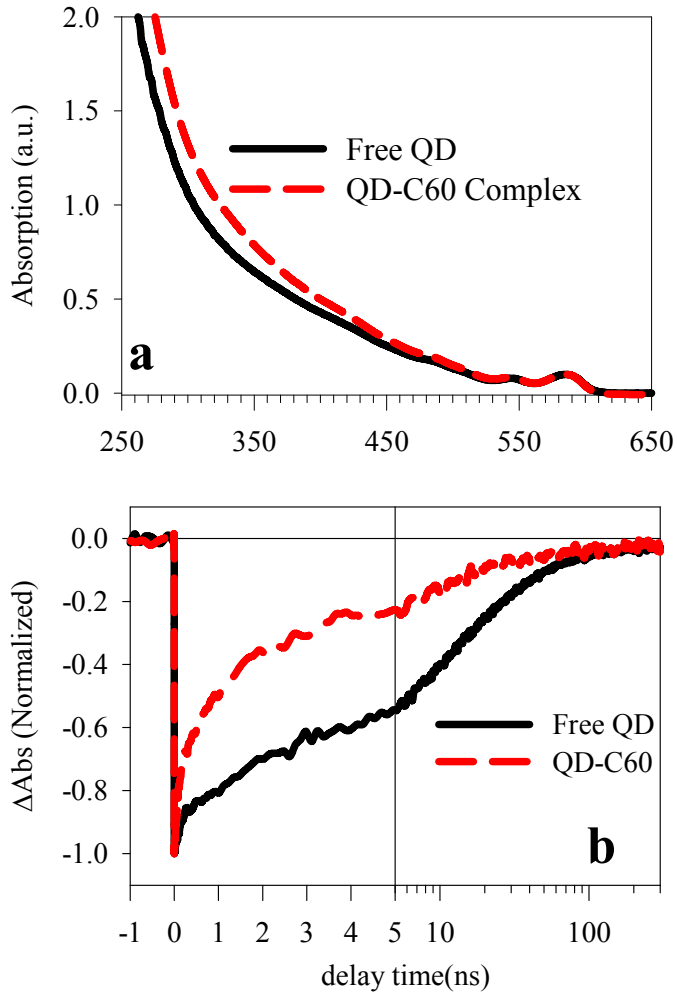

Figure 3.3 a) UV-VIS absorption spectra of free QD (black solid line) and QD-C_{60} complex (red dashed line) solutions in water. Absorption spectrum of C_{60} in ethanol is

plotted with pink solid line. b) 1S exciton band bleach recovery kinetics of QD and QD-C_{60} complexes.

To provide additional evidence of the ET pathway, we also carried out a transient absorption study of the QD-C_{60} complexes. Two samples were prepared: free QD and QD-C_{60} complex solutions in water. The UV-VIS absorption spectra of the two samples are plotted in Figure 3.3a. The increase in absorption below 500 nm of the spectrum of QD-C_{60} solution compared with free QD solution indicates the binding of C_{60} to QD. 1S exciton band bleach recovery kinetics of QD and QD-C_{60} complexes, shown in Figure 3.3b, suggests that, in the presence of C_{60}, the QD 1S exciton bleach shows a faster recovery on the nanosecond time scale than the free QDs. The bleach of 1S exciton absorption results from the filling of the 1S level in the conduction band by the excited electron and its recovery indicates the removal of the 1S electron. Faster bleach recovery in the QD-C_{60} complexes suggests an additional decay pathway for the 1S electron - by electron transfer to the C_{60} molecules. We have previously shown that the kinetics of QD exciton bleach recovery agrees with the formation of reduced adsorbates, confirming the assignment of the exciton bleach recovery to the interfacial ET process.[15,16,47,48] Unfortunately, the absorption band of reduced C_{60} molecules falls in the near IR, beyond the spectral window of our current setup. Together, these results suggest that exciton quenching in the QD-C_{60} complexes can be attributed to the electron transfer from excited QDs to adsorbed C_{60} molecules.

3.2.2 Single QD Electron Transfer Dynamics

For single QD experiment, four samples (1-4) of QD-C_{60} complexes were prepared according to the procedure in Chapter 2.1, followed by dilution. The C_{60}-to-

QD ratios varied with different mixing time, and increased from sample 1 (free QD) to sample 4. However, the exact ratio cannot be determined due to the inability to record accurate absorption spectra under such low concentration (~ 10 pM) of QDs.

Fifty single QDs from each sample were detected and examined, and each QD was followed for about 5 minutes, within which, no noticeable permanent photo-bleach was observed. For each detected photon, both the delay time (relative to the excitation pulse) and the arrival time (relative to the start of experiment) were recorded. For each QD, photons within 50 ms arrival time windows were binned to construct the intensity trajectory. And the delay time histograms of photons within 2 s arrival time windows were constructed and fitted to single exponential decay functions (by a non-linear least square fit) to obtain the lifetime or decay rate (inverse of lifetime) trajectory. Typical intensity and lifetime trajectories of single QD and QD-C_{60} complexes from these samples are shown in panels a1-4 in Figure 3.4. The lifetime trajectory follows the intensity trajectory for both free QDs and QD-C_{60} complexes, consistent with the reported positive correlation between the fluorescence intensity and lifetime of single QDs.[14,40,49-61] States with higher fluorescence intensity (on-state) have longer exciton lifetimes, and states of low intensity (off-state) have shorter lifetimes. The off-states have been attributed to charged QDs, formed by photoinduced Auger ionization and/or charge transfer to trap states.[33,51-53,55,61-63] We attribute all points with intensity within three standard deviation of the background level to off-states and all points with higher intensities to on-states. The exciton decay rate distributions for the single QDs shown in Figures 3.4 a1-4 are plotted in Figures 3.4 b1-4. The green bar in each histogram indicated the occurrence of off-states with decay rates larger than 2 ns^{-1} (or lifetimes < 0.5 ns). The decay rates at these points cannot be accurately determined because of limited photon numbers.

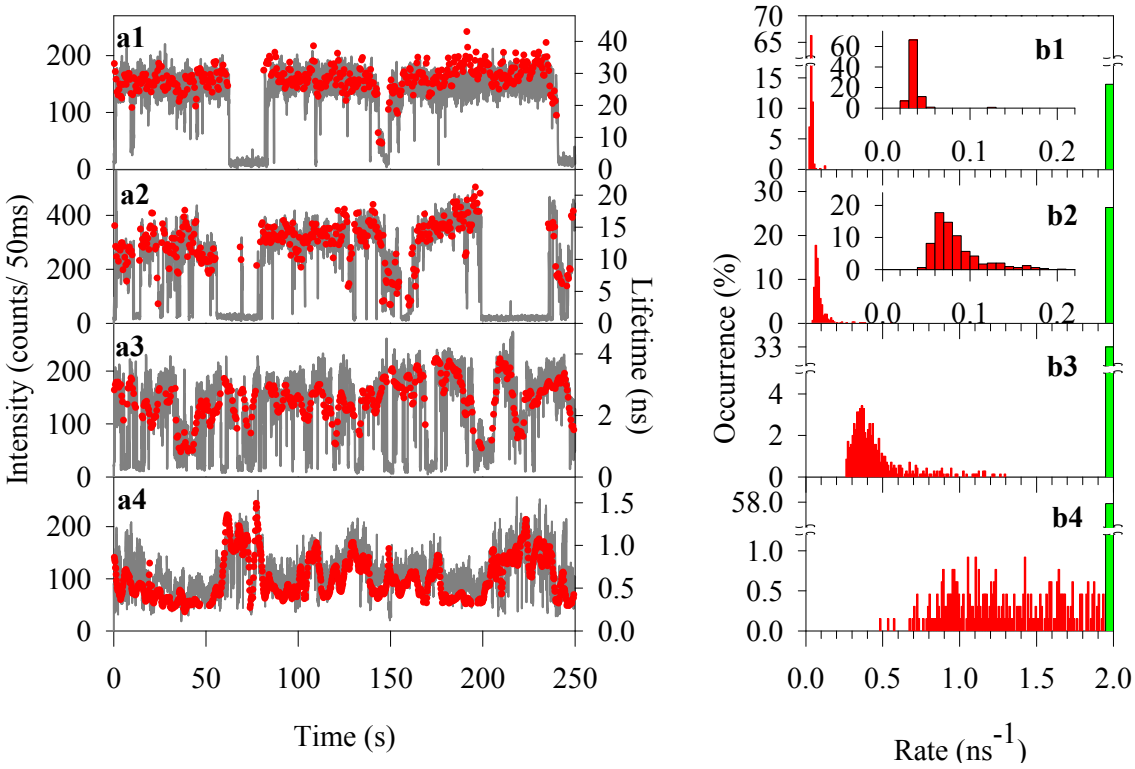

Figure 3.4 Typical fluorescence intensity (gray line) and lifetime (red circles) trajectories (ai) and histograms of exciton quenching rate (with a 0.01 ns^{-1} bin) (bi) of a representative single QD or QD-C_{60} complex from each sample (i=1-4 for samples 1-4, respectively). Green bars in bi) indicate the occurrence of low fluorescence intensity points along the trajectories, for which the rates have been assumed to be > 2 ns^{-1}

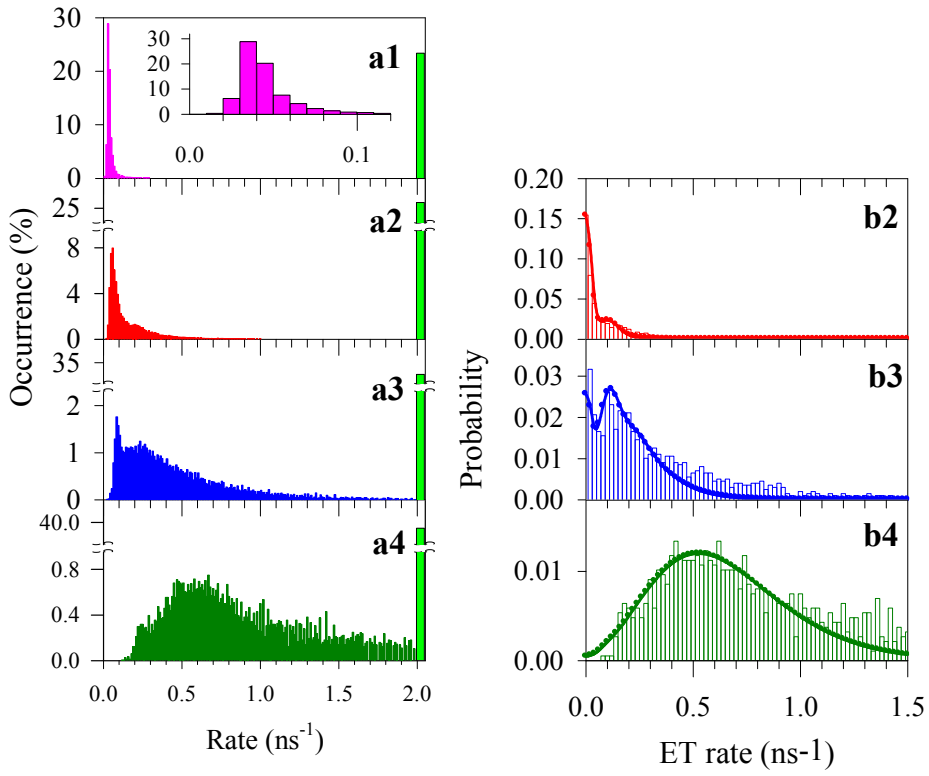

Figure 3.5 ai) Total histogram of exciton quenching rates constructed from 50 particles in each sample. Green bars in bi and ci indicate the occurrence of low fluorescence intensity points along the trajectories, for which the rates have been assumed to be > 2 ns^{-1}.bi) Histograms of ET rates for QD-C_{60} complexes from samples i (=2, 3, 4). Bars are experimental data and solid lines are fits to Poisson distributions according to the model described in the text.

Similar fluorescence decay rate distributions were found in other single QDs and QD-C_{60} complexes. Total histograms of exciton decay rate distributions were constructed from the sum of 50 single particles in each sample and are plotted in Figure 3.5 a1-a4. In free QDs (Figure 3.5 a1), the exciton decay rate fluctuates from ~ 0.03 ns^{-1} in the on state to > 0.5 ns^{-1} in the off state. The QD on-state decay rate increases from 0.1 to 0.6 ns^{-1} in samples 2 to 4 as the average C_{60}-to-QD ratios increase. The occurrence of off-state increases in these samples, and their decay rates

remain too fast to be measured. This behavior is similar to a previous study of ET from single QDs to TiO_2, where the presence of ET pathway increases the probability density of long off-states.[49] The presence of off-state in QDs complicates the analysis of ET rates from QD to C_{60}. And it was shown that for single QDs on TiO_2, the off-state decay rate was much faster than the ET rate and was dominated by Auger recombination process in charged QDs.[49] Thus, the off-state decay rates will not be used to calculate the ET rate and are not further discussed here. We will focus on the distribution and fluctuation of the on-state decay rates.

From Figure 3.5 a1-a4, the on-state decay rates increase in single QD-C_{60} complexes with higher C_{60}-to-QD ratios. This trend is consistent with the ensemble-averaged fluorescence decay results shown in Figure 3.1b and indicates increased ET rates from sample 2 to 4. The distribution of on-state exciton decay rates in free QDs (Figure 3.5 a1), with an average intrinsic decay rate k_0 at 0.048 ns^{-1}, is much narrower compared with those in QD-C_{60} complexes (Figure 3.5 c2-4). Thus, ET rate trajectories for QD_i ($k_{ET,i}(t)$) can be calculated from the exciton decay rate trajectory $k_i(t)$ following equation (3.1):

$$k_{ET,i}(t) = k_i(t) - k_0 \qquad (3.1)$$

Using equation (3.1), the total histogram of ET rates for all QD-C_{60} complexes with different C_{60}-to-QD ratios can be obtained, as plotted in Figure 3.5 b.

To quantify the static heterogeneity of ET rates in different QD-C_{60} complexes, the average ET rate of each single QD, $\langle k_{ET,i} \rangle$, was calculated as the arithmetic mean of ET rates along its trajectory:

$$\left\langle k_{ET,i} \right\rangle = \frac{1}{N}\sum_{j=1}^{N} k_{ET,i}(t_j) \qquad (3.2)$$

Here, t_j and N is the j_{th} and total number of on-state points, respectively, along the trajectory. The probability distributions of the average ET rates of samples 2-4 are shown in Figure 3.6a.

We assume that ET from QD to C_{60} adds an additional decay pathway, $k_{ET}(t)$, but does not affect the distribution of intrinsic exciton decay processes (with an average rate k_0) in the QD-C_{60} complexes. Thus, the fluctuation of the exciton on-state decay rates in QD-C_{60} complexes results mainly from the fluctuation of ET rates. To characterize the fluctuation, we calculate the standard deviation (SD) of ET rates for each complex:

$$SD_i = \sqrt{\frac{1}{N}\sum_{j=1}^{N}\left(k_{ET,i}(t_j) - \left\langle k_{ET,i} \right\rangle\right)^2} \qquad (3.3)$$

Histograms of SD for the three QD-C_{60} samples are compared in Figure 3.6 b. With the C_{60}-to-QD ratios increasing, the fluctuation of ET rates become larger.

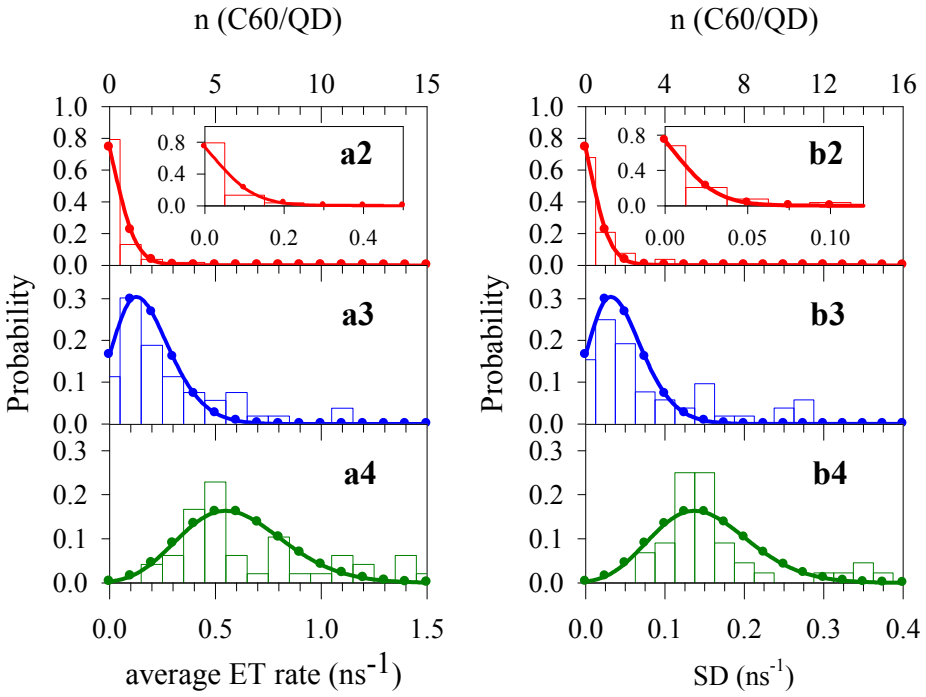

Figure 3.6 Histograms of average ET rates (ai), and standard deviations of ET rates (b) for QD-C_{60} complexes from samples i (=2, 3, 4). Bars are experimental data and solid lines are fits to Poisson distributions according to the model described in the text. The histograms were constructed using bin sizes that equal the average ET rate k_1 (0.10 ns^{-1}) and standard deviation SD_1 (0.025 ns^{-1}), respectively, of the 1:1 C_{60}-QD complex. The number of C_{60} (n) corresponding to the average ET rate and standard deviation is labeled as the top horizontal axes of panel a1 and b1.

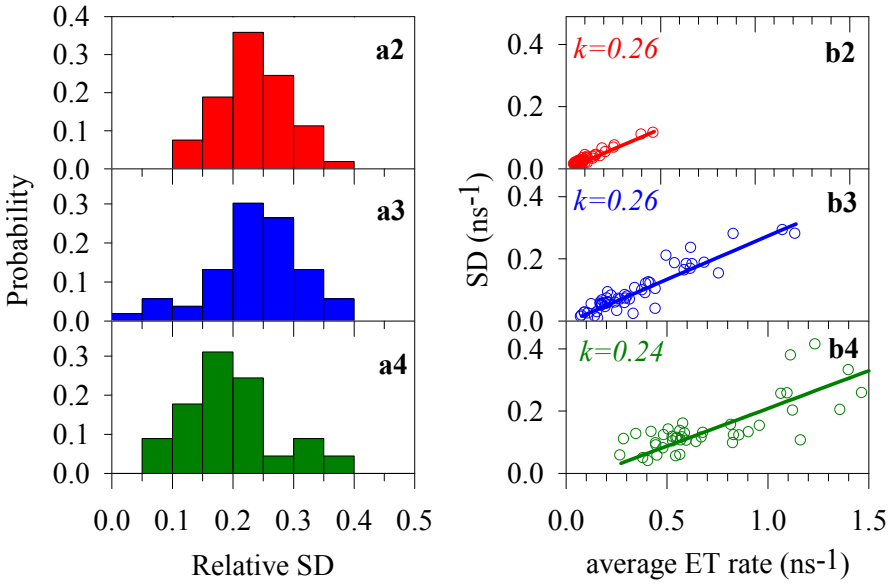

Figure 3.7 ai) Histograms of relative standard deviations of ET rates and bi) plots of standard deviations *vs.* average ET rates for QD-C_{60} complexes from samples 2(red), 3(blue), and 4(green).

The relative standard derivative (RSD) of each complex is defined as the ratio of the SD to the average ET rate and histograms of RSD of ET rates for QD-C_{60} complexes from samples 2 to 4 are shown in Figure 3.7 a. For these complexes, the distributions are similar, which suggests that the standard deviation increases linearly with the average ET rate for single QD-C_{60} complexes. In Figure 3.7 b, we plot the SD as a function of the average ET for all single QDs. A linear function can be used to fit these plots and approximately equal slopes of 0.26, 0.26, and 0.24 were obtained for samples 2, 3, and 4, respectively.

As shown in Figure 3.6 a and b, the histograms of the averages and standard deviations of ET rates for single QD-C_{60} complexes show Poisson-like distributions, and these quantities are positively correlated. This suggests that the heterogeneities in both the average and standard deviation are caused by a common underlying

distribution, which we assume is the distribution of the number of adsorbates on each QD within that sample.

In the self-assembly process of QD-C_{60} complexes, a distribution of the number of C_{60}s on QDs will be generated. Each C_{60} has only two closely spaced COOH groups and can only bind to one QD, but each QD, with its larger surface area, can accommodate more than one C_{60}. If the adsorption process can be assumed to be random, then the number (*n)* of adsorbates per QD obeys a Poisson distribution:[17,37,48]

$$p(n;m) = \frac{m^n e^{-m}}{n!} \quad (3.4)$$

Here, *p(n,m)* is the probability of finding QDs with *n* adsorbates and *m* the average number of adsorbates per QD for the sample.

Let k_1 and SD_1 denote the average and standard deviation of ET rates in the 1:1 C_{60}-QD complexes. It is further assumed that in the *n*:1 C_{60}-QD complex, the *n* C_{60} molecules act as *n* independent electron acceptors. As a result, the average, k_n, and standard deviation, SD_n, of ET rates in the *n*:1 C_{60}-QD complex are given by:

$$k_n = nk_1 \quad (3.5)$$

$$SD_n = nSD_1 \quad (3.6)$$

In a sample with an average C_{60}-to-QD ratio of *m*, the probability distribution of average ET rates and standard deviations in QD-C_{60} complexes is given by:

$$p(m;k_n)=\frac{m^{(\frac{k_n}{k_1})}e^{-m}}{\left(\frac{k_n}{k_1}\right)!} \qquad (3.7)$$

$$p(m;SD_n)=\frac{m^{(\frac{SD_n}{SD_1})}e^{-m}}{\left(\frac{SD_n}{SD_1}\right)!} \qquad (3.8)$$

Within this model, the dynamic fluctuation of ET rates for the *n*:1 complexes should lead to a Gaussian distribution of ET rates with a center at nk_1 and width of nSD_1. Furthermore, there is a distribution of the number of C_{60} molecules on the QDs in the ensemble of self-assembled single QD-C_{60} complexes. Accounting for both effects, the total distribution of ET rate in each sample of single QD-C_{60} complexes can be written as:

$$p(k_{ET})=\sum_{n=1}^{\infty}\frac{m^n e^{-m}}{n!}\cdot\frac{1}{\sqrt{2\pi}(n\cdot SD_1)}e^{-\frac{(k_{ET}-nk_1)^2}{2(n\cdot SD_1)^2}}+e^{-m}\delta(k_{ET}) \qquad (3.9)$$

where the last term represents the contribution of free QDs in the ensemble.

The distributions shown in Figures 3.5 b and 3.6 can be fitted according to equations (3.9), (3.7) and (3.8), respectively. For each sample, the same value of *m* is used to fit the total distribution of ET rates, and the distributions of the average and standard deviations of ET rates. Furthermore, for samples of different ratios, the same k_1 and SD_1 values are used, whereas the *m* values are allowed to change. Because of the linear relationship between k_1 and SD_1 (shown in Figure 3.7 b), we have restrained the value of SD_1 to be $0.25k_1$. In the fitting process, Figure 3.5 b was first fitted to obtain the value for k_1 (and SD_1) and three *m* values (one for each sample). The

histograms in Figure 3.6 were then binned according to the values of k_1 and SD_1, and fitted using the same sets of four fitting parameters. This process is repeated until the best fits for all nine sets of distributions is obtained. These parameters, *m, k_1 and SD_1,* obtained from the best fits (shown in Figure 3.5 b and 3.6) are listed in Table 3.1. From the fitting parameter k_1 (SD_1), we can also calculate the number of adsorbates, *n*, for each average ET rate (standard deviation) according to equation 3.5 (3.6), which is also labeled in Figure 3.6 a (b).

Table 3. 1 Fitting parameters for the distributions of the average and standard deviation of ET rate in single QD-C_{60} complexes. k_1 and SD_1 is the average and standard deviation of ET rates in 1:1 C_{60}-to-QD complexes; *m* is the average C_{60}-to-QD ratio of the samples.

Single experiments				Ensemble experiments	
k_1 (ns^{-1})	SD_1 (ns^{-1})	Sample #	m	Sample #	m
0.1	0.025	2	0.3	B	0.3
		3	1.8	C	1.2
		4	6.0	D	2.2

This model was implemented to describe the ensemble averaged fluorescence decay curves shown in Figure 3.1b and the parameters obtained from the single QD measurement were used. The ensemble averaged fluorescence decay can be described by the following expression:

$$[N(t)] = [N(0)]\left[\int_0^\infty p(k_{ET})e^{-k_{ET}t}dk_{ET}\right]\cdot f_{Free}(t) \qquad (3.10)$$

where *[N(t)] and [N(0)]* are the population of excited QDs at time *t* and 0, respectively. $f_{Free}(t)$ is the fluorescence decay of free QDs, which can be independently measured and fitted.The values of k_1 and SD_1 were determined from fitting the data for single QD-C_{60} complexes, leaving only the average C_{60}-to-QD ratio *m* as a fitting parameter. As shown in Figure 3.1b, the ensemble-averaged fluorescence decay curves for ratio B, C, and D can be well fitted to this model. The average ratios obtained from the fits are 0.3, 1.2, and 2.2, respectively, as listed in Table 3.1. These values agree with the trend of C_{60} absorption in the UV-visible spectra (Figure 3.1a) of these samples. Unfortunately, a quantitative comparison is not possible because the exact ratios of C_{60}-to-QD are not known in these samples due to the non-negligible solubility of modified C_{60} molecules in water.

Both the distributions of the average and standard deviation of ET rates in single QD-C_{60} complexes as well as the ensemble averaged fluorescence decay kinetics can be described by the proposed model. It indicates that in self-assembled QD heterostructures, such as the QD-C_{60} complexes, the Poissonian statistical distribution of the number of partners on the QD is the most dominating heterogeneity. This implies that other heterogeneities, such as the distribution of QD sizes, are much smaller in comparison. In the proposed model, the assembly process is assumed to be random, which should be obeyed when the interaction between the adsorbates is negligible or is much smaller than the adsorbate-QD interaction. Under these conditions, it is also reasonable to assume that these adsorbates act as independent electron acceptors, which leads to the observed correlated Poissonian distributions of the standard deviations and averages of ET rates. We believe that these assumptions are likely valid for many other self-assembly QD nanostructures and the averages and standard deviations of their properties (such as electron and energy transfer rates) may

also follow the correlated Poissonian distributions reported here for QD-C_{60} complexes.

3.3 Summary

To summarize, single QD fluorescence spectroscopy and ensemble-averaged transient absorption and fluorescence decay measurements were utilized to study the electron transfer dynamics in self-assembled QD-C_{60} complexes. It is shown by both the single QD and ensemble-averaged measurements that the exciton quenching rate increases with the C_{60}-to-QD ratio and can be attributed to the increasing electron transfer rates from the QD to C_{60} in these samples. By comparing with the fluorescence decay trajectories of free QDs, we find that the ET rates of single QD-C_{60} complexes exhibit large fluctuation with time. In addition, the fluctuation degree, measured by the standard deviation, increases linearly with the average ET rate, and both show Poisson like distributions. This finding suggests that the distributions in these quantities are caused by a common heterogeneity in the sample. A model is proposed to quantify the distributions of averages and standard deviations of ET rates in each QD-C_{60} complex sample. In this model, a random adsorption process for C_{60} on QDs is assumed and the adsorbates act as independent electron acceptors. Under these assumptions, both the averages and standard deviations of ET rates obey Poisson distribution, which is caused by the Poisson distribution of the number of adsorbates on the QDs. It is found that our model can satisfactorily describe the distributions measured in single QD-C_{60} complexes (i.e. histograms of the ET rates, average ET rates and standard deviations) and the ensemble-averaged fluorescence decays kinetics. Based on our finding, we conclude that in many self-assembled QD nanostructures, such as QD-C_{60} complexes, the statistical distribution of the number

of adsorbed partners on the QDs exists, and it is the origin of distributions of the averages and fluctuations of their interfacial dynamic properties.

Reference

(1) Bruchez, M.; Moronne, M.; Gin, P.; Weiss, S.; Alivisatos, A. P. *Science* **1998**, *281*, 2013.

(2) Chan, W. C. W.; Nie, S. *Science* **1998**, ***281***, 2016.

(3) Medintz, I. L.; Clapp, A. R.; Brunel, F. M.; Tiefenbrunn, T.; Uydea, H. T.; Chang, E. L.; Deschamps, J. R.; Dawson, P. E.; Mattoussi, H. *Nat. Mater.* **2006**, *5*, 581.

(4) Achermann, M.; Petruska, M. A.; Koleske, D. D.; Crawford, M. H.; Klimov, V. I. *Nano Lett* **2006**, *6*, 1396.

(5) Steckel, J. S.; Snee, P.; Coe-Sullivan, S.; Zimmer, J. P.; Halpert, J. E.; Anikeeva, P.; Kim, L.-A.; Bulovic, V.; Bawendi, M. G. *Angew. Chem., Int. Ed.* **2006**, *45*, 5796.

(6) Colvin, V. L.; Schlamp, M. C.; Alivisatos, A. P. *Nature* **1994**, *370*, 354.

(7) Huynh, W. U.; Dittmer, J. J.; Alivisatos, A. P. *Science* **2002**, *295*, 2425.

(8) Robel, I.; Subramanian, V.; Kuno, M.; Kamat, P. V. *J. Am. Chem. Soc.* **2006**, *128*, 2385.

(9) Tachibana, Y.; Akiyama, H. Y.; Ohtsuka, Y.; Torimoto, T.; Kuwabata, S. *Chem. Lett.* **2007**, *36*, 88.

(10) Funston, A. M.; Jasieniak, J. J.; Mulvaney, P. *Adv. Mater.* **2008**, *20*, 4274.

(11) Curutchet, C.; Franceschetti, A.; Zunger, A.; Scholes, G. D. *J. Phys. Chem. C* **2008**, *112*, 13336.

(12) Medintz, I. L.; Mattoussi, H. *Phys. Chem. Chem. Phys.* **2009**, *11*, 17.

(13) Dayal, S.; Burda, C. *J. Am. Chem. Soc.* **2007**, *129*, 7977.

(14) Issac, A.; Jin, S.; Lian, T. *J. Am. Chem. Soc.* **2008**, *130*, 11280.

(15) Boulesbaa, A.; Issac, A.; Stockwell, D.; Huang, Z.; Huang, J.; Guo, J.; Lian, T. *J. Am. Chem, Soc.* **2007**, *129*, 15132.

(16) Huang, J.; Stockwell, D.; Huang, Z.; Mohler, D. L.; Lian, T. *J. Am. Chem. Soc.* **2008**, *130*, 5632.

(17) Huang, J.; Huang, Z.; Jin, S.; Lian, T. *J. Phys. Chem. C* **2008**, *112*, 19734.

(18) Kamat, P. *J. Phys. Chem. C* **2008**, *112*, 18737.

(19) Rossetti, R.; Beck, S. M.; Brus, L. E. *J. Am. Chem. Soc.* **1984**, *106*, 980.

(20) Rossetti, R.; Brus, L. E. *J. Phys. Chem.* **1986**, *90*, 558.

(21) Ramsden, J. J.; Gratzel, M. *Chem. Phys. Lett.* **1986**, *132*, 269.

(22) Henglein, A. *Pure & Appl. Chem.* **1984**, *56*, 1215.

(23) Logunov, S.; Green, T.; Marguet, S.; El-Sayed, M. A. *J. Phys. Chem. A* **1998**, *102*, 5652.

(24) Burda, C.; Green, T. C.; Link, S.; El-Sayed, M. A. *J. Phys. Chem. B* **1999**, *103*, 1783.

(25) Blackburn, J. L.; Ellingson, R. J.; Micic, O. I.; Nozik, A. J. *Journal of Physical Chemistry B* **2003**, *107*, 102.

(26) Robel, I.; Kuno, M.; Kamat, P. V. *J. Am. Chem. Soc.* **2007**, *129*, 4136.

(27) Spanhel, l.; Weller, H.; Henglein, A. *J. Am. Chem. Soc.* **1987**, *109*, 6632.

(28) Nair, G.; Bawendi, M. G. *Phys Rev Lett* **2007**, *76*, 081304.

(29) McGuire, J. A.; Joo, J.; Pietryga, J. M.; Schaller, R. D.; Klimov, V. I. *Acc. Chem. Res.* **2008**, *41*, 1810.

(30) Pijpers, J. J. H.; Ulbricht, R.; Tielrooij, K. J.; Osherov, A.; Golan, Y.; Delerue, C.; Allan, G.; Monn, M. *Nature Physics* **2009**, *5*, 811.

(31) Beard, M. C.; Midgett, A. G.; Hanna, M. C.; Luther, J. M.; Hughes, B. K.; Nozik, A. J. *Nano Lett* **2010**, *10*, 3019.

(32) Sudeep, P. K.; Early, K. T.; McCarthy, K. D.; Odoi, M. Y.; Barnes, M. D.; Emrick, T. *J Am Chem Soc* **2008**, *130*, 2384.

(33) Nirmal, M.; Dabbousi, B. O.; Bawendi, M. G.; Macklin, J. J.; Trautman, J. K.; Harris, T. D.; Brus, L. E. *Nature* **1996**, *383*, 802.

(34) Empedocles, S.; Bawendi, M. *Acc. Chem. Res.* **1999**, *32*, 389.

(35) Moerner, W. E.; Barbara, P. F. *Accounts of Chemical Research* **1996**, *29*, 561.

(36) Tamarat, P.; Maali, A.; Lounis, B.; Orrit, M. *J. Phys. Chem. A* **2000**, *104*, 1.

(37) Pons, T.; Medintz, I. L.; Wang, X.; English, D. S.; Mattoussi, H. *J. Am. Chem. Soc.* **2006**, *128*, 15324.

(38) Brus, L. E. *J. Chem. Phys.* **1983**, *79*, 5566.

(39) Brus, L. E. *J. Chem. Phys.* **1984**, *80*, 4403.

(40) Jin, S.; Song, N.; Lian, T. *ACS Nano* **2010**, *4*, 1545.

(41) Dubois, D.; Kadish, K. M.; Flanagan, S.; Haufler, R. E.; Chibante, L. P. F.; Wilson, L. J. *Journal of the American Chemical Society* **1991**, *113*, 4364.

(42) Kira, A.; Umeyama, T.; Matano, Y.; Yoshida, K.; Isoda, S.; Park, J. K.; Kim, D.; Imahori, H. *J. Am. Chem. Soc.* **2009**, *131*, 3198.

(43) Zhang, J. Z.; Geselbracht, M. J.; Ellis, A. B. *Journal of the American Chemical Society* **1993**, *115*, 7789.

(44) Brown, P.; Kamat, P. V. *Journal of the American Chemical Society* **2008**, *130*, 8890.

(45) Biebersdorf, A.; Dietmuller, R.; Susha, A. S.; Rogach, A. L.; Poznyak, S. K.; Talapin, D. V.; Weller, H.; Klar, T. A.; Feldmann, J. *Nano Letters* **2006**, *6*, 1559.

(46) Biebersdorf, A.; Dietmueller, R.; Ohlinger, A.; Klar, T. A.; Feldmann, J.; Talapin, D. V.; Weller, H. *App. Phys. B* **2008**, *93*, 239.

(47) Huang, J.; Huang, Z.; Yang, Y.; Zhu, H.; Lian, T. *J Am Chem Soc* **2010**, *132*, 4858.

(48) Boulesbaa, A.; Huang, Z.; Wu, D.; Lian, T. *J. Phys. Chem. C* **2010**, *114*, 962.

(49) Jin, S.; Lian, T. *Nano Lett* **2009**, *9*, 2448.

(50) Fisher, B. R.; Eisler, H.-J.; Stott, N. E.; Bawendi, M. G. *J. Phys. Chem. B* **2004**, *108*, 143.

(51) Efros, A. L.; Rosen, M. *Phys. Rev. Lett.* **1997**, *78*, 1110.

(52) Shimizu, K. T.; Neuhauser, R. G.; Leatherdale, C. A.; Empedocles, S. A.; Woo, W. K.; Bawendi, M. G. *Phys. Rev. B* **2001**, *63*, 205316/1.

(53) Kuno, M.; Fromm, D. P.; Johnson, S. T.; Gallagher, A.; Nesbitt, D. J. *Phys. Rev. B:* **2003**, *67*, 125304/1.

(54) Peterson, J. J.; Nesbitt, D. J. *Nano Lett.* **2009**, *9*, 338.

(55) Zhang, K.; Chang, H.; Fu, A.; Alivisatos, A. P.; Yang, H. *Nano Lett* **2006**, *6*, 843.

(56) Montiel, D.; Yang, H. *J. Phys. Chem. A* **2008**, *112*, 9352.

(57) Pelton, M.; Smith, G.; Scherer, N. F.; Marcus, R. A. *Proc. Natl. Acad. Sci. U. S. A.* **2007**, *104*, 14249.

(58) Tang, J.; Marcus, R. A. *J. Chem. Phys.* **2006**, *125*, 044703/1.

(59) Issac, A.; von Borczyskowski, C.; Cichos, F. *Phys.l Rev. B* **2005**, *71*, 161302/1.

(60) Schlegel, G.; Bohnenberger, J.; Potapova, I.; Mews, A. *Phys. Rev. Lett.*. **2002**, *88*, 137401.

(61) Verberk, R.; van Oijen, A. M.; Orrit, M. *Phys. Rev. B* **2002**, *66*, 233202/1.

(62) Krauss, T. D.; O'Brien, S.; Brus, L. E. *J. Phys. Chem. B* **2001**, *105*, 1725.

(63) Shimizu, K. T.; Woo, W. K.; Fisher, B. R.; Eisler, H. J.; Bawendi, M. G. *Phys. Rev. Lett.* **2002**, *89*, 117401/1.

Chapter 4 Hole Transfer from Quantum Dot to PTZ Molecule

4.1 Introduction

The dynamics of charge transfer from and to QDs has brought broad interest to researchers in many fields due to their potential application in solar cells.[1-4] For instance, in QD solar cells based on QD sensitized TiO_2 nanocrystalline thin films, in addition to many other processes, the efficiencies of the initial electron transfer from the QDs to TiO_2 and subsequent filling of the holes in the QD by the redox mediators can greatly affect the device performance.[5] Thus, exciton dissociation in CdX and PbX (X=S, Se and Te) QDs by ultrafast electron transfer (ET) to molecular electron acceptor or semiconductors has been investigated.[5-19] Examples of hole transfer (HT) are relatively few and the rate of hole transfer is considerably slower for reasons yet to be understood.[20-24] Our understanding of ET dynamics from QDs is mostly derived from ensemble averaged measurements, which show that these processes are highly heterogeneous. Studies of electron transfer from single QD to electron acceptors led to further insights into the heterogeneity of ET dynamics within single QD-electron acceptor complexes.[25-31] From these studies, it has been found that the ET activity in these complexes is intermittent, modulated by the blinking dynamics of single QDs.[25-31] Because the important roles of these interfacial electron and hole transfer activities in QD-solar cells, further studies of their dependences on single QD blinking dynamics are needed.

Under continuous excitation, single QDs fluctuate between on-states (with high fluorescence intensity and long lifetime) and off-states (with low fluorescence intensity at or near the background level and short lifetimes).[25,27,28,32-54] The off-states have been attributed to photoinduced charging of QDs by Auger ionization and/or electron transfer to trap states in QDs or the surrounding matrix.[32-34,36,45,48,53,54] The probability densities of the on- and off- times obey a power-law distribution with an exponent of ~ 1.5,[33,36,55,56] and this dependence can be explained by models that assume diffusion controlled electron transfer (ET).[33,48,52,53,56-58] These models suggest that the blinking dynamics can be suppressed by a number of approaches, including filling of the electron trap states (by surface ligands[39,41,42] or n-doped semiconductors[28]), increasing the emission yield of the charged QD (by either increasing the radiative decay rate[36,44] or reducing the Auger recombination rate[38,40,59]) and decreasing the probability of accessing the off states.[60,61] Despite these abilities to manipulate the blinking behavior, the nature of the trap states remains unclear and has yet to be systematically controlled.

Single particle spectroscopy has been proven to be an effective technique in understanding the single QD blinking dynamics. In QD-electron (hole) acceptor complexes, the exciton dissociates by electron (hole) transfer to the acceptor, generating charge separated states with the hole (electron) left in the QD. The nature of the off-states can be probed by investigating the effect of these charge separate states on the blinking dynamics. Furthermore, in QD-acceptor complexes, the charge transfer rate can be controlled by the number as well as the nature of the acceptors, offering the possibility to test the relationship between the blinking dynamics and charge transfer rate. In recent studies of single QD-electron acceptor complexes, we and others have shown that the electron transfer rate and the blinking dynamics are

correlated: the QDs exhibit larger probability of off states in complexes with higher ET rate.[25-31] This finding supports the current model for the off-states because electron transfer to acceptors left a hole in the QDs, which is similar to the proposed off-state generated by Auger ionization or electron transfer to trap states. It also suggests that in QD-hole acceptor complexes, due to the presence of hole transfer pathway, the duration of off-states can be shortened and therefore the blinking dynamics will be suppressed. However, direct observations of the hole transfer process and correlations of the blinking dynamics with hole transfer rate on the single QD level have not been reported.

In this chapter, we report a study of hole transfer dynamics in single QD-hole acceptor complexes. Ensemble average transient absorption (TA) and fluorescence decay measurements confirm that in QD-phenothiazine (PTZ, see Figure 2.5a) complexes, excitons dissociate by hole transfer to PTZ, consistent with a previous study of related complexes.[20] At the single QD-PTZ level, QD shows correlated fluctuations of lifetime and intensity. The on-state fluorescence lifetime deceases, consistent with hole transfer. Unlike in electron transfer process, the hole transfer pathway does not suppress the blinking or significantly alter the statistics of the on- and off- state distributions of QDs. Instead, it increases the probability of grey-states. We propose a model to account for the observed effects of hole transfer on single QD blinking dynamics.

4.2 Experiment and Discussion

4.2.1 Ensemble Averaged Hole Transfer Dynamics

Three samples, A, B and C, with different PTZ-to-QD ratios were prepared according to the procedure in Chapter 2. CdSe/CdS_{3ML}/$CdZnS_{2ML}$/ZnS_{2ML} core/multi-shell QDs with first exciton (1S) peak at 605 nm were used for this study. The ultraviolet-visible (UV-VIS) absorption spectra of samples A, B, C are displayed in Figure 4.1. These spectra show the same QD absorption (from 400- 605 nm) and different PTZ absorption (~ 320 nm), indicating a constant QD concentration and increasing PTZ-to-QD ratios from samples A (free QD without PTZ) to C. The exact ratios of adsorbed PTZ-to-QD could not be determined from the absorption spectra because the extinction coefficient of the QD is unknown and there is a partition of free and QD bound PTZ molecules. Both the exciton absorption and emission peak positions (see inset of Figure 4.1) have negligible changes with increased PTZ-to-QD ratios.

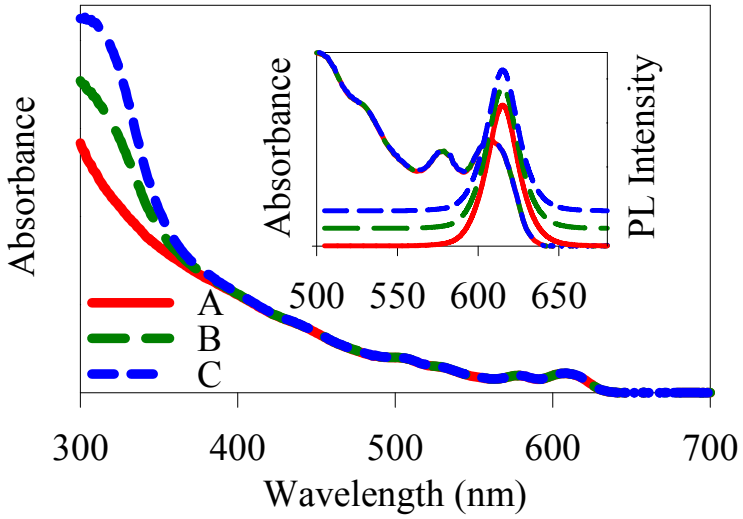

Figure 4.1 UV-VIS absorption spectra of QD-PTZ complexes of samples A (red, free QDs), B (green) and C (blue). The fluorescence spectra of the three samples are compared in the inset of figure a, along with an expanded view of the absorption spectra near the 1S exciton band.

Ensemble averaged fluorescence decays of these samples are plotted in Figure 4.2a. These samples were excited at 500 nm and the resulting QD emission from 540-625 nm was collected by time-correlated single photon counting. It can be seen that exciton fluorescence decay is faster in QD-PTZ complexes than free QDs and the exciton quenching rate increases with the PTZ-to-QD ratio.

Possible pathways for the observed exciton quenching in QD-PTZ complexes can be determined from the relative energy levels of QD and PTZ shown in Figure 4.2c. From the first exciton peak position of the QDs, the conduction and valence band levels can be estimated to be -3.89V and -5.79 V (relative to vacuum) according to the method reported in previous works.[28,62,63] The lowest-unoccupied and highest occupied molecular-orbitals (LUMO and HOMO) levels of PTZ molecules were reported to be -1.6 and -5.5 V, respectively.[64] Exciton dissociation by ET from the QD to the PTZ LUMO level is energetically forbidden in this system. Energy transfer is not possible either due to the lack of spectral overlap of the QD emission with PTZ absorption (Figure 4.1). Hole transfer from the QD valence band to the HOMO of PTZ is energetically allowed and has been reported in our previous work.[20]

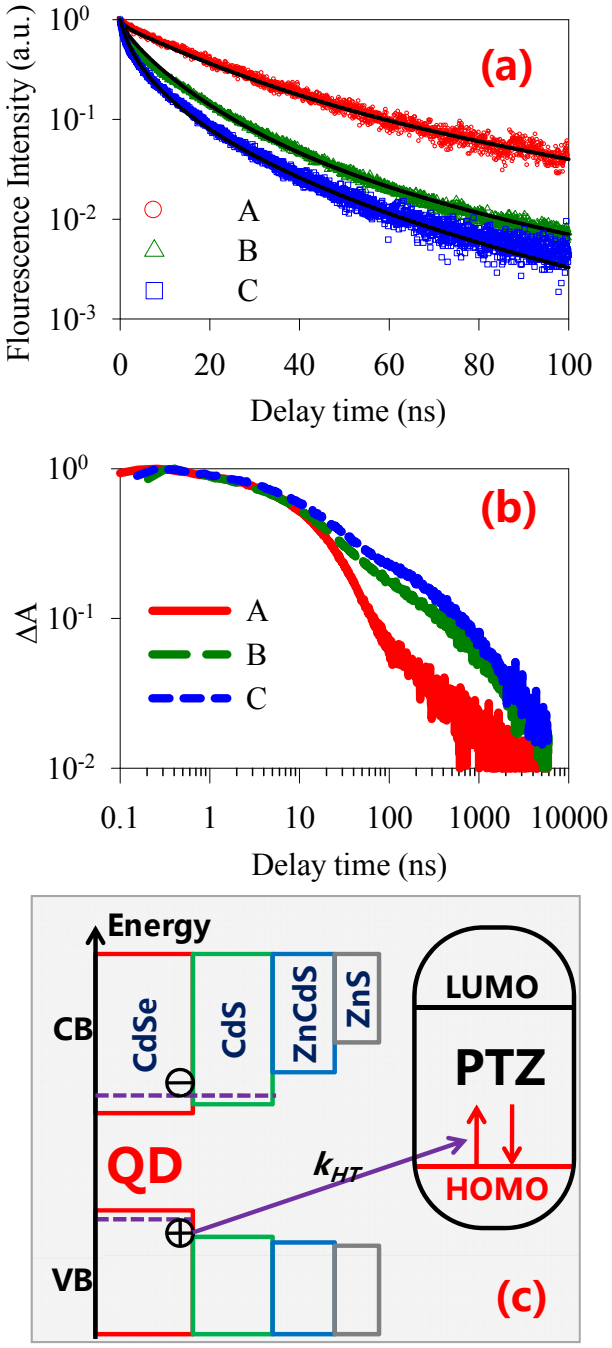

Figure 4.2 a) Ensemble-averaged fluorescence decays (open symbols) and b) 1S exciton bleach recovery kinetics of QD-PTZ complexes of samples A (red, free QDs), B (green) and C (blue). Solid lines in a) are best fits according to the Poisson distribution model described in the text. c) Energetic diagram of the QD-PTZ complex and possible charge transfer processes: hole transfer from the QD valence band (VB) to PTZ HOMO followed by charge recombination (not shown), in which

the electron is transferred from the conduction band (CB) of the reduced QD to the oxidized PTZ.

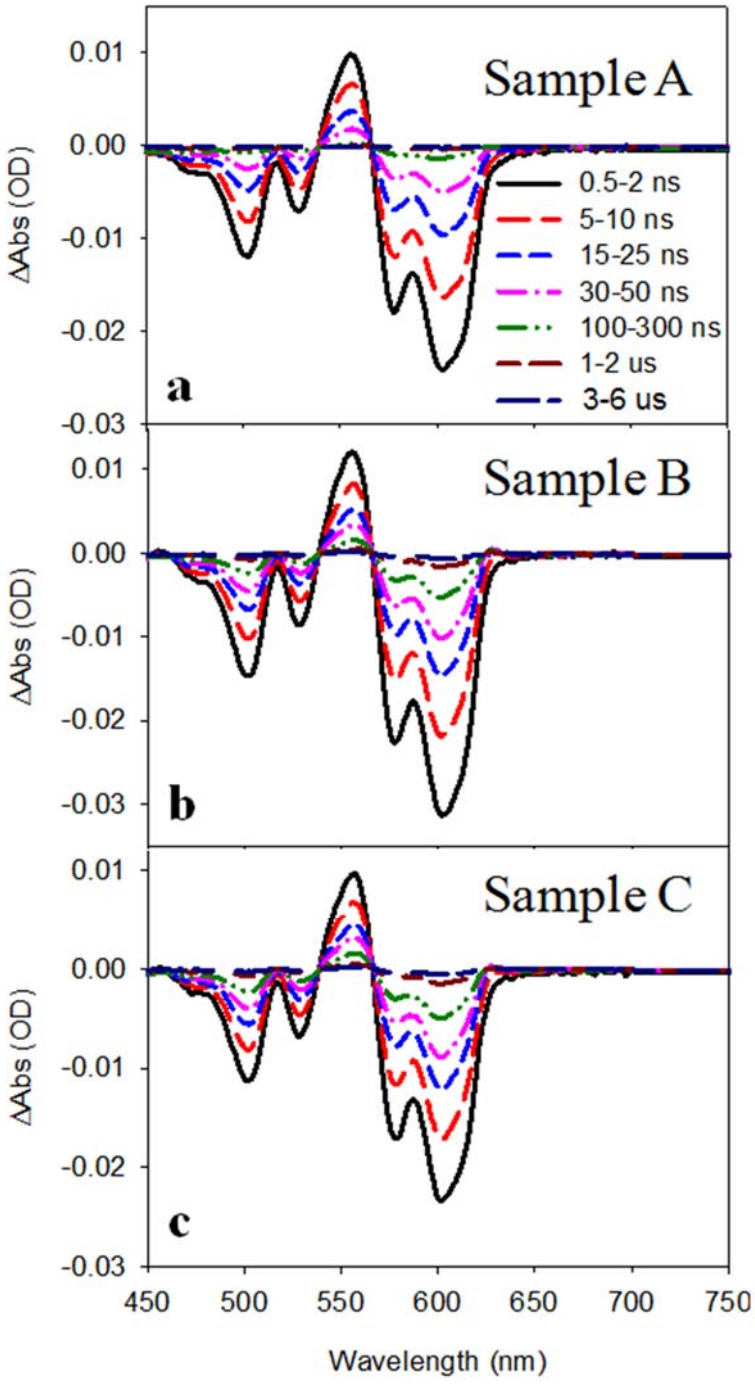

Figure 4.3 Transient absorption spectra of a) sample A (free QDs), b) sample B, and c) sample C at indicated delay times after 400 nm excitation. The average PTZ-to-QD ratio increases from samples B to C. The spectra are dominated by state filling

induced QD exciton bleach signatures, which are the same for all samples. They differ in the kinetics of the bleach recovery (shown in Figure 4.2c).

Exciton quenching by hole transfer generates a charge separated state with a reduced QD and oxidized PTZ radical. The 1S electron in the reduced QD can eventually recombine with the hole at the HOMO level of the oxidized PTZ radical to regenerate the complex in the ground state. To probe this charge recombination process and to provide further evidence for the HT pathway, we have also carried out transient absorption study of the QD-PTZ complexes. As shown in Figure 4.2b and Figure 4.3, in samples A, B and C, excitation by 400 nm pulses generates excited QDs, in which the filling of the 1S electron level leads to the bleach (or decrease of absorption) of the 1S exciton band.[20,65,66] The 1S exciton bleach recovery kinetics directly monitors the removal rate of the 1S electron. In QD-PTZ complexes, the QD 1S exciton bleach shows a slower recovery (or longer lived 1S electron on the 10 ns to a few seconds scale) than the free QDs. It indicates that in the QD-PTZ complexes, excitons dissociate by HT from the QD to PTZ, which increases the lifetime of the 1S electron by removing the 1S electron – 1S hole recombination pathway. Exciton quenching by both electron and energy transfers would have shortened the 1S electron lifetime. Furthermore, it was previously shown that in CdSe QD-PTZ complexes, the decay of the QD 1S exciton fluorescence leads to the formation of PTZ radicals (at ~ 520 nm), directly confirming the interfacial HT process.[20] In the current system, the overlap of the strong exciton bleach signatures with the much weaker PTZ radical absorption hinders a direct measurement of the latter. The recovery of 1S exciton bleach in the QD-PTZ complex on the 100 ns to a few microseconds time scale is assigned to the charge recombination process, transferring the 1S electron to the PTZ radical to regenerate the complex in the ground state.

4.2.2 HT Dynamics in Single QD-PTZ Complexes

To examine the effect of hole transfer on the blinking dynamics of single QDs, we examine three samples (1-3) of QD-PTZ complexes by single QD fluorescence spectroscopy. The PTZ-to-QD ratios, controlled by the amount of PTZ added, increase from sample 1 (free QD) to 3. About forty to fifty single QDs from each sample were detected and each QD was followed for about 5 minutes. Two times were associated with each detected photon: the delay time (relative to excitation pulse) and the arrival time (relative to the start of the experiment) were recorded. For each QD, intensity trace was constructed by counting the number of photons within 50 ms arrival time windows. The delay time histograms of photons within 1 s arrival time windows were constructed and fitted to single exponential decay functions (by a non-linear least square fit) to obtain the lifetime trajectory. Typical intensity and lifetime trajectories of single QD and QD-PTZ complexes from these samples are shown in panels b1-3 of Figure 4.4. Typical fluorescence decay curves at selected times along the trajectories shown in panels b2 and b3 of Figure 4.4 are shown in Figure 4.5. All trajectories show single-step bleaching of fluorescence intensity to the background level, consistent with the behavior of single emitters, although the possibility of a small number of aggregates of two or three emitters cannot be excluded. Recent studies show that aggregates of two or three nanorods show blinking statistics that are indistinguishable from single QDs, but different statistics are observed in aggregates with five or more nanorods.[67,68] The lifetime trajectory follows the intensity trajectory for both free QDs and QD-PTZ complexes, consistent with the reported positive correlation between the fluorescence intensity and lifetime of single QDs.[25,27,28,33,45-54] Intensity and lifetime histograms of these single QDs are plotted in Figure 4.4a and 4.4c, respectively. We attribute all points with intensity within six

standard deviation of the background level to off-states and all points with higher intensities to on-states. The intensity threshold separating the "on" and "off" states are indicated by black dashed lines in Figure 4.4a. For states with emission intensity at the background level, the exciton lifetimes cannot be accurately obtained because of limited photon numbers and are estimated to be smaller than 0.5 ns. The occurrence of these states are counted and plotted with in the lifetime histograms in Figure 4.4c.

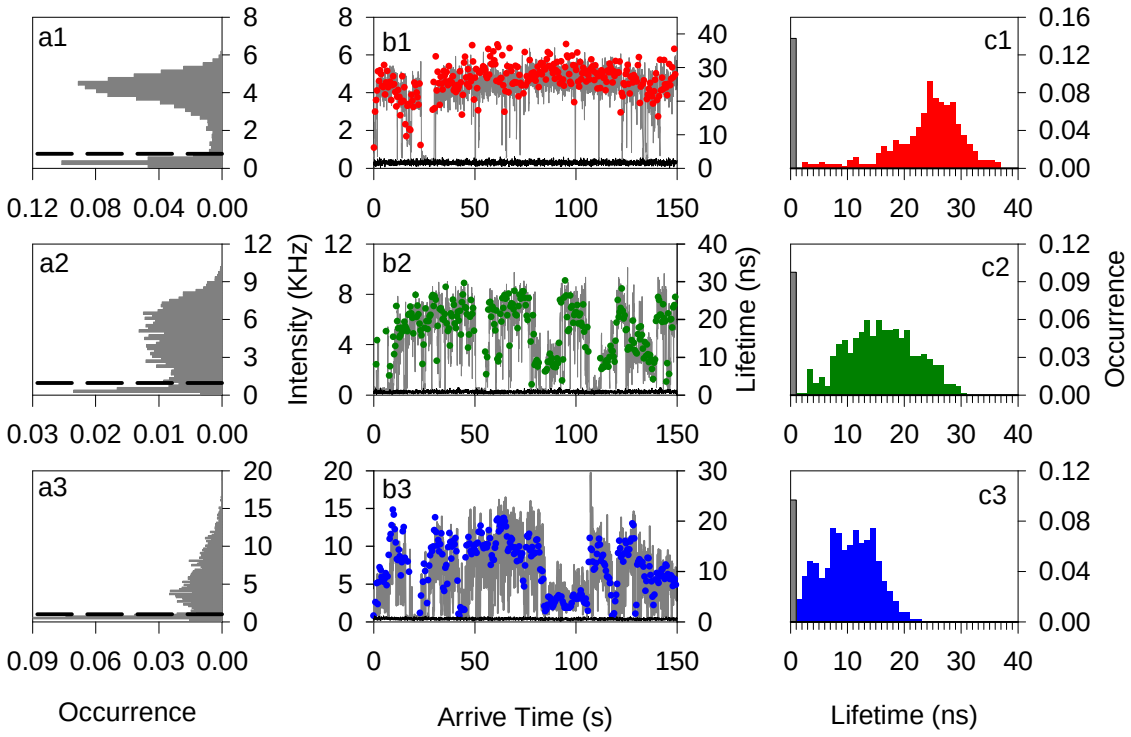

Figure 4.4 Typical fluorescence intensity (gray line) and lifetime (circles) trajectories (bi) and histograms of fluorescence intensity (with a 0.2 KHz bin) (ai) and lifetime (ci) of a representative single QD or QD-PTZ complex from each sample (i=1-3 for samples 1- 3, respectively). Black dashed lines in ai) indicate the threshold separating the on- and off- states. The black lines in bi) are the background emission level in this measurement. Gray bars in ci) indicates the occurrence of states with emission intensity at the background level, whose lifetime is estimated to be smaller than 0.5 ns.

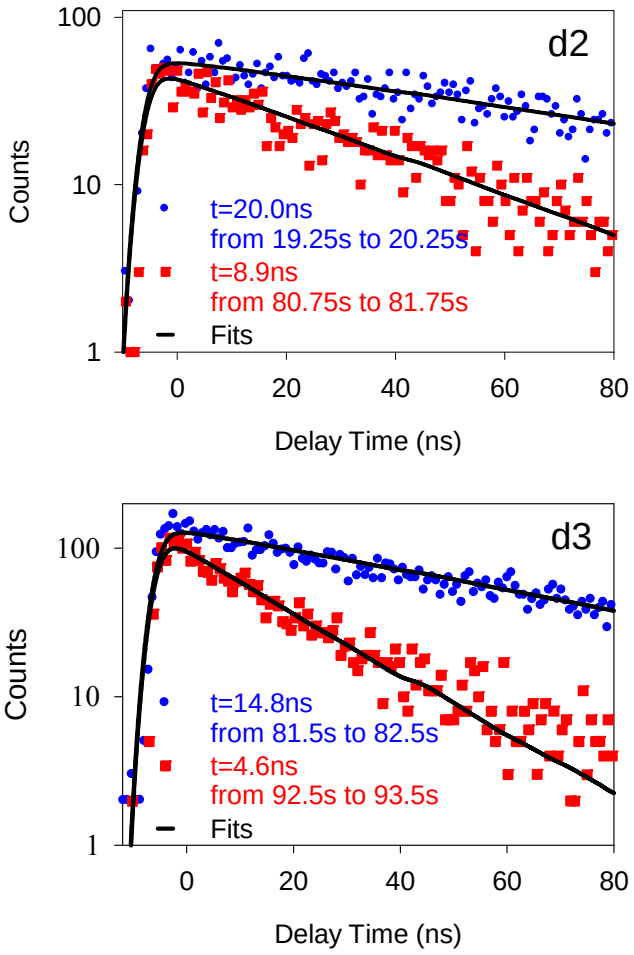

Figure 4.5 Typical fluorescence decay curves for single QD-PTZ complexes

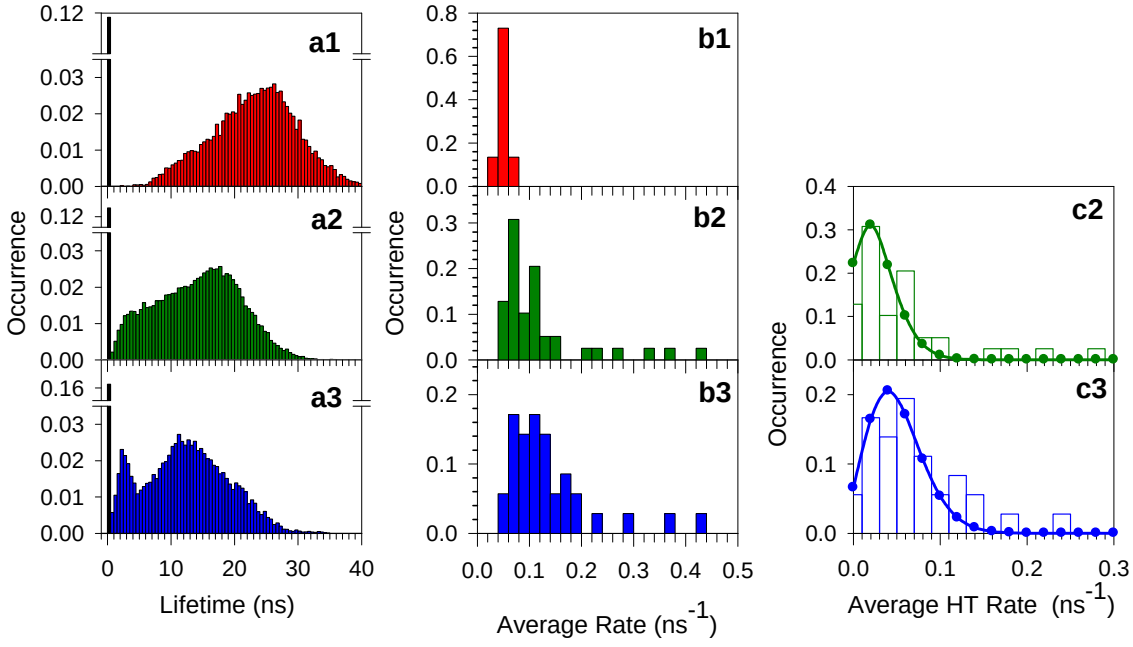

Figure 4.6 Histograms of total fluorescence lifetime distributions (ai), average total decay rates (bi) and average hole transfer rates (ci) for samples i (=1, 2, 3). Histograms of total lifetime distributions were constructed by summing up the lifetime distributions of all QDs in each sample. Black bars indicate the occurrence of low fluorescence intensity points along the trajectories, for which the lifetimes have been assumed to be 0.5 ns. The solid dots (connected by lines) in panels c2 and c3 are fits according to equation 4.1 with fitting parameters listed in Table 4.1.

The total lifetime histograms constructed from 40, 50 and 50 QDs from samples **1**, **2** and **3**, respectively, are shown in Figure 4.6a. With increasing PTZ to QD ratios, the distribution of the "on" state lifetimes shifts to the shorter lifetime region. This behavior is similar to what was observed in single QD-molecular electron acceptor complexes, in which the increase in exciton decay rate (due to electron transfer process) caused a decrease of the average on-state lifetime.[29,31] Similarly, in QD-PTZ complexes, hole transfer from the valence band of QDs to the HOMO of PTZ molecules results in the reduction of exciton lifetime, as shown by the ensemble averaged measurement. On the single QD-PTZ level, this leads the observed shift of the on-state lifetime distribution to the shorter lifetime. For each QD and QD-PTZ complexes, an average exciton decay, defined as the inverse of the average on-state lifetime of each particle along its trajectory, was computed, from which histograms of average decay rates were constructed for each sample. As can be seen in Figure 4.6b, the free QDs show relatively small variation of average decay rates between different QDs. The variation becomes bigger in QD-PTZ complexes. Because of the relatively narrow distribution of the average intrinsic decay rate (k_0) of free QDs, the average HT rates for each QD-PTZ complexes can be calculated by subtracting k_0 from the total decay rate k. As shown in Figure 4c, compared to sample 2, the distribution of

average HT rates shifts to higher values in sample 3, consistent with the higher PTZ-to-QD ratio in this sample.

The distributions of the average HT rates are broad and asymmetric, showing a long tail in the high HT rate side. Similar asymmetric distribution of average ET rates was observed previously in QD-PTZ complexes.[31] We have shown previously that in QD-molecular acceptor complexes prepared by self-assembly, the Poisson distribution of the number of adsorbates on the QD leads to Poisson distributions of average ET rates and fluctuations in single QD-adsobrate complexes and non-exponential ensemble-averaged fluorescence decay kinetics.[29,31] For the same reason, the number of adsorbed PTZs should also obey the Poisson distribution in the QD-PTZ complexes studied here.[20] Following this model, we assume that the number (*n)* of adsorbed PTZ molecule per QD obeys a Poisson distribution.[20,69,70] In *n*:1 PTZ-QD complexes, the average, k_n, and standard deviation, SD_n, of HT rates are given by $k_n = nk_1$ and $SD_n = nSD_1$, respectively, where k_1 and SD_1 denote the average and standard deviation of HT rates in the 1:1 PTZ-QD complexes. It can be shown that in a sample with an average PTZ-to-QD ratio of *m*, the probability distribution of the average HT rates of single PTZ-QD complexes is given by: [29,31]

$$p(m;k_n) = \frac{m^{\left(\frac{k_n}{k_1}\right)} e^{-m}}{\left(\frac{k_n}{k_1}\right)!} \qquad (4.1)$$

The total distribution of HT rates measured in an ensemble of single QD-PTZ complexes is:

$$p(k_{HT}) = \sum_{n=1}^{\infty} \frac{m^n e^{-m}}{n!} \cdot \frac{1}{\sqrt{2\pi}(n \cdot SD_1)} e^{-\frac{(k_{HT} - nk_1)^2}{2(n \cdot SD_1)^2}} + e^{-m}\delta(k_{HT}) \qquad (4.2)$$

Here the last term represents the contribution of free QDs (without adsorbates) in the PTZ-QD samples. In the ensemble averaged fluorescence measurement, the distributions of HT rates from the individual PTZ-QD complexes are not explicitly measured and only the average fluorescence decay of all QDs is monitored. This ensemble-averaged fluorescence decay can be expressed as a sum of all single QD decays: [29,31]

$$[S(t)] = [S(0)]\left[\int_0^{\infty} p(k_{HT}) e^{-k_{HT}t} dk_{HT}\right] \cdot f_{Free}(t) \qquad (4.3)$$

Here *[S(t)] and [S(0)]* are the population of excited QDs at time *t* and 0, respectively. $f_{Free}(t)$ is the fluorescence decay of free QDs, which is independently measured and fitted.

The data shown in Figures 4.6c and 4.2a are fitted simultaneously by equations 4.1 and 4.3, respectively. The same k_1 and SD_1 values are used for all samples, but the *m* values are allowed to change to reflect different average ratios in these samples. The histograms in Figure 4.6c were binned to reflect the value of k_1. This model leads to satisfactory fit to the data, as shown in Figures 4.6c and 4.2a, and the fitting parameters, *m,* k_1 *and* SD_1*,* are listed in Table 4.1.

Table 4.1 Fitting parameters for the distributions of the average HT rates in single PTZ-QD complexes (Figure 4.4b) and the ensemble averaged fluorescence decay of PTZ-QD complexes (Figure 4.1c) according to equations 4.1-4.3. k_1 and SD_1 are the

average and standard deviation, respectively, of the HT rate in 1:1 PTZ-QD complexes; *m* is the average PTZ-to-QD ratio of the sample.

Single QD-PTZ fluorescence decay				Ensemble-averaged fluorescence decay	
k_1 (ns^{-1})	SD_1 (ns^{-1})	Sample #	m	Sample #	m
0.02	0.03	2	1.4	B	2.8
		3	2.5	C	3.4

The HT rate in the 1:1 complexe is $2x10^{-7}$ s^{-1} (correspond to a HT time of 50 ns). Our previous study showed that the hole transfer time in the 1:1 CdSe/PTZ complex is around 2.5 ns.[20] In the current system, the observed hole transfer rate is 20 times slower and it can be attributed to the retardation of HT rate by the multiple layers of insulating ZnS shells on CdSe core.[71] From the average intrinsic decay rate of $5x10^{-7}$ s^{-1}, a hole transfer quantum yield of 29% in 1:1 PTZ-QD complexes can be estimated. This yield increases in complexes with more adsorbed PTZ molecules.

4.2.3 Blinking Dynamics in Single QD-PTZ Complexes

To examine the effect of the hole transfer process on the statistics of the single QD blinking dynamics, we have calculated the probability densities *P(t)* of a QD in the on- or off- states for a duration time of *t* according to eq. 4.[33,48,52,53,56-58]

$$P_i(t) = \frac{N_i(t)}{N_{i,total}} \times \frac{1}{\Delta t_{avg}} \quad (i = \text{on or off}) \qquad (4.4)$$

Here, *N(t)* is the number of on- or off- events with duration time of *t*, N_{total} is the total number of on- or off- events, and Δt_{avg} is the average of the time intervals to the

preceding and subsequent events. Recent studies have shown that the on- and off-time statistics can depend on the choice of threshold that separates the on- and off-states.[67,72-75] We have constructed on- and off- probability distributions using a thresholds of 0.6, 0.9, and 1.2 KHz, corresponding to the count rates at the background level plus 3, 6 and 9 standard deviations, respectively. As shown in Figure 4.7, within this range of threshold values, the on- and off- probability distributions have negligible dependence on the choice of thresholds. We have chosen a threshold level of 0.9 KHz.

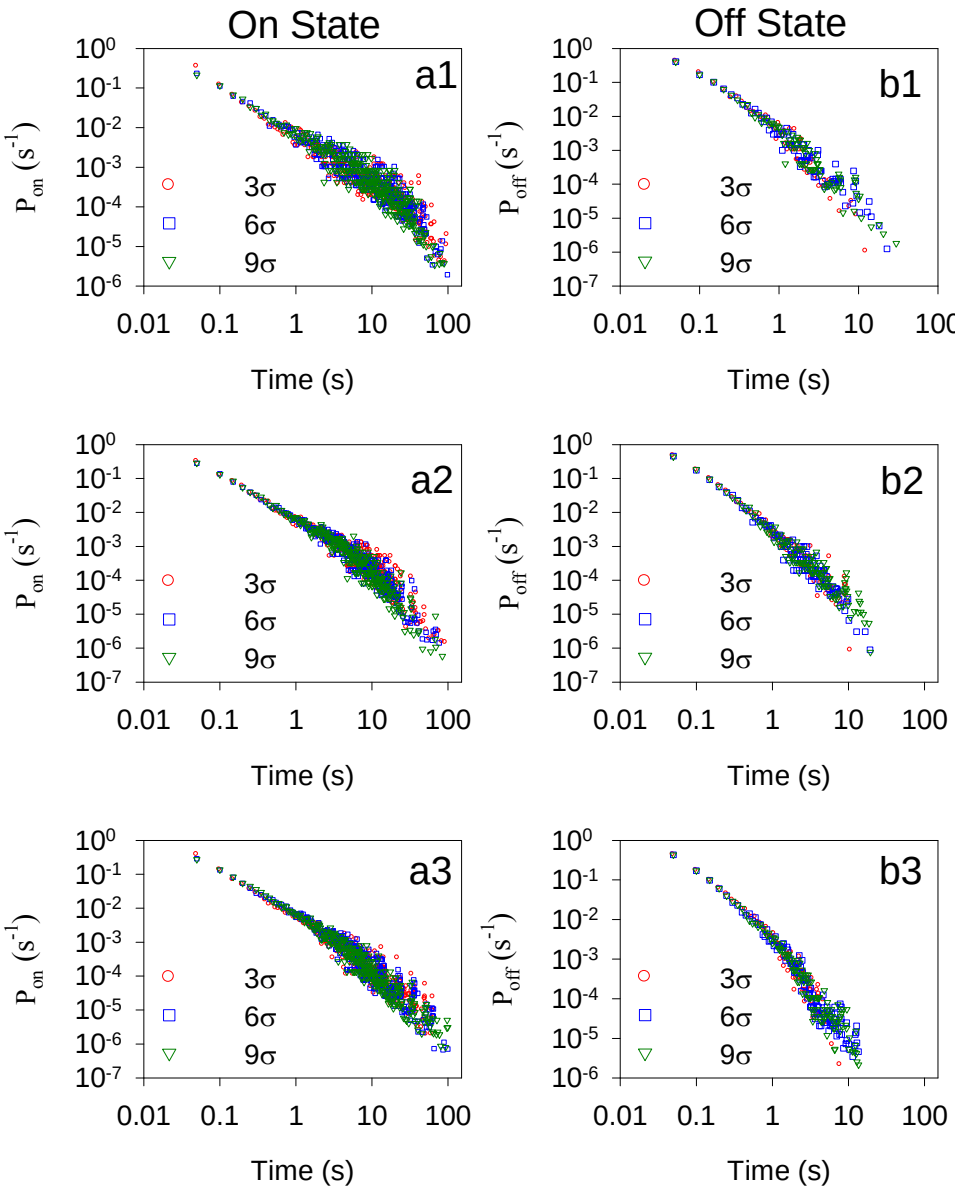

Figure 4.7 On- and off- state probability distributions constructed with different on/off threshold values. No significant difference exists in either on- or off- state probability distributions among different threshold levels.

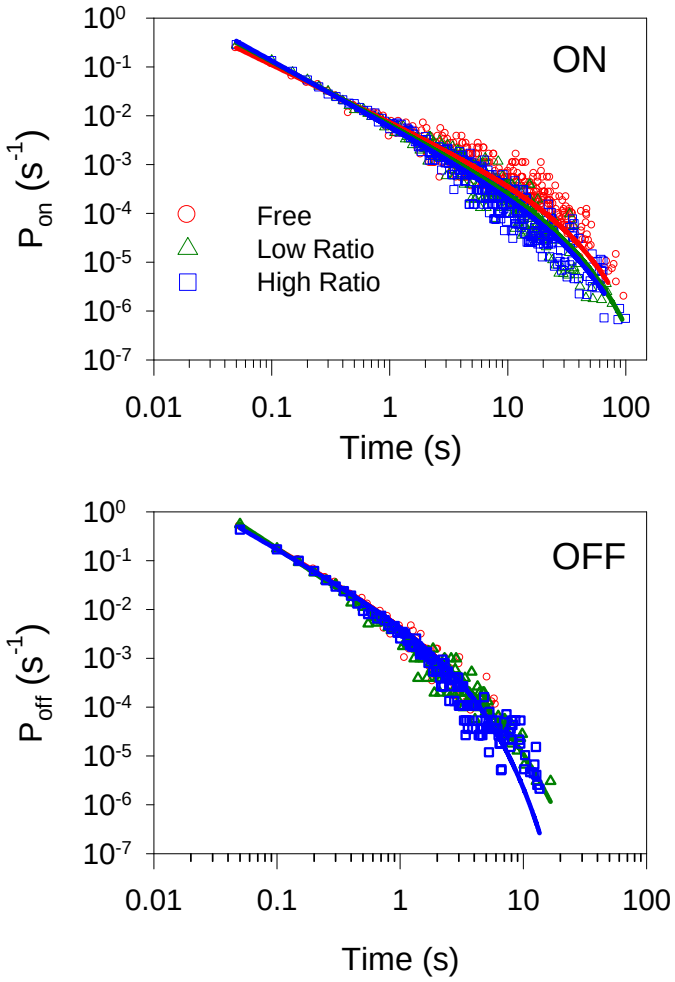

Figure 4.8 Probability density distributions of (a) on states (P_{on}) and (b) off states (P_{off}) as a function of on (off) time intervals, constructed from 40 free QDs from sample 1 (red circle), 50 complexes from sample 2 (green triangle) and 50 complexes from sample 3 (blue square). The solid lines are the best fits according to equation (4.5).

As shown in Figure 4.8, both $P_{on}(t)$ and $P_{off}(t)$ for single QDs from samples **1**, **2** and **3** show power law distributions at short times but deviate from this behavior at

longer times, similar to results reported for free QDs and QD-electron acceptor complexes. These *P(t)* distributions can be fit by a truncated power law: [33,48,52,53,56-58]

$$P_i(t) = B_i t^{-\alpha_i} \exp(-\Gamma_i t) \quad (i = \text{on or off}) \qquad (4.5)$$

where B is the amplitude, α is the power law exponent, and Γ is the saturation rate. The fitting parameters are listed in Table 4.2. The probabilities of "on" time and "off" time in QD-PTZ complexes remain similar to bare QD and do not change significantly with PTZ-to-QD ratios. This indicates that the hole transfer process does not significantly affect the occurrence and the probability density distributions of the on and off states in QD-PTZ complexes within the limited time range (0.1 to 100 s for on-state and 0.1 – 10 s for off-state) probed in this experiment. This observation is different from QD-molecular electron acceptor complexes, where the possibilities of long "on" ("off") and short "off" ("on") events deceases (increases) with molecule-to-QD ratios (or electron transfer rates).[29,31]

Table 4.2 Fitting parameters of $P_{on}(t)$ and $P_{off}(t)$ for single QDs from samples 1, 2 and 3.

Sample #	α_{on}	$1/\Gamma_{on}$(s)	α_{off}	$1/\Gamma_{off}$(s)
1	1.17±0.04	27±3	1.5±0.2	2.2±0.1
2	1.28±0.03	28±3	1.6±0.1	4.4±0.3
3	1.34±0.04	29±3	1.2±0.1	2.2±0.1

A closer inspection of the total lifetime histograms in Figure 4.6a shows a significant increase in states with lifetime between 1 and 5 ns in QD-PTZ complexes compared to free QDs. These states, often labeled as "grey states",[38,40,59,76,77] fall between the high intensity region of the off-states distribution and the low intensity of the on-states distribution. The increase of grey states affect both the on- and off- states, which may account for the lack of changes in the probability distributions of on- and off- states in the presence of the HT pathway.

4.2.4 A Model Explaining the HT Dynamics and Blinking Dynamics in QD-PTZ Complexes

The experimental findings of the single QD-PTZ complex studies are the following: 1) The HT process shortens the average lifetime of the on states; and 2) The presence of a HT pathway does not significantly alter the occurrence of off-states. Instead, it increases the probability of "grey" states with lifetimes between 1-5 ns. To account for effect of the hole acceptor on the dynamics of single QDs, we propose a model for various states and their inter-conversion processes in the QD-PTZ complexes. As shown in Figure 4.9, when a neutral QD is excited from the ground state (**1**), an on state (**1***) is generated, which can relax to state **1** by intrinsic radiative or nonradiative relaxation with a total decay rate of approximately 10^8-10^7 s^{-1}. As the QD cycles between the excitation and emission processes, there is a chance for the excited electron to be transferred to trap states in or near the QD (with rate constant k_{on}), thus forming the off state (state **2**). The emission quantum yield for QDs in state **2** is at or near the background level because optical excitation of state **2** generates a positive trion which relaxes *via* a rapid non-radiative Auger recombination process (not shown).[66] When the trapped electron recombines with the positively charged QD

(rate constant k_{off}), state **1** is regenerated. These states and rate constants for their inter-conversion are assumed to be the same in free QDs and QD-PTZ complexes.

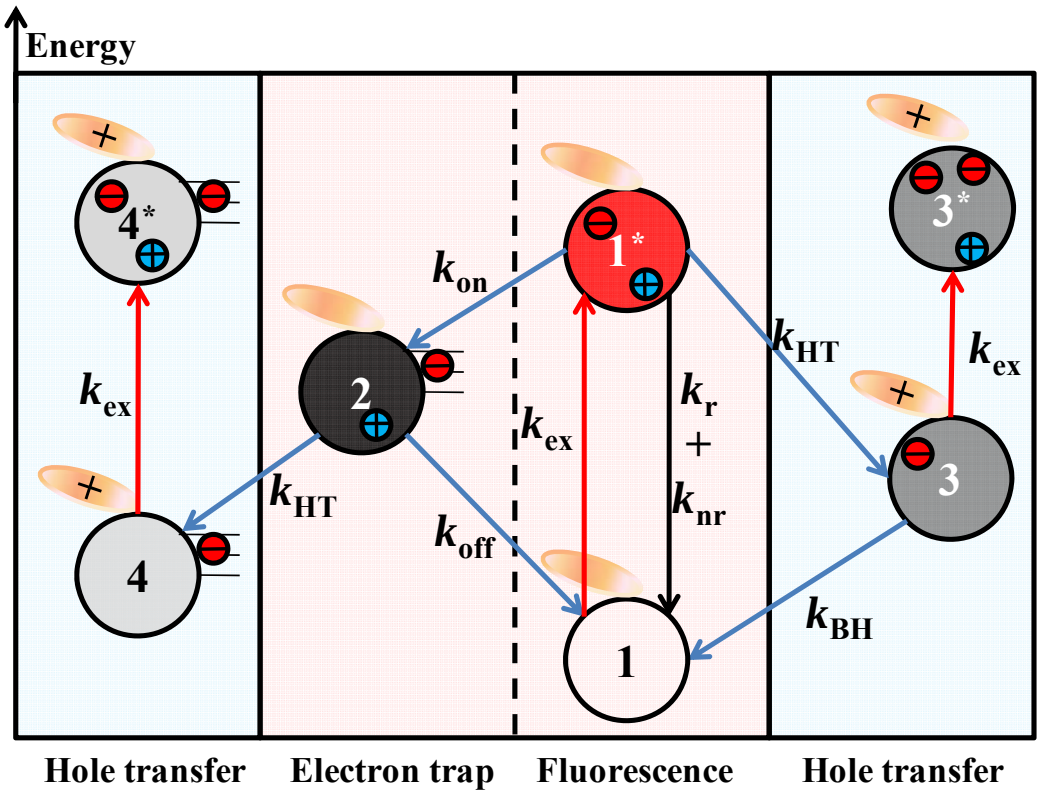

Figure 4.9 Possible states and charge transfer processes in QD-PTZ complexes. On state **1** and **1*** are the ground and excited states of the neutral QD-PTZ complex. k_{ex} is the excitation rate of QDs and k_r and k_{nr} are intrinsic raidative and nonradiative decay rates of QDs. Electron ionization or transfer to trap state converts (with rate constant k_{on}) **1*** to state **2** (off-state), which can convert back (with rate constant k_{off}) to the on-state by charge recombination. In the presence of hole acceptors, two additional pathways are created. **1*** can be quenched by hole transfer to the hole acceptor (with rate constant k_{HT}), forming state **3**. State **3** is a grey state because upon its excitation a negative trion is generated inside the QD, which has a low but detectable emission quantum yield. Hole transfer from the off-state (**2**) generates state **4**, which should be emissive.

The presence of hole acceptors creates two additional states and pathways for their inter-conversion. Hole transfer process from the excited neutral QD (state **1***) generates a charge separated state (state **3**) consisting of a PTZ cation and a negatively charged QD with a conduction band electron. Excitation of **3** generates a negative trion state in the QD, similar to the one studied by Jha and Sionnest.[78] These authors show that trions in CdSe/CdS QDs with core diameter around 4 nm has a total lifetime of the 0.7 - 1.5 ns and a radiative decay rate of 10^8 s^{-1}, which should have weak but detectable emissions under single QD conditions. Therefore, we attribute this charge separated state (**3**) to the grey state. This state can relax back to the ground state (**1**) by transferring the electron from the QD to oxidized PTZ (i.e. the charge recombination process), with a rate constant of $10^6 \sim 10^7$ s^{-1} as determined by the TA kinetics shown in Figure 4.2b. The TA data also show that the charge separated state has a highly dispersive decay process, with a small but non-negligible probability for existing beyond 6 microseconds (the longest time measured in the transient study). Thus, it is possible that the increased probability of grey states observed in the experiment can be attributed to the charge separated state (with negatively charged QDs) generated by the hole transfer process.

The presence of the hole acceptor is also expected to remove the hole in the dark state (**2**), converting to state **4**, which is a neutral QD with adsorbed PTZ cation and a trapped electron on the QD surface. This state should be emissive upon excitation, and, therefore, this process should alter the fate of the dark state and the distribution of the off-state probability density. However, as shown in Figure 4.8, the on- and off-state distributions have not been significantly changed in the current system. The reason for this is unclear. We tentatively attribute this to the competing effects of the hole acceptors on the off-state distribution of QDs. On one hand, it can remove the

off-state (**2**) by transferring the hole to the acceptors, reducing the off-state probabilities. On the other hand, it can quench the excited QDs, generating the charge separated state (**3**). As discussed above, this grey state has low emission quantum yield and can increase the probability of the off-states. Another possibility is that the hole in the dark state may also be trapped and cannot be effectively removed by PTZ because of reduced electronic coupling strength and driving force.[79] A trapped hole should have a reduced wave function overlap with the PTZ, decreasing the electronic coupling strength for HT. As shown in Figure 4.2c, the driving force for transferring the 1S hole to the PTZ is estimated to be ~ 0.3 eV. Trapping the hole to defect states over 0.3 eV above the valence band would make it energetically not favorable for transferring to PTZ.

It is interesting to compare the effect of electron and hole acceptors on the dynamics of single QDs. While both pathways shorten the exciton lifetime and lead the reduced average on-state lifetime of the QDs, they have different effects on the blinking dynamics of QDs. In QD - electron acceptor complexes, the electron transfer process leaves a hole in the QD, which increases the probability of grey and off-states.[29] However, unlike the hole acceptor, the electron acceptor cannot remove the hole in the dark state. Therefore, the net effect of the electron acceptor is to increase the off-state probability densities in the QD-acceptor complexes, leading to a correlated electron-transfer and QD blinking dynamics.

4.3 Summary

In summary, photoinduced hole transfer dynamics from single QDs to adsorbed phenothiazine molecules have been studied by single QD fluorescence spectroscopy. The hole transfer process was independently verified by ensemble-averaged transient

absorption and fluorescence decay measurements. Single QD-PTZ complexes show fluctuation of fluorescence intensity and lifetime similar to those in free QDs. The hole transfer process shortens the lifetimes of on-states in the QD-hole acceptor complexes. There is a broad distribution of average hole transfer rates in different complexes, likely reflecting the distribution in the PTZ-to-QD ratio in the samples. Both the distributions of average hole transfer rates in single QD-PTZ complexes and ensemble average fluorescence decay kinetics can be fit by a kinetics model that assumes a Poisson distribution of adsorbed PTZ molecules per QD, from which an average HT time of 50 ns in the 1:1 PTZ-QD complex was obtained. Unlike the correlated electron transfer and blinking dynamics observed in QD-electron acceptor complexes, the hole acceptors do not significantly alter the on- and off- state probability density distributions in the QD-PTZ complexes. Instead, it increases the probability of weakly emissive grey states. We attribute this to two competing effects of the hole acceptors. On one hand, the HT process generates a negatively charged QD, increasing the probability of grey- and off- states. On the other hand, the hole acceptor can remove the hole in the off-state, reducing the probability of observing this state.

Reference

(1) Pattantyus-Abraham, A. G.; Kramer, I. J.; Barkhouse, A. R.; Wang, X.; Konstantatos, G.; Debnath, R.; Levina, L.; Raabe, I.; Nazeeruddin, M. K.; Gratzel, M.; Sargent, E. H. *Acs Nano* **2010**, *4*, 3374.

(2) Sambur, J. B.; Novet, T.; Parkinson, B. A. *Science (Washington, DC, United States)* **2010**, *330*, 63.

(3) Huynh, W. U.; Dittmer, J. J.; Alivisatos, A. P. *Science* **2002**, *295*, 2425.

(4) Robel, I.; Subramanian, V.; Kuno, M.; Kamat, P. V. *J. Am. Chem. Soc.* **2006**, *128*, 2385.

(5) Kamat, P. *J. Phys. Chem. C* **2008**, *112*, 18737.

(6) Kamat, P. V.; Tvrdy, K.; Baker, D. R.; Radich, J. G. *Chemical Reviews* **2010**, *110*, 6664.

(7) Tisdale, W. A.; Williams, K. J.; Timp, B. A.; Norris, D. J.; Aydil, E. S.; Zhu, X.-Y. *Science (Washington, DC, United States)* **2010**, *328*, 1543.

(8) Boulesbaa, A.; Issac, A.; Stockwell, D.; Huang, Z.; Huang, J.; Guo, J.; Lian, T. *J. Am. Chem, Soc.* **2007**, *129*, 15132.

(9) Huang, J.; Stockwell, D.; Huang, Z.; Mohler, D. L.; Lian, T. *J. Am. Chem. Soc.* **2008**, *130*, 5632.

(10) Rossetti, R.; Beck, S. M.; Brus, L. E. *J. Am. Chem. Soc.* **1984**, *106*, 980.

(11) Rossetti, R.; Brus, L. E. *J. Phys. Chem.* **1986**, *90*, 558.

(12) Ramsden, J. J.; Gratzel, M. *Chem. Phys. Lett.* **1986**, *132*, 269.

(13) Henglein, A. *Pure & Appl. Chem.* **1984**, *56*, 1215.

(14) Logunov, S.; Green, T.; Marguet, S.; El-Sayed, M. A. *J. Phys. Chem. A* **1998**, *102*, 5652.

(15) Burda, C.; Green, T. C.; Link, S.; El-Sayed, M. A. *J. Phys. Chem. B* **1999**, *103*, 1783.

(16) Kamat, P. V.; Dimitrijevic, N. M.; Fessenden, R. W. *Journal of Physical Chemistry* **1987**, *91*, 396.

(17) Blackburn, J. L.; Selmarten, D. C.; Nozik, A. J. *J. Phys. Chem. B* **2003**, *107*, 14154.

(18) Robel, I.; Kuno, M.; Kamat, P. V. *J. Am. Chem. Soc.* **2007**, *129*, 4136.

(19) Spanhel, l.; Weller, H.; Henglein, A. *J. Am. Chem. Soc.* **1987**, *109*, 6632.

(20) Huang, J.; Huang, Z.; Jin, S.; Lian, T. *J. Phys. Chem. C* **2008**, *112*, 19734.

(21) Sharma, S. N.; Pillai, Z. S.; Kamat, P. V. *J. Phys. Chem. B* **2003**, *107*, 10088.

(22) Landes, C. F.; Burda, C.; Braun, M.; El-Sayed, M. A. *J. Phys. Chem. B.* **2001**, *105*, 2981.

(23) Landes, C. F.; Braun, M.; El-Sayed, M. A. *J. Phys. Chem. B* **2001**, *105*, 10554.

(24) Guyot-Sionnest, P. *Structure and Bonding (Berlin, Germany)* **2005**, *118*, 59.

(25) Issac, A.; Jin, S.; Lian, T. *J. Am. Chem. Soc.* **2008**, *130*, 11280.

(26) Cui, S.-C.; Tachikawa, T.; Fujitsuka, M.; Majima, T. *J. Phys. Chem. C* **2008**, *112*, 19625.

(27) Jin, S.; Lian, T. *Nano Letters* **2009**, *9*, 2448.

(28) Jin, S.; Song, N.; Lian, T. *Acs Nano* **2010**, *4*, 1545.

(29) Jin, S.; Hsiang, J.-C.; Zhu, H.; Song, N.; Dickson, R. M.; Lian, T. *Chemical Science* **2010**, *1*, 519.

(30) Cui, S.-C.; Tachikawa, T.; Fujitsuka, M.; Majima, T. *The Journal of Physical Chemistry C* **2011**, *115*, 1824.

(31) Song, N.; Zhu, H.; Jin, S.; Zhan, W.; Lian, T. *Acs Nano* **2011**, *5*, 613.

(32) Nirmal, M.; Dabbousi, B. O.; Bawendi, M. G.; Macklin, J. J.; Trautman, J. K.; Harris, T. D.; Brus, L. E. *Nature* **1996**, *383*, 802.

(33) Shimizu, K. T.; Neuhauser, R. G.; Leatherdale, C. A.; Empedocles, S. A.; Woo, W. K.; Bawendi, M. G. *Phys. Rev. B* **2001**, *63*, 205316/1.

(34) Krauss, T. D.; O'Brien, S.; Brus, L. E. *Journal of Physical Chemistry B* **2001**, *105*, 1725.

(35) Empedocles, S.; Bawendi, M. *Acc. Chem. Res.* **1999**, *32*, 389.

(36) Shimizu, K. T.; Woo, W. K.; Fisher, B. R.; Eisler, H. J.; Bawendi, M. G. *Physical Review Letters* **2002**, *89*, 117401/1.

(37) Chen, Y.; Vela, J.; Htoon, H.; Casson, J. L.; Werder, D. J.; Bussian, D. A.; Klimov, V. I.; Hollingsworth, J. A. *J. Am. Chem. Soc.* **2008**, *130*, 5026.

(38) Mahler, B.; Spinicelli, P.; Buil, S.; Quelin, X.; Hermier, J.-P.; Dubertret, B. *Nature Materials* **2008**, *7*, 659.

(39) Hohng, S.; Ha, T. *Journal of the American Chemical Society* **2004**, *126*, 1324.

(40) Wang, X.; Ren, X.; Kahen, K.; Hahn, M. A.; Rajeswaran, M.; Maccagnano-Zacher, S.; Silcox, J.; Cragg, G. E.; Efros, A. L.; Krauss, T. D. *Nat.* **2009**, *459*, 686.

(41) Odoi, M. Y.; Hammer, N. I.; Early, K. T.; McCarthy, K. D.; Tangirala, R.; Emrick, T.; Barnes, M. D. *Nano Letters* **2007**, *7*, 2769.

(42) Hammer, N. I.; Early, K. T.; Sill, K.; Odoi, M. Y.; Emrick, T.; Barnes, M. D. *J. Phys. Chem. B* **2006**, *110*, 14167.

(43) Ray, K.; Badugu, R.; Lakowicz, J. R. *Journal of the American Chemical Society* **2006**, *128*, 8998.

(44) Fomenko, V.; Nesbitt, D. J. *Nano Lett.* **2008**, *8*, 287.

(45) Efros, A. L.; Rosen, M. *Physical Review Letters* **1997**, *78*, 1110.

(46) Fisher, B. R.; Eisler, H.-J.; Stott, N. E.; Bawendi, M. G. *J. Phys. Chem. B* **2004**, *108*, 143.

(47) Issac, A.; von Borczyskowski, C.; Cichos, F. *Phys.l Rev. B* **2005**, *71*, 161302/1.

(48) Kuno, M.; Fromm, D. P.; Johnson, S. T.; Gallagher, A.; Nesbitt, D. J. *Phys. Rev. B:* **2003**, *67*, 125304/1.

(49) Montiel, D.; Yang, H. *J. Phys. Chem. A* **2008**, *112*, 9352.

(50) Peterson, J. J.; Nesbitt, D. J. *Nano Lett.* **2009**, *9*, 338.

(51) Schlegel, G.; Bohnenberger, J.; Potapova, I.; Mews, A. *Phys. Rev. Lett.*. **2002**, *88*, 137401.

(52) Tang, J.; Marcus, R. A. *J. Chem. Phys.* **2006**, *125*, 044703/1.

(53) Verberk, R.; van Oijen, A. M.; Orrit, M. *Phys. Rev. B* **2002**, *66*, 233202/1.

(54) Zhang, K.; Chang, H.; Fu, A.; Alivisatos, A. P.; Yang, H. *Nano Letters* **2006**, *6*, 843.

(55) Kuno, M.; Fromm, D. P.; Hamann, H. F.; Gallagher, A.; Nesbitt, D. J. *J. Chem. Phys.* **2001**, *115*, 1028.

(56) Tang, J.; Marcus, R. A. *J. Chem. Phys.* **2005**, *123*, 204511/1.

(57) Tang, J.; Marcus, R. A. *Phys. Rev. Lett.* **2005**, *95*, 107401/1.

(58) Tang, J.; Marcus, R. A. *J. Chem. Phys.* **2005**, *123*, 054704/1.

(59) Hollingsworth, J. A.; Vela, J.; Chen, Y.; Htoon, H.; Klimov, V. I.; Casson, A. R. *Proceedings of SPIE* **2009**, *7189*, 718904/1.

(60) Ito, Y.; Matsuda, K.; Kanemitsu, Y. *Physical Review B* **2007**, *75*, 033309.

(61) Bharadwaj, P.; Novotny, L. *Nano Lett.* **2011**, *11*, 2137.

(62) Brus, L. *J. Chem. Phys.* **1983**, *79*, 5566.

(63) Brus, L. E. *J. Chem. Phys.* **1984**, *80*, 4403.

(64) Tierney, M. T.; Grinstaff, M. W. *J. Org. Chem.* **2000**, *65*, 5355.

(65) Klimov, V. I. *Ann. Rev. Phys. Chem.* **2007**, *58*, 635.

(66) Klimov, V. I.; Mikhailovsky, A. A.; McBranch, D. W.; Leatherdale, C. A.; Bawendi, M. G. *Science* **2000**, *287*, 1011.

(67) Drndic, M.; Wang, S.; Querner, C.; Fischbein, M. D.; Willis, L.; Novikov, D. S.; Crouch, C. H. *Nano Lett* **2008**, *8*, 4020.

(68) Drndic, M.; Wang, S.; Querner, C.; Dadosh, T.; Crouch, C. H.; Novikov, D. S. *Nature Communications* **2011**, *2*.

(69) Boulesbaa, A.; Huang, Z.; Wu, D.; Lian, T. *Journal of Physical Chemistry C* **2010**, *114*, 962.

(70) Pons, T.; Medintz, I. L.; Wang, X.; English, D. S.; Mattoussi, H. *J. Am. Chem. Soc.* **2006**, *128*, 15324.

(71) Zhu, H.; Song, N.; Lian, T. *Journal of the American Chemical Society* **2010**, *132*, 15038.

(72) Tang, J.; Lee, D. H.; Yuan, C. T.; Tachiya, M. *Appl Phys Lett* **2009**, *95*.

(73) Frantsuzov, P. A.; Volkan-Kacso, S.; Janko, B. *Phys Rev Lett* **2009**, *103*.

(74) Tang, J.; Lee, D. H.; Yeh, Y. C.; Yuan, C. T. *J Chem Phys* **2009**, *131*.

(75) Crouch, C. H.; Sauter, O.; Wu, X. H.; Purcell, R.; Querner, C.; Drndic, M.; Pelton, M. *Nano Lett* **2010**, *10*, 1692.

(76) Ma, X.; Tan, H.; Kipp, T.; Mews, A. *Nano Lett.* **2010**, *10*, 4166.

(77) Gómez, D. E.; van Embden, J.; Mulvaney, P.; Fernée, M. J.; Rubinsztein-Dunlop, H. *ACS Nano* **2009**, *3*, 2281.

(78) Jha, P. P.; Guyot-Sionnest, P. *Acs Nano* **2009**, *3*, 1011.

(79) Marcus, R. A.; Sutin, N. *Biochem. Biophys. Acta* **1985**, *811*, 265.

Chapter 5 Photoinduced Charging of QDs on Sb Doped SnO_2 Film

5.1 Introduction

QDs have been studied extensively and been shown promising in various applications due to their outstanding properties.[1-12] In QD based optoelectronic devices, transparent conducting electrodes (TCE), such as Sn doped In_2O_3 (ITO), F doped SnO_2 (FTO) and Sb doped SnO_2 (ATO) are widely utilized as both windows for light illumination or collection and electrical contact for carrier extraction or injection.[7,8,10,13-16] The presence of TCE and applied external bias was shown to affect exciton dynamics of QDs and modify the single QD blinking dynamics.[17-24] The mechanism by which these changes occur remains unclear.

Because the conduction band edge of the oxide materials (such as In_2O_3, SnO_2) is lower than QDs (e.g. CdSe), electron transfer from excited QDs to the TCE film is energetically favored and has been observed previously.[22,25-28] As shown in Figure 5.2, n-doping of these materials raises the Fermi levels near their conduction band edges, which also opens up a possible hole transfer pathway for excited QDs in addition to quenching by electron transfer. Furthermore, for QDs on n-doped TCE films, the equilibration of their Fermi levels likely leads to the charging of QDs, which can also affect the exciton dynamics. Previously, we and others reported shortened fluorescence lifetime and suppressed blinking for QDs on n-type ITO films.[19,22,23] We speculated that QDs are charged on n-type ITO due to the electron filling of trapped states and the shortened QD fluorescence lifetime can be attributed to Auger

recombination of charged QDs and/or exciton quenching by hole transfer to the trapped electron or to ITO.[22] Charging of QDs on an ITO substrate has been experimentally confirmed and quantitatively studied by electrostatic force microscopy by Barnes and coworkers.[23] Guyot-Sionnest and coworkers proposed that for QDs in contact with ITO, energy transfer between QDs and ITO film is responsible for the observed shortened fluorescence lifetime for the QDs.[19] The same study also reported that electrochemical charging of QDs to form negative trions (exiton + electron) leads to shortened fluorescence lifetime. More recently, electrochemical charging induced change of QD lifetime and blinking behavior has also been reported and the role of mid-gap trap state was proposed by Klimov and coworkers.[21] These previous studies are based on fluorescence measurements, which by themselves are not sufficient to differentiate the multiple pathways (electron transfer, hole transfer, energy transfer and Auger recombination) for exciton quenching at the QD/ITO interface.

In an effort to reveal the mechanism of exciton quenching at QD/electrode interface, we report here a study of QDs on ATO film. Unlike ITO, the absorption of ATO at QD emission range is negligible (see Figure 5.1), which precludes energy transfer from excited QDs to substrate as a competitive exciton quenching pathway. In addition to QD fluorescence, the ability to prepare nanoporous ATO films also enables the study of the same system by transient absorption spectroscopy. By combining transient absorption measurement and single QD fluorescence dynamics and comparing QDs on sapphire window and nanoporous SnO_2 and ATO films, we show that for QDs on n-type ATO film charging induced fast Auger relaxation is the dominant excited state quenching pathway. The effect of QD charging on single QD blinking behavior is also examined.

5.2 Experiment and Discussion

5.2.1 Ultrafast Transient Absorption and Ensemble Averaged Fluorescence Measurements

To examine the interaction mechanism of excited QDs on SnO_2 and ATO films, which were prepared according to the procedure discussed in Chapter 2, combined ensemble-averaged transient absorption (TA) and fluorescence (FL) decay measurements were conducted for QDs on sapphire windows, SnO_2 films and ATO films. The samples were prepared by dropping water-soluble QDs with carboxylate group (-COOH) terminated capping ligands on flat sapphire windows, nanocrystalline SnO_2 and ATO films and drying the films in air. For QD-SnO_2 and QD-ATO samples, prior to drying, the films were washed with water for 30 seconds to remove any weakly bound QDs. Because of nanoporous structure of SnO_2 and ATO film, a sufficiently high loading for ensemble TA measurement can be obtained after several drop casting-washing cycles. For QDs on sapphire windows, several cycles of QDs drop-casting without washing were needed. Steady-state UV-Vis absorption and emission spectra of the core/multi-shell ($CdSe/CdS_{3ML}ZnCdS_{2ML}ZnS_{2ML}$) quantum dots used in this study are shown in Figure 5.1. It has to be noted that energy transfer between QDs cannot be precluded for QDs on Sapphire windows where closely packed QDs layers likely formed on the flat surface.[29,30] This can be seen from the fluorescence lifetime differences between the ensemble-averaged and single QD measurements (see below). Nevertheless, even with energy transfer, the lifetime of QDs on sapphire is still longer than those on other substrates. The trend of ensemble averaged lifetimes for QDs on different substrates remains comparable; meanwhile, the comparison between TA and FL decay for each sample will not be affected since

inter-QDs energy transfer contribute to TA and FL decay kinetics in the same way. Therefore, we will identify the quenching mechanism based on qualitative comparison by ensemble averaged measurements and extract the precise quenching rate and its distribution based on single QDs measurement later where energy transfer between QDs can be avoided.

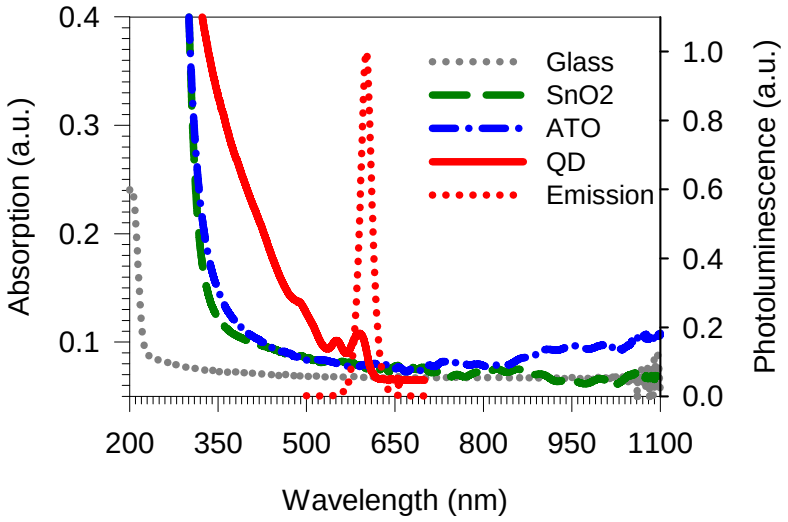

Figure 5.1 Absorption spectra (left y-axis) of a QD colloidal solution (QD, red solid line), sapphire window (grey line), and SnO_2 film (dark green line) and ATO film (blue line) prepared on sapphire windows. Also shown in red dashed line is the emission spectrum of QDs (right y-axis).

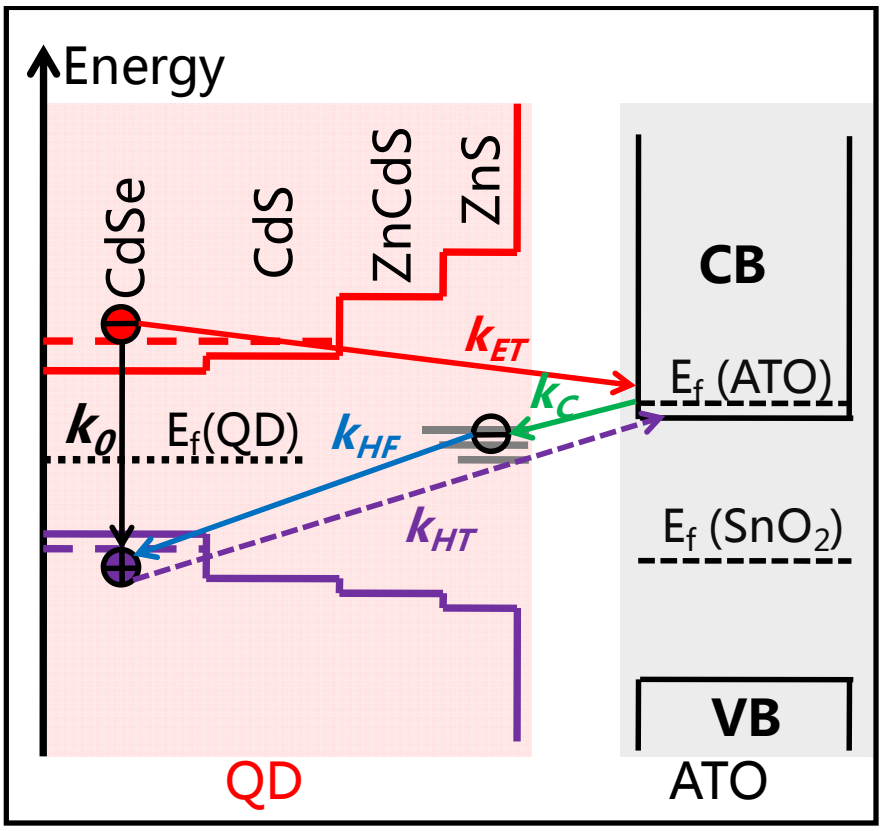

Figure 5.2 Schematic diagram of relative energy levels of QD and- SnO_2/ATO and possible exciton quenching pathways (see the main text).

From the first exciton peak position (585nm) of the QDs, the conduction and valence band levels can be estimated to be -0.90 and 1.03 V (*vs.* SCE) according to the method reported in previous studies.[22,31] The flat band potential of SnO_2 conduction band edge (E_c) depends on pH and ranges from +0.067V (SCE) at pH= 0 to -0.35V at pH= 7.[32,33] In this study, the conduction band edge is assumed to be -0.35V because all measurements are done at neutral conditions. Based on the SnO_2 bandgap (3.6 eV), the valance band edge (E_v) and Fermi level (E_f) are deduced to be +3.25 V and +1.4 V.[33,34] As can be seen, the Fermi level of SnO_2 lays below the valance band edge of QDs. In ATO films (10% Sb in mole fraction), prepared according to published method,[33,34] the Fermi level is shifted to ~ 0.09 V above the E_c of SnO_2, i.e. -0.44 V, making it an n-type semiconductor.[33,34] The Fermi level is

calculated from the free electron density estimated from the Plasmon band absorption of the ATO in the near- to mid- IR range.[33,34] From the relative energy levels of QDs, SnO_2, and ATO (Figure 5.2), the excitons in QDs on SnO_2/ATO surface can decay by e-h recombination (with the rate k_0), electron transfer from conduction band (CB) of QD to the CB of SnO_2/ATO (k_{ET}) and/or hole transfer from valence band of the QD to the filled electron levels in ATO (k_{HT}).

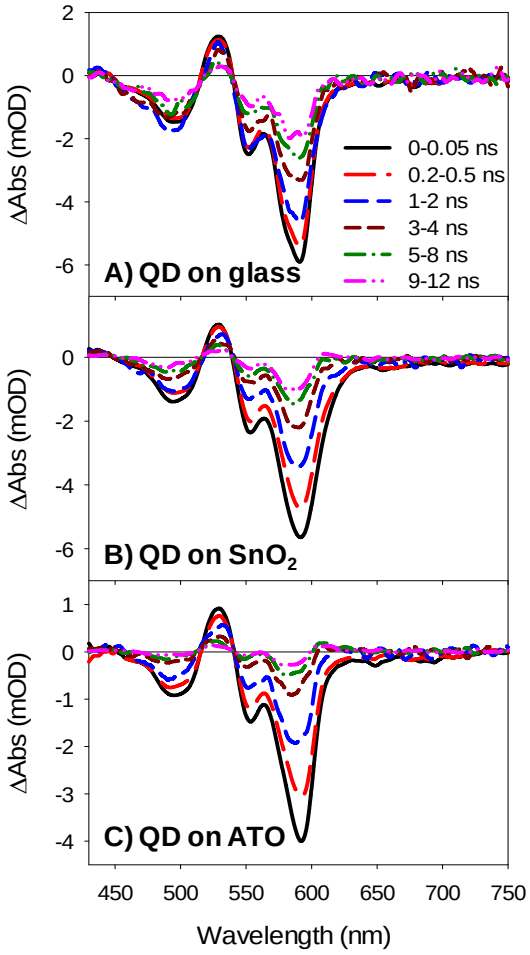

Figure 5.3 TA spectra (0-12 ns) of QDs on glass (A), SnO_2 (B) and ATO (C).

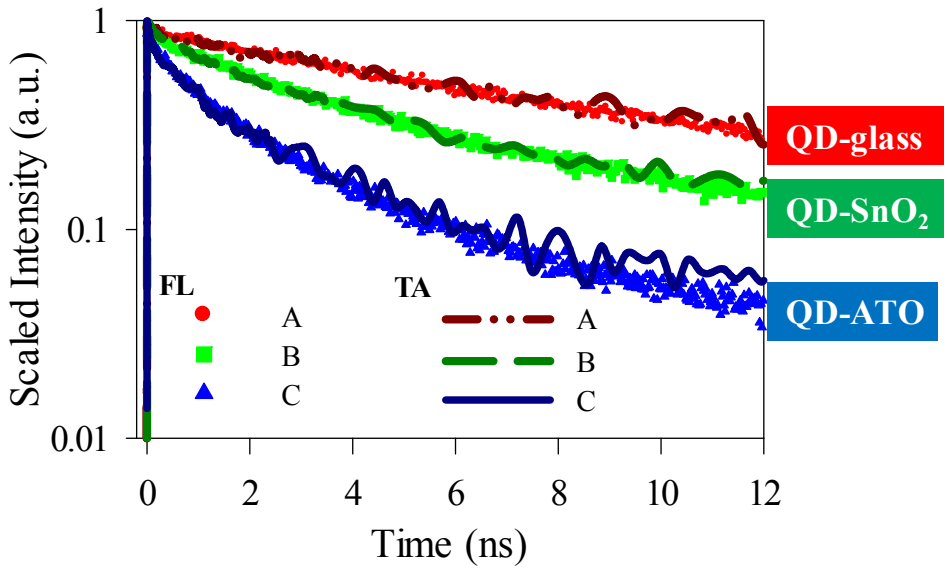

Figure 5.4 Transient absorption (TA, solid lines) kinetics at 605 nm (averaged from 601 to 610 nm) and ensemble averaged fluorescence (FL, open symbols) decays of QDs deposited on sapphire windows (A), SnO_2 films (B), and ATO films (C). The TA kinetics have been inverted and normalized for better comparison with the FL kinetics.

The transient spectra of these samples recorded after 400 nm excitation are shown in Figure 5.3. These spectra show the characteristic bleach of the 1S exciton band and the shift of higher energy exicton bands result from the formation of 1S exciton. The decay of these features are different in these samples, which can be better seen in the comparison of the 1S exciton TA bleach recovery and FL decay kinetics for these three samples shown in Figure 5.4. For better comparison, the 1S bleach recovery kinetics from TA measurement have been inverted and normalized. The TA and FL decay kinetics agree reasonably well with each other for all samples and show a trend of decreasing decay rates: ATO > SnO_2 > glass. A biexponential fit of fluorescence decay kinetics yields the amplitude-weighted-average lifetime of QDs on glass (~ 13 ns), SnO_2 (~ 7 ns) and ATO (~ 2 ns). Because the 1S exciton transient bleach signal in CdSe QDs is dominated by the state filling of 1S conduction band electron level with

negligible contribution from the holes,[35,36] the bleach recovery kinetics reflects the 1S CB electron depopulation process. The decay rate of the 1S electron TA signal is $k_{TA} = k_{ET} + k_{e\text{-}h}$, where k_{ET} is 1S electron transfer/trapping rate and $k_{e\text{-}h}$ is the rate of direct 1S electron-1S hole recombination. Because the transient fluorescence intensity is proportional to the concentration of both 1S electrons and holes, the fluorescence decay kinetics is given by: $k_{FL} = k_{ET} + k_{e\text{-}h} + k_{HT} = k_{TA} + k_{HT}$, where k_{HT} is hole transfer/trapping rate.[31,37]

As we can see in Figure 5.4, a good agreement between excited state TA and FL decay kinetics is observed, which rules out the hole transfer/trapping/filling process for these samples. Therefore, it is the 1S electron depopulation process ($k_{ET} + k_{e\text{-}h}$) that leads to the different excited state decay dynamics on different substrates. Compared with QDs on glass, interfacial electron transfer (with rate k_{ET}) from QDs to SnO_2/ATO leads to the faster 1S electron decay on these films, consistent with previous report for QDs on SnO_2 films.[25-27] According to our previous study of adsorbed dye molecules on ATO films, the forward electron transfer rate (k_{ET}) from excited dye molecules to ATO doesn't depend on Sb doping level because conduction band states mostly remain unoccupied even after Sb doping and the electron accepting state density are similar for SnO_2 and ATO.[33] Therefore, it is reasonable to assume similar k_{ET} rates from QDs to SnO_2 and ATO. However, the 1S electron decays much faster for QDs on ATO film than on SnO_2, suggesting additional electron depopulation pathway for QD-ATO sample. Additional internal/surface electron trapping process for QDs on ATO compared with SnO_2 is unlikely since Sb doping in SnO_2 should not introduce electron trapping states on QDs. Then the faster electron decay component on ATO films (compared with SnO_2) can only be attributed to faster electron-hole recombination process ($k_{e\text{-}h}$), which contains intrinsic radiative decay rate (k_0) and any

additional nonradiative decay rate. The former can be assumed to be unchanged on these three substrates, so the significantly faster electron decay rate indicates additional nonradiative electron-hole recombination pathway for QDs on ATO than on SnO_2.

Similar to the charging of QDs on ITO,[22,23] it is likely that QDs on ATO are also negatively charged and we attribute the faster nonradiative electron-hole recombination process to Auger recombination in charged QDs. It is well established now that exciton lifetime (several ns) in charged CdSe/CdS and CdSe/ZnS core shell QDs are shortened due to fast Auger recombination.[18,38-40] In addition to the quantum confined electron/hole states, the nanometer-size QDs also have surface states located within the bandgap due to large surface-to-volume ratio and incomplete surface passivation.[41-44] Since the Fermi level in ATO is raised from 1.4 V in SnO_2 (below the QDs valance band edge) to -0.44 V (1.5 V above the QDs valance band edge and 0.5 V below the conduction band edge) after Sb doping, it is reasonable to assume that Fermi level equilibration should lead to electron transfer from ATO to empty surface mid-gap states in QDs, forming negatively charged QDs.[22,23] Therefore, photoexcited electron-hole pairs recombine nonradiatively by transferring energy to surface state electron which gets excited to higher energy level and then relaxes back. Similar electron charging of midgap surface states in QDs has been achieved before by applying electrochemical potentials[21,45-49] and reducing agents.[50] In these charged QDs, the QD excitons decays through nonradiative multicarrier Auger recombination which has a much shorter lifetime than radiative recombination.[18,22,38-40,51] In principle, the photoexcited holes can also recombine nonradiatively with the surface trap electrons on QDs through hole filling (k_{HF}) process.[21,49] However, this process should lead to faster FL decay kinetics (than TA), which is not observed experimentally

(Figure 5.4), suggesting it is much slower compared with the Auger recombination rate (~ 2 ns). The slow hole transfer/filling is likely caused by slower hole tunneling from the CdSe core through the thick CdS/CdZnS/ZnS shell.[52,53]

5.2.2 Single Quantum Dot Exciton Quenching Dynamics

To facilitate the comparison of ensemble averaged and single QD studies, the same batch of QDs, SnO_2 films and ATO films were used, although the films were prepared on different substrates: glass cover slips and sapphire windows for single QD and ensemble averaged measurements, respectively. To prepare samples for single QD measurement, a QD solution with a diluted concentration of ~ 10 pM was spin-coated on bare glass cover slips (sample 1), SnO_2 film (sample 2) and ATO films (sample 3). About fifty single QDs from each sample were detected and each QD was followed for about 5 minutes, during which permanent photo-bleach was not observed. Two times were associated with each detected photon: the delay time (relative to excitation pulse) and the arrival time (relative to the start of the experiment) were recorded. For each QD, the intensity trace was constructed by counting the number of photons within 50 ms arrival time windows. The delay time histograms of photons within 1 s arrival time windows were constructed and fitted to single exponential decay functions (by nonlinear least square fit) to obtain the lifetime trajectory.

Typical intensity and lifetime trajectories of single QDs on different substrates are shown in panels a1-3 (1-glass, 2- SnO_2, 3-ATO) of Figure 5.5. The lifetime trajectory follows the intensity trajectory for QDs in all three samples, consistent with the reported positive correlation between the fluorescence intensity and lifetime of single QDs.[54-64] We attribute all points with intensity within six standard deviation of the background level to off-states and all points with higher intensities to on-states. It is

clear that QDs in sample 2 and 3 have more short on-states compared with the QD in sample 1 and less long on-states. The histograms of exciton decay rate (calculated as the inverse of lifetime) distributions for a representative single QD are plotted in Figure 5.5 b1-3. For off states, their exciton decay rates cannot be accurately determined because of limited photon numbers and are estimated to be bigger than 2 ns^{-1}. The occurrence of these states are counted and plotted with grey bars in the rate histograms as shown in Figure 5.5b. In sample 1 (Figure 5.5 b1), the QD has a typical intrinsic exciton decay rate centered at 0.03 ns^{-1}. For sample 2 (b2), the QD shows a faster exciton quenching compared with QDs on glass and the peak of the distribution shifts to 0.08 ns^{-1}. QDs deposited on ATO films (b3), have the fastest exciton decay rates, centering at ~ 0.4 ns^{-1}.

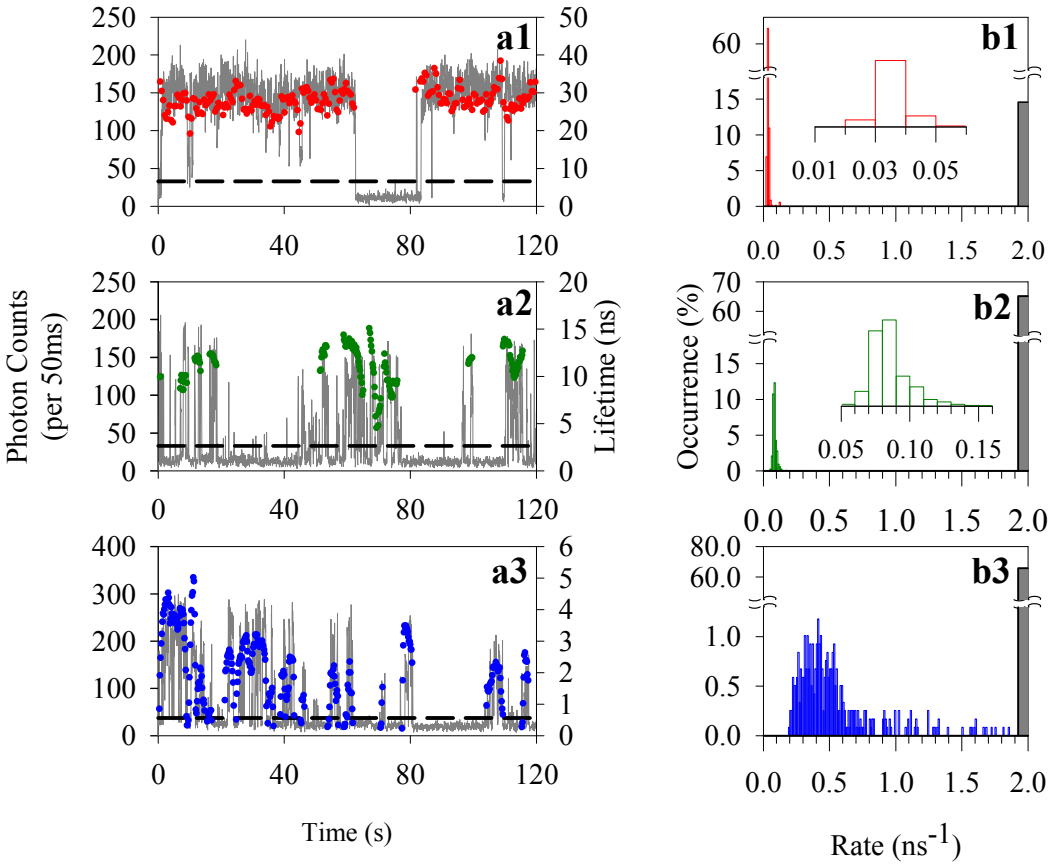

Figure 5.5 (a_i) Typical fluorescence intensity (gray line) and lifetime (color dots) trajectories and (b_i) histograms of exciton decay rates of a representative single QD from each sample (i=1-3 for samples 1- 3). Black dashed lines in a_i) indicate the threshold separating the on- and off- states. Grey bars in b_i) indicates the occurrence of states with emission intensity at the background level, which has exciton quenching (EQ) rates bigger than $2ns^{-1}$ and lifetimes shorter than 0.5 ns).

Similar distributions were observed in different QDs and total histograms of 50 single QD on-state exciton decay rate distributions are shown in Figure 5.6 a1-3. The exciton fluorescence decay rates in QDs increase from sample 1 to 3, consistent with the observed trend in ensemble averaged measurements (Figure 5.4). The average intrinsic exciton decay rate of QDs on glass is estimated to be 0.045 ns^{-1} (Figure 5.6 a1). The distributions of fluorescence intensity of QDs in the three samples are plotted in Figure 5.7. The "on-state" fluorescence intensity of QDs on SnO_2 and ATO films are shifted to the low level and the "off-state" probability increases due to electron transfer from QDs to SnO_2 film and additional exciton quenching by Auger relaxation on ATO film.

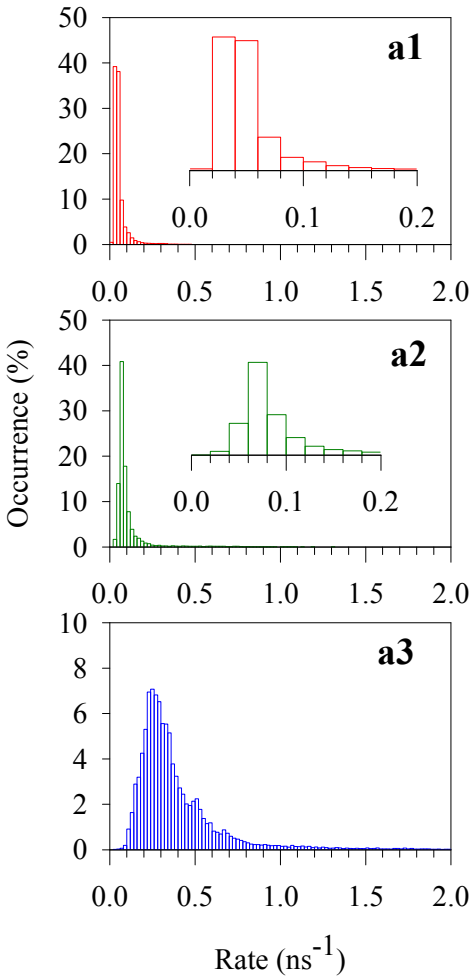

Figure 5.6 Total histograms of on state exciton decay rates for all (50) measured single QDs in sample i (1-3).

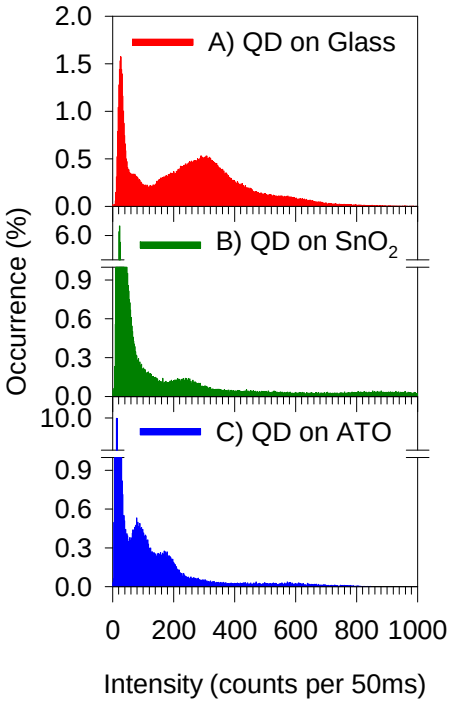

Figure 5.7 Intensity histograms of QDs on glass (A), SnO_2 (B), and ATO (C).

The exciton quenching rate (k_{EQ}) in SnO_2 or ATO is calculated by the subtraction of exciton decay rate on SnO_2 (a2) and ATO (a3) by the intrinsic average exciton decay rate on glass (0.045 ns^{-1}). The histograms of the calculated k_{EQ} distributions for QDs on SnO_2 and ATO are depicted in Figure 5.8 a2 and a3, respectively. The average k_{EQ} in sample 2 is ~ 0.04 ns^{-1}, which represents the average electron transfer rate from QDs to SnO_2. This average electron transfer rate is much slower than the previously reported value for core-only CdSe QDs on SnO_2;[27] it can be attributed to the existence of ZnS shells on the core/shell QDs which act as electron tunneling barrier to reduce the surface electron density.[52,53] The average EQ rate in sample 3 (QD-ATO) is estimated to be 0.25 ns^{-1}, which contains electron transfer rate (~ 0.04 ns^{-1} obtained from QD-SnO_2) and Auger recombination rate (~ 0.21 ns^{-1} after subtraction). This Auger recombination rate is slower than the negative trion decay in electrochemically charged CdSe/CdS QDs,[18] suggesting the Auger recombination

process involving trapped electron is slower. The full width at half maximum of k_{EQ} distribution ($FWHM_{EQ}$) in Figure 5.8a is 0.05 ns^{-1} on SnO_2 and 0.22 ns^{-1} on ATO, as listed in Table 5.1, indicating much higher heterogeneity in the exciton quenching dynamics for QDs on ATO.

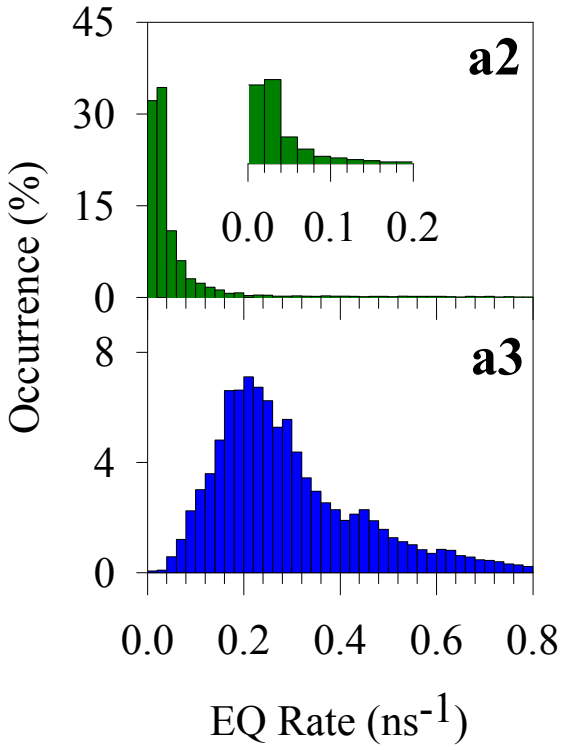

Figure 5.8 Histograms of total exciton quenching rates.

To reveal the origin of the heterogeneity of exciton quenching rates in sample 2 and 3, we calculate the average exciton quenching rate ($k_{AEQ,i}$) and associated standard deviation (SD_i) of each QD.[31,56] $k_{AEQ,i}$ is the arithmetic mean of exciton quenching rates averaged over its trajectory. Standard deviation, representing the extent of dynamic fluctuation of EQ rates in single each QD, is defined by the following expression,

$$SD_i = \sqrt{\frac{\sum_{j=1}^{N}\left(k_{EQ,i}(t_j) - \left\langle k_{AEQ,i}\right\rangle\right)^2}{N}} \qquad (5.1)$$

where $k_{EQ,i}$ is the EQ rate at time t_j and the sum is over the whole trajectory. Histograms of $k_{AEQ,i}$ and SD_i for each studied QDi (50 in total) in sample 2 and 3 are plotted in Figure 5.9 b2-3 and c2-3, respectively, and the averaged SD_i over 50 QDs are listed in Table 5.1. The distribution of k_{AEQ} reflects how the average quenching rates differ among QDs, which can be used as rough indicator of "static" heterogeneity. The standard deviation represents how the exciton quenching rates varies with time for each QD, which provides a measure of the dynamic heterogeneity. From Figure 5.9 b2 and b3, the full-width-at-half- maximum (FWHM) of k_{AEQ} distribution ($FWHM_{AEQ}$) are calculated to be 0.02 ns^{-1} for sample 2 and 0.2 ns^{-1} for sample 3 (listed in Table 5.1).

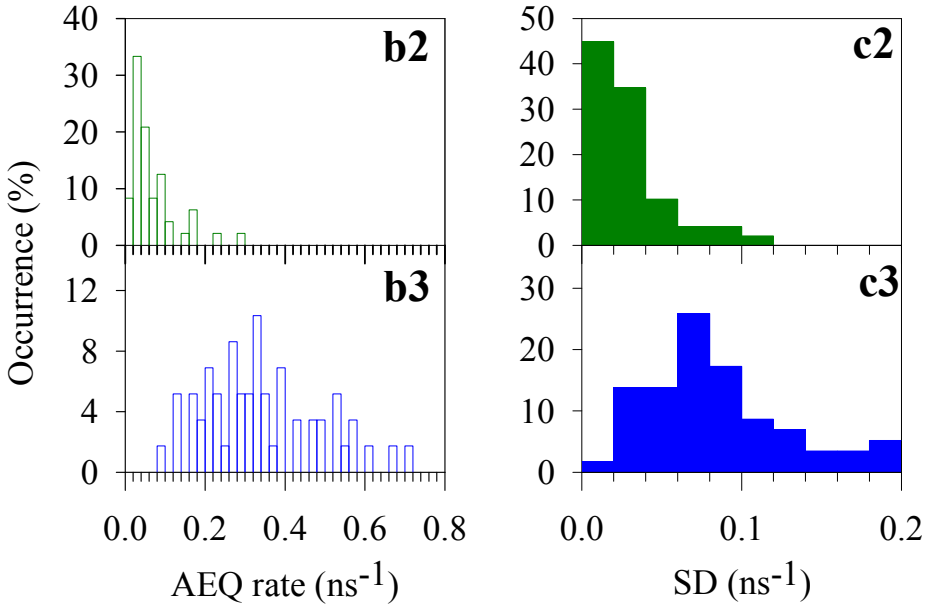

Figure 5.9 Histograms of average exciton decay rates (bi) and standard deviations (ci) for sample 2 and sample 3.

For QDs on SnO_2, $FWHM_{AEQ}$ (0.02 ns^{-1}) is smaller than $FWHM_{EQ}$ (0.05 ns^{-1}) by 0.03 ns^{-1}, a value that is similar to the average SD. This result suggests that the exciton quenching rate for QDs on SnO_2 contains similar contributions of static heterogeneity and dynamic fluctuation. However, for QDs on ATO, $FWHM_{AEQ}$ is ~ 10 fold larger than that on SnO_2 and it is close to $FWHM_{EQ}$, indicating that static heterogeneity dominates the distributions of exciton quenching rates. Because QDs from the same batch are used for the measurements on SnO_2 and ATO films, they should have similar distribution of intrinsic exciton decay rates. On the basis of the ensemble averaged study presented above, we attribute the faster exciton decay rate for QDs on ATO to Auger recombination caused charging of QDs. Therefore, the broad distribution of exciton quenching rates among QDs on ATO can be attributed to the distribution of Auger recombination rates, which likely indicates the heterogeneity of the number of charges and charging sites. Although the nature of surface trap states is still poorly understood, it is reasonable to assume that they are sensitive to surface chemistry and environment and can vary dramatically among QDs.

Table 5.1 Full width at half maxima of exciton quenching rates and average exciton quenching rate and average standard deviations in sample 2 and 3 (calculated from the distributions in Figure 5.8 and 5.9).

Sample #	$FWHM_{EQ}$ (ns^{-1})	$FWHM_{AEQ}$ (ns^{-1})	Average SD (ns^{-1})
2	0.05	0.02	0.03
3	0.22	0.20	0.08

5.2.3 Blinking Dynamics of Single QD-SnO_2 and QD-ATO Complexes

To examine the effect of charging on the statistics of the on- and off- state distributions, we have calculated the probability densities *P(t)* of a QD in the "on" or "off" states for a duration time of *t* according to eq. 2. [59,62,65-69]

$$P_i(t) = \frac{N_i(t)}{N_{i,total}} \times \frac{1}{\Delta t_{avg}} \quad (i = \text{on or off}) \qquad (5.2)$$

Here, *N(t)* is the number of "on" or "off" events with duration time of *t*, N_{total} is the total number of "on" or "off" events, and Δt_{avg} is the average of the time intervals to the preceding and subsequent events.

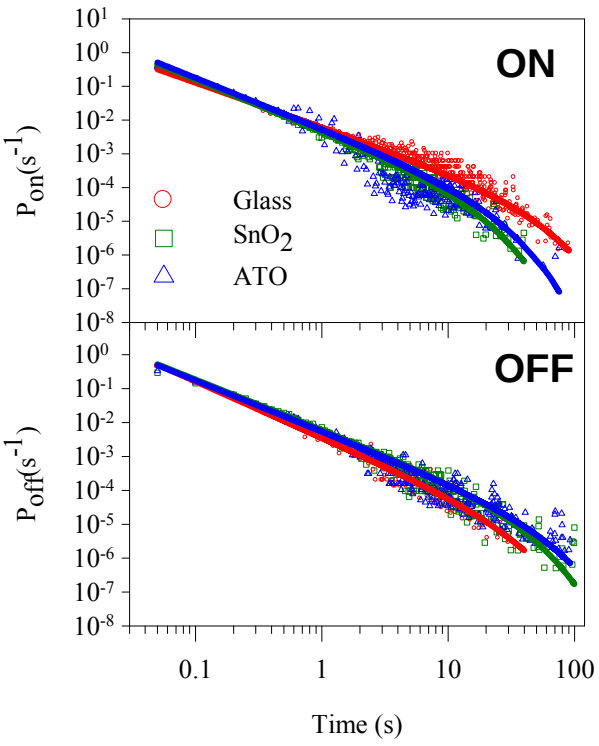

Figure 5.10 Probability density distributions of (a) on states (P_{on}) and (b) off states (P_{off}) as a function of on (off) time intervals, constructed from 50 QDs from sample 1

(red circle), sample 2 (green square) and sample 3 (blue triangle). The solid lines are the best fits according to equation (5.3).

As shown in Figure 5.10, both $P_{on}(t)$ and $P_{off}(t)$ for single QDs from samples **1**, **2** and **3** show power law distributions at short times but deviate from this at longer times, similar to results reported for free QDs and QD-electron acceptor complexes.[59,62,65-69] These *P(t)* distributions can be fit by a truncated power law:

$$P_i(t) = B_i t^{-m_i} \exp(-\Gamma_i t) \quad (i = \text{on or off}) \qquad (5.3)$$

where B is the amplitude, m the power law exponent, and Γ the saturation rate. The fitting parameters are listed in Table 5.2. Noticeable differences between QDs on glass and on SnO_2/ATO are observed: compared to QDs on glass, QDs on SnO_2 have larger m_{on} and Γ_{on} as well as smaller m_{off} and Γ_{off}. This suggests that electron transfer from QDs to SnO_2 reduces probability densities of long on events and increases probability densities of long off events, which is consistent with the findings of previous works.[54-56] For QDs on ATO films, the probabilities of "on" time and "off" time remain similar to QDs on SnO_2 except for slightly decreased Γ_{off}. This indicates that the charging of QDs on ATO does not significantly affect the occurrence and the probability density distributions of the "on" and "off" states compared with SnO_2.

Although the blinking of QD was observed more than 10 years ago, its origin remains an intensely debated subject.[21,70-74] The on/off states of QDs are commonly ascribed to charged/neutral QDs. Once a carrier (electron or hole) is ejected from the QD core to surface traps and surrounding matrix, the QD is charged and much faster (compared with radiative recombination) multicarrier Auger recombination process annihilate the subsequent photoexcited e-h pair nonradiatively, leading to off states

with reduced emission intensity and shortened lifetime.[57,70,71] QDs can return to on-states (and become bright) again when they are neutralized. However, recent observations of biexciton emission (which should have lower emission quantum yield than a positive trion), negative trion emission[17-19] and size independent off state lifetime in single QDs, have led to reexamination of the nature of the off-state.[18,72,73] Many combined electrochemistry and single QD measurements show that negatively charged QDs can still be emissive although with lower emission intensity and lifetime.[17-19,21] Our previous study of QD-hole acceptor complexes shows that negatively charge QDs generated by hole transfer to the acceptor are also emissive, showing an enhanced probability of low emission ("grey") states.[31]

For QDs on ATO, the Fermi level equilibration leads to negatively charged QDs, a condition that is similar to QDs under negative external bias. From the observed exciton quenching rate (0.25 ns^{-1}), the emission quantum yield can be calculated to be 15% assuming the same e-h radiative recombination rate as QDs on glass (0.045 ns^{-1}). The emission from these charged QDs is weaker than neutral QD but still high enough to be observed and attributed to "on" or "grey" state, consistent with the experimental observation. Therefore, compared with QDs on SnO_2, the charging of QDs on ATO, which shortens exciton lifetime due to nonradiative Auger recombination, does not increase the "off" state or decrease the "on" state probability densities. Both the observed lifetime and blinking dynamics of single QDs on ATO are consistent with experimental observations of negatively charged QDs.[17-19,21]

The observed shortened on-state fluorescence lifetime of QDs on ATO is similar to that previously reported for the similar QDs on ITO, suggesting that fast Auger recombination due to negatively charged QD is also a likely quenching mechanism in

the latter. However, the blinking behaviors in these systems are quite different. It has been reported that single QDs in contact with electron-donating molecules or (n-doped) ITO substrates show suppressed blinking dynamics,[22,75] which was attributed to the efficient removal of the extra holes in the off-state by the electrons from molecules or ITO, reducing the off-state probability. According to this model, the different blinking dynamics on ATO and ITO films likely indicates different hole removal rates for QDs on these films. This difference may be caused by the lower free electron density in ATO, which is typically ~ 10 fold or more lower than ITO.[22,34]

Table 5.2 Fitting parameters of $P_{on}\ (t)$ and $P_{off}\ (t)$ for single QDs from samples 1, 2 and 3.

Sample #	m_{on}	$1/\Gamma_{on}$(s)	m_{off}	$1/\Gamma_{off}$(s)
1	1.32±0.04	36.5±4.3	1.65±0.05	25.1±3.9
2	1.52±0.06	12.0±1.5	1.49±0.04	27.4±2.9
3	1.51±0.08	16.4±3.4	1.50±0.07	42.6±3.9

5.3 Summary

The exciton quenching dynamics of core/multi-shell ($CdSe/CdS_{3ML}ZnCdS_{2ML}ZnS_{2ML}$) quantum dots deposited on glass, SnO_2, and ATO films has been studied by transient absorption spectroscopy and ensemble-averaged and single QD fluorescence spectroscopy. The exciton quenching rates on these substrates increases from glass to SnO_2 to ATO. Comparison of ensemble averaged TA and FL decay kinetics show that these kinetics agree with each other, reflecting the decay of the 1S electron population. Compared to QDs on glass, the faster exciton

quenching on SnO_2 is attributed to electron transfer from the excited QDs to SnO_2. Because similar electron transfer rates are expected on SnO_2 and ATO, the faster exiton quenching rate for QDs on ATO suggests additional electron decay pathway and is attributed to fast Auger recombination in charged QDs formed by Fermi level equilibration between QDs and n-doped ATO films. Single QDs on all substrates show correlated fluorescence intensity and emission lifetime, i.e. blinking dynamics. The blinking dynamics of QDs on ATO and SnO_2 are similar, and show similar on and off time probability densities. Compared to QDs on glass, they show decreased probabilities of long on states and increased probabilities of long off states. For QDs on SnO_2, we observe comparable contributions of static and dynamic heterogeneity to the total distribution of exciton quenching rates. On ATO surfaces, the static heterogeneity is greatly increased compared to QDs on SnO_2, indicating a large heterogeneity of Auger recombination rates in charged QDs, which is likely caused by a distribution of the number of charges and/or charging sites on the QD surface.

Reference

(1) Yu, W. W.; Qu, L. H.; Guo, W. Z.; Peng, X. G. *Chem. Mater.* **2003**, *15*, 2854.

(2) Zhu, H.; Song, N.; Lian, T. *J. Am. Chem. Soc.* **2011**, *133*, 8762.

(3) Zhu, H.; Lian, T. *Energy Environ. Sci.* **2012**, *5*, 9406.

(4) Alivisatos, A. P. *Science* **1996**, *271*, 933.

(5) Bruchez Jr, M.; Moronne, M.; Gin, P.; Weiss, S.; Alivisatos, A. *Science* **1998**, *281*, 2013.

(6) Chan, W. C. W.; Nie, S. M. *Science* **1998**, *281*, 2016.

(7) Colvin, V. L.; Schlamp, M. C.; Alivisatos, A. P. *Nature* **1994**, *370*, 354.

(8) Coe, S.; Woo, W.-K.; Bawendi, M.; Bulovic, V. *Nature* **2002**, *420*, 800.

(9) Konstantatos, G.; Howard, I.; Fischer, A.; Hoogland, S.; Clifford, J.; Klem, E.; Levina, L.; Sargent, E. H. *Nature* **2006**, *442*, 180.

(10) Huynh, W. U.; Dittmer, J. J.; Alivisatos, A. P. *Science* **2002**, *295*, 2425.

(11) Robel, I.; Subramanian, V.; Kuno, M.; Kamat, P. V. *J. Am. Chem. Soc.* **2006**, *128*, 2385.

(12) Zhu, H.; Song, N.; Lv, H.; Hill, C. L.; Lian, T. *J. Am. Chem. Soc.* **2012**, *134*, 11701.

(13) Greenham, N. C.; Peng, X.; Alivisatos, A. P. *Phys. Rev. B* **1996**, *54*, 17628.

(14) Klem, E. J. D.; MacNeil, D. D.; Levina, L.; Sargent, E. H. *Adv. Mater.* **2008**, *20*, 3433.

(15) Leschkies, K. S.; Beatty, T. J.; Kang, M. S.; Norris, D. J.; Aydil, E. S. *ACS Nano* **2009**, *3*, 3638.

(16) Rivest, J. B.; Swisher, S. L.; Fong, L.-K.; Zheng, H.; Alivisatos, A. P. *ACS Nano* **2011**, *5*, 3811.

(17) Jha, P. P.; Guyot-Sionnest, P. *J. Phys. Chem. C* **2007**, *111*, 15440.

(18) Jha, P. P.; Guyot-Sionnest, P. *ACS Nano* **2009**, *3*, 1011.

(19) Jha, P. P.; Guyot-Sionnest, P. *J. Phys. Chem. C* **2010**, *114*, 21138.

(20) White, M. A.; Weaver, A. L.; Beaulac, R. m.; Gamelin, D. R. *ACS Nano* **2011**, *5*, 4158.

(21) Galland, C.; Ghosh, Y.; Steinbruck, A.; Sykora, M.; Hollingsworth, J. A.; Klimov, V. I.; Htoon, H. *Nature* **2011**, *479*, 203.

(22) Jin, S.; Song, N.; Lian, T. *ACS Nano* **2010**, *4*, 1545.

(23) Yalcin, S. E.; Yang, B.; Labastide, J. A.; Barnes, M. D. *J. Phys. Chem. C* **2012**, *116*, 15847.

(24) Qin, W.; Guyot-Sionnest, P. *ACS Nano* **2012**.

(25) Leventis, H. C.; O'Mahony, F.; Akhtar, J.; Afzaal, M.; O'Brien, P.; Haque, S. A. *J. Am. Chem. Soc.* **2010**, *132*, 2743.

(26) Pijpers, J. J. H.; Koole, R.; Evers, W. H.; Houtepen, A. J.; Boehme, S.; de Mello Donegá, C.; Vanmaekelbergh, D.; Bonn, M. *J. Phys. Chem. C* **2010**, *114*, 18866.

(27) Tvrdy, K.; Frantsuzov, P. A.; Kamat, P. V. *Proc. Natl. Acad. Sci.* **2011**, *108*, 29.

(28) Hossain, M. A.; Jennings, J. R.; Koh, Z. Y.; Wang, Q. *ACS Nano* **2011**, *5*, 3172.

(29) Crooker, S. A.; Hollingsworth, J. A.; Tretiak, S.; Klimov, V. I. *Phys. Rev. Lett.* **2002**, *89*, 186802.

(30) Kagan, C. R.; Murray, C. B.; Nirmal, M.; Bawendi, M. G. *Phys. Rev. Lett.* **1996**, *76*, 1517.

(31) Song, N.; Zhu, H.; Jin, S.; Lian, T. *ACS Nano* **2011**, *5*, 8750.

(32) Ai, X.; Anderson, N. A.; Guo, J. C.; Lian, T. Q. *J. Phys. Chem. B* **2005**, *109*, 7088.

(33) Guo, J. C.; She, C. X.; Lian, T. Q. *The Journal of Physical Chemistry B* **2005**, *109*, 7095.

(34) Guo, J. C.; She, C. X.; Lian, T. Q. *The Journal of Physical Chemistry C* **2008**, *112*, 4761.

(35) Klimov, V. I. *J. Phys. Chem. B* **2000**, *104*, 6112.

(36) Klimov, V. I. *Annu. Rev. Phys. Chem.* **2007**, *58*, 635.

(37) Knowles, K. E.; McArthur, E. A.; Weiss, E. A. *ACS Nano* **2011**, *5*, 2026.

(38) Gómez, D. E.; van Embden, J.; Mulvaney, P.; Fernée, M. J.; Rubinsztein-Dunlop, H. *ACS Nano* **2009**, *3*, 2281.

(39) Spinicelli, P.; Buil, S.; Quelin, X.; Mahler, B.; Dubertret, B.; Hermier, J. P. *Phys. Rev. Lett.* **2009**, *102*, 136801.

(40) Yalcin, S. E.; Labastide, J. A.; Sowle, D. L.; Barnes, M. D. *Nano Lett.* **2011**, *11*, 4425.

(41) Sercel, P. C.; Efros, A. L.; Rosen, M. *Phys. Rev. Lett.* **1999**, *83*, 2394.

(42) Fu, H.; Zunger, A. *Phys. Rev. B* **1997**, *56*, 1496.

(43) Hässelbarth, A.; Eychmüller, A.; Weller, H. *Chem. Phys. Lett.* **1993**, *203*, 271.

(44) Lifshitz, E.; Dag, I.; Litvitn, I. D.; Hodes, G. *J. Phys. Chem. B* **1998**, *102*, 9245.

(45) Wang, C.; Shim, M.; Guyot-Sionnest, P. *Science* **2001**, *291*, 2390.

(46) Weaver, A. L.; Gamelin, D. R. *J. Am. Chem. Soc.* **2012**, *134*, 6819.

(47) Schäfer, S.; Wang, Z.; Kipp, T.; Mews, A. *Phys. Rev. Lett.* **2011**, *107*, 137403.

(48) Wang, C.; Wehrenberg, B. L.; Woo, C. Y.; Guyot-Sionnest, P. *J. Phys. Chem. B* **2004**, *108*, 9027.

(49) Gooding, A. K.; Gómez, D. E.; Mulvaney, P. *ACS Nano* **2008**, *2*, 669.

(50) Bang, J.; Chon, B.; Won, N.; Nam, J.; Joo, T.; Kim, S. *J. Phys. Chem. C* **2009**, *113*, 6320.

(51) Klimov, V. I.; Mikhailovsky, A. A.; McBranch, D. W.; Leatherdale, C. A.; Bawendi, M. G. *Science* **2000**, *287*, 1011.

(52) Zhu, H.; Song, N.; Lian, T. *J. Am. Chem. Soc.* **2010**, *132*, 15038.

(53) Zhu, H.; Song, N.; Rodríguez-Córdoba, W.; Lian, T. *J. Am. Chem. Soc.* **2012**, *134*, 4250.

(54) Jin, S.; Lian, T. *Nano Lett.* **2009**, *9*, 2448.

(55) Jin, S.; Hsiang, J.-C.; Zhu, H.; Song, N.; Dickson, R. M.; Lian, T. *Chemical Science* **2010**, *1*, 519.

(56) Song, N.; Zhu, H.; Jin, S.; Zhan, W.; Lian, T. *ACS Nano* **2011**, *5*, 613.

(57) Efros, A. L.; Rosen, M. *Phys. Rev. Lett.* **1997**, *78*, 1110.

(58) Schlegel, G.; Bohnenberger, J.; Potapova, I.; Mews, A. *Phys. Rev. Lett.* **2002**, *88*, 137401.

(59) Kuno, M.; Fromm, D. P.; Johnson, S. T.; Gallagher, A.; Nesbitt, D. J. *Phys. Rev. B* **2003**, *67*, 125304.

(60) Fisher, B. R.; Eisler, H. J.; Stott, N. E.; Bawendi, M. G. *J. Phys. Chem. B* **2004**, *108*, 143.

(61) Issac, A.; von Borczyskowski, C.; Cichos, F. *Phys. Rev. B* **2005**, *71*, 161302.

(62) Tang, J.; Marcus, R. A. *J. Chem. Phys.* **2006**, *125*, 044703.

(63) Issac, A.; Jin, S. Y.; Lian, T. Q. *J. Am. Chem. Soc.* **2008**, *130*, 11280.

(64) Montiel, D.; Yang, H. *J. Phys. Chem. A* **2008**, *112*, 9352.

(65) Shimizu, K. T.; Neuhauser, R. G.; Leatherdale, C. A.; Empedocles, S. A.; Woo, W. K.; Bawendi, M. G. *Phys. Rev. B* **2001**, *63*, 205316.

(66) Verberk, R.; van Oijen, A. M.; Orrit, M. *Phys. Rev. B* **2002**, *66*, 233202.

(67) Tang, J.; Marcus, R. A. *J. Chem. Phys.* **2005**, *123*, 204511.

(68) Tang, J.; Marcus, R. A. *Phys. Rev. Lett.* **2005**, *95*, 107401.

(69) Jau, T.; Marcus, R. A. *J. Chem. Phys.* **2005**, *123*, 54704.

(70) Nirmal, M.; Dabbousi, B. O.; Bawendi, M. G.; Macklin, J. J.; Trautman, J. K.; Harris, T. D.; Brus, L. E. *Nature* **1996**, *383*, 802.

(71) Kuno, M.; Fromm, D. P.; Hamann, H. F.; Gallagher, A.; Nesbitt, D. J. *J. Chem. Phys.* **2001**, *115*, 1028.

(72) Rosen, S.; Schwartz, O.; Oron, D. *Phys. Rev. Lett.* **2010**, *104*, 157404.

(73) Zhao, J.; Nair, G.; Fisher, B. R.; Bawendi, M. G. *Phys. Rev. Lett.* **2010**, *104*, 157403.

(74) Frantsuzov, P.; Kuno, M.; Janko, B.; Marcus, R. A. *Nat. Phys.* **2008**, *4*, 519.

(75) Hohng, S.; Ha, T. *J. Am. Chem. Soc.* **2004**, *126*, 1324.

Chapter 6 Charging of Quantum Dots by Sulfide Electrolyte: Implications for Quantum Dot Sensitized Solar Cell

6.1 Introduction

Because of their size tunable properties, versatile surface and interior modification, and low cost solution processing and device integration, QDs have been widely investigated as an alternative to molecular dyes in sensitized solar cell.[1-4] More recently, this interest has been intensified due to the possibility of multiexciton and hot carrier extraction from QDs, which potentially can improve the efficiency of QD sensitized solar cells (QDSSCs).[5-7] The working principle of regenerative type QDSSCs, including charge separation from photoexcited sensitizers, charge transport and collection in regenerative electrolyte or electrodes, and charge recombination processes, possess strong similarities to dye sensitized solar cells (DSSCs) which have been extensively studied in past two decades.[8,9] Therefore, the potential advantages of QDs and the rich background knowledge gained on DSSCs should boost the advancement of QDSSCs. However, the highest solar energy conversion efficiency of QDSSCs has reached only ~ 5% using CdS/CdSe co-sensitized TiO_2,[10,11] significantly inferior to that of DSSC analogue (~ 12%).[12-14] The reason for the rather low efficiencies of QDSSCs is still yet to be understood.[4,15-17]

As a key step, the electron injection efficiency from photoexcited QDs to semiconductor metal oxide (MO) films depends on the competition between electron

transfer process and intrinsic electron relaxation process. Although the interfacial charge transfer process from QDs (such as CdSe) to MO films and the intrinsic carrier relaxation process have been extensively measured with either colloidal solution or dry film samples,[18-21] regenerative electrolyte is present in real QDSSCs to scavenge photoexcited holes and stabilize the devices.[22-25] The effect of redox electrolyte on the photophysical properties of QDs including optical properties and carrier dynamics has been much less studied, but is critical to the performance assessment and device design of QDSSCs.[25] Various electrolytes including iodide,[26] cobalt complexes[17,27] and iron complexes[23] have been developed. To date, sulfide/polysulfide redox couple (-0.45 V *vs*. NHE[23]) still remains as the favorite choice due to appealing device efficiency and durability.[4,25] Kamat's group recently has shown both emission quenching and faster fluorescence decay for CdSe QDs in the presence of Na_2S which were assigned to valance band hole transfer process from photo excited QDs to sulfide.[25] Because fluorescence is sensitive to all possible exciton decay process and any carrier depopulation process (including electron/hole transfer/trapping, Auger recombination) will contribute to fluorescence quenching/decay, it is still not clear how the presence of sulfide electrolyte will affect the photophysical properties of QDs including optical properties and carrier dynamics.

In this study, we employed both steady state and time resolved absorption and fluorescence spectroscopy to investigate the effect of sulfide on CdSe based QDs. To prevent the possible surface corrosion by sulfide which has been reported to form a thin $CdSe_xS_{1-x}$ surface layer on CdSe QDs and complications to the analysis,[25] we use a water soluble type I core/multishell QDs ($CdSe/CdS_{3ML}ZnCdS_{2ML}ZnS_{2ML}$) capped with carboxylic acid functional group in this study. By ensemble averaged absorption and fluorescence results, we found at the presence of sulfide electrolyte, QDs actually

are charged and instead of slow single electron-hole radiative recombination in neutral QDs, charging induced fast Auger recombination process dictates the intrinsic carrier lifetime of QDs. The hole transfer from QDs to sulfide is also observed but with a much slower rate compared with charging induced Auger recombination process. The effects of QDs charging on QDSSC performance, especially on the electron injection efficiency, are discussed, which help understand the rather low efficiency of CdSe QDSSCs. In addition, using single QD fluorescence spectroscopy, we investigate the evolution of QDs properties during the charging process as a function of charging time. From the single QD study, we conclude that, the off-states in charged QDs are suppressed blinking activity due to the efficient recombination between trapped electrons donated by S^{2-} and the positive charge inside QDs. A distribution in the average decay rates was observed in different charged samples. This distribution is attributed to the different changing degree among charged QDs. It is also found that the distribution becomes broader as charging time increases, which is a result of the different charging degree and charging sites in different QDs.

6.2 Experiments and Discussion

6.2.1 Ensemble-Averaged Absorption and Emission Measurements

QD-S^{2-} solution was prepared by mixing 0.01 M Na_2S solution with water soluble QDs in the dark as discussed in Chapter 2. Because of hydrolysis, a large portion of the sulfide ions are in the SH^- form and the solution pH is 11.5, although for simplicity we still refer the dissolved sulfide as S^{2-} below.[25] To account for the possible effect of solution pH on QD exciton dynamics, we also prepared a reference QD solution by mixing QDs (10^{-6} M) with NaOH (pH = 11.5) without adding Na_2S. We first monitored the reaction process between the QD and sulfide by measuring the

QD emission spectra and decay kinetics in the mixed solution as a function of time. As shown in Figure 6.1(a) and inset, the QD emission intensity decreased and emission peak red-shifted gradually with mixing time. The solution reached a steady state after ~ 150 min when the emission intensity was ~ 7% of the initial value and the peak position has red-shifted by ~ 14 meV. Ensemble-averaged emission decay measurement (Figure 6.1b) shows shorter emission lifetimes at increasing mixing time. The QD absorption and emission spectra before (denoted as QD) and at 5 hour after S^{2-} mixing (when steady state has reached, denoted as QD-S^{2-}) are compared in Figure 6.2a. Compared to QDs, the emission peak of QD-S^{2-} shows a redshift of ~ 14 meV and a broadening in peak width by 5%. The UV-Vis absorption spectra of QD and QD-S^{2-} solutions of the same QD concentration also show different absorption profiles. The lowest energy 1S exciton peak (~ 2.04 eV) in the QD-S^{2-} solution shows a clear red-shift and broadening compared to the QD sample. In the spectral region above ~ 2.7 eV (data not shown), where featureless bulk-like transitions dominate, the absorption are nearly identical in these samples. The differences in these absorption spectra can be more clearly seen in their absorption difference spectra (QD-S^{2-} minus QD) shown in the Figure 6.2b, which shows a derivative feature of exciton bands below ~ 2.7 eV.

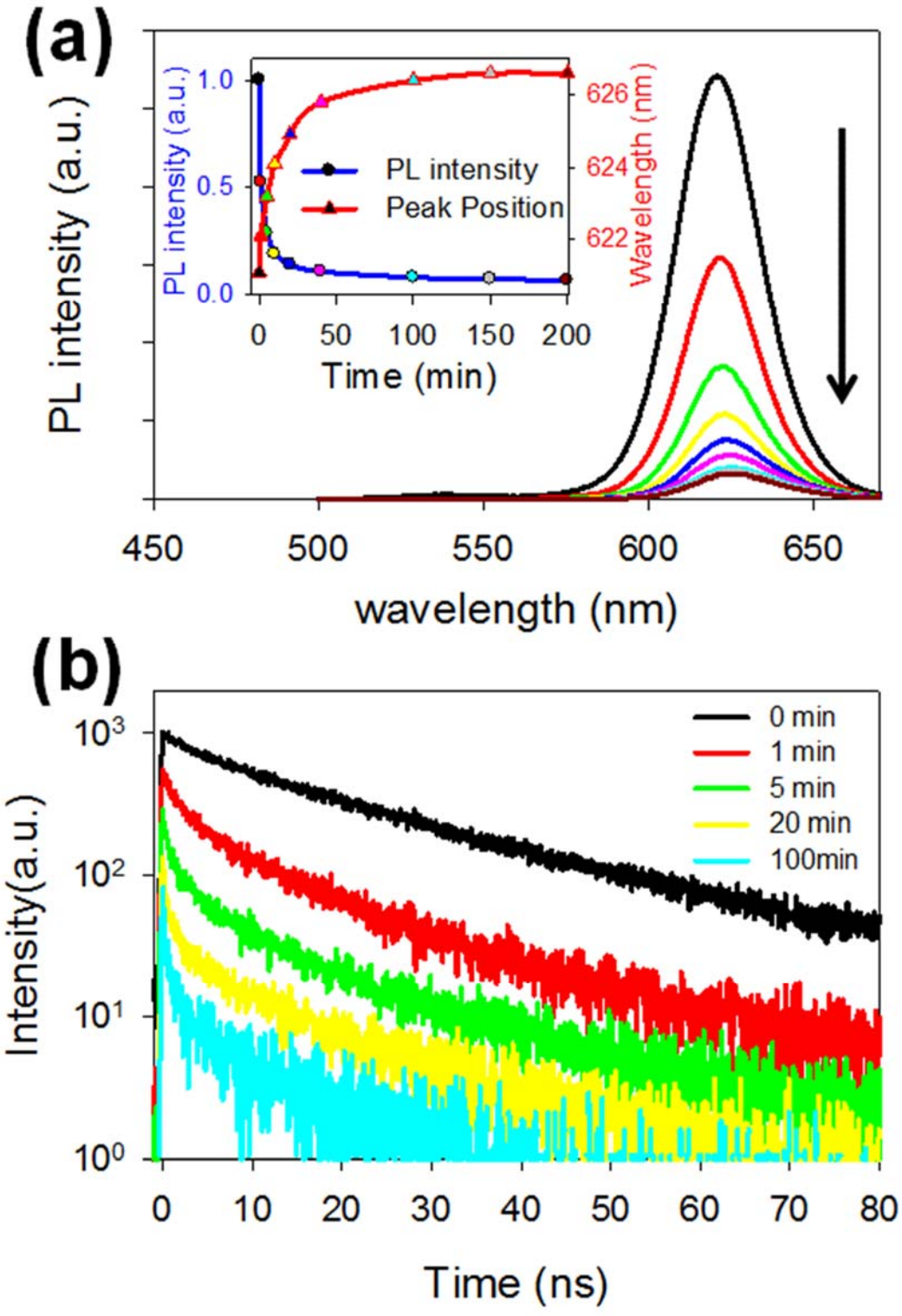

Figure 6.1 (a) Steady state emission spectra and (b) time-resolved emission decay of QDs (10^{-6} M) solution at indicated times after mixing with Na_2S (0.01 M) in the dark. The excitation wavelength was 400 nm and the samples were kept in the dark during

the measurements. Inset in (a) is the integrated emission intensity (blue line) and peak position (red line) as a function of time. QD emission from 580 nm to 650 nm was collected in (b). The 0 min sample was prepared by mixing QDs (10^{-6} M) with NaOH (pH = 11.5) without adding Na_2S.

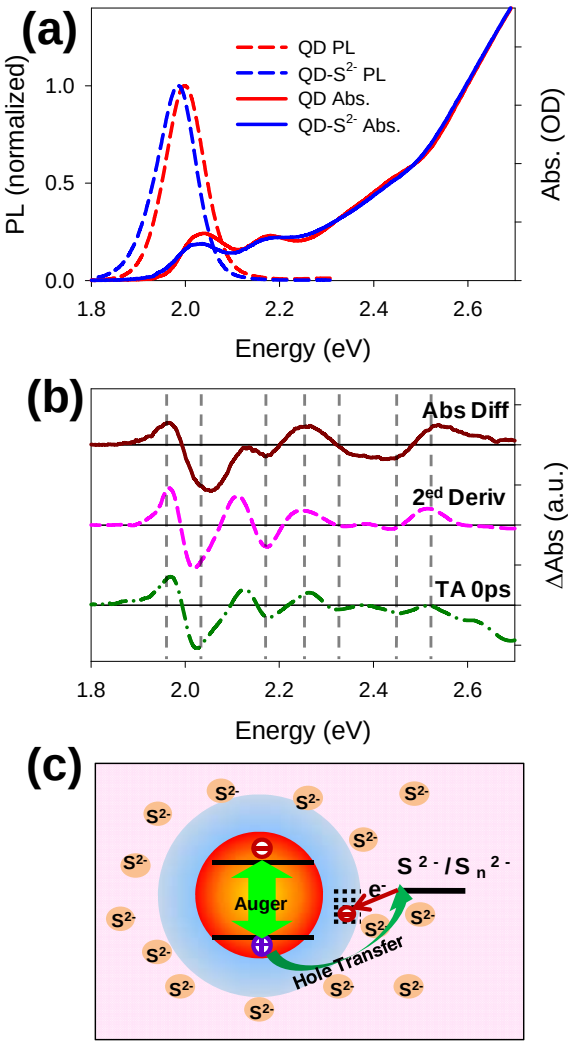

Figure 6.2 (a) Upper panel: UV-Vis absorption (solid lines) and emission spectra (dashed lines) of QDs before (QD) and at 5h after mixing with S^{2-}(QD-S^{2-}). The concentrations of QDs are same for QD and QD-S^{2-} samples and for better comparison the emission spectrum of QD-S^{2-} have been scaled by a factor of 14.3. (b)

Comparison of the absorption difference spectrum between QD-S^{2-} and QD (QD-S^{2-} minus QD, brow solid line), 2nd derivative line shape of QD absorption spectrum (pink dashed line) and TA spectra of QDs at early delay time (0 ps) after 400 nm excitation (green dash-dot line). These spectra have been vertically displaced for clarity, and the black horizontal lines indicate the zero intensity level in each figure. (c) Schematic diagram showing key carrier relaxation pathways: charging of QD surface states by sulfide (black arrow), hole transfer from excited QDs to sulfide (dark green) and electron-hole Auger recombination in charged QDs (green arrow).

Emission quenching (reduction of intensity and lifetime) and red-shift of exciton bands have been reported previously for CdSe QDs in the presence of S^{2-}.[25] Emission quenching was attributed to hole transfer process from photoexcited QDs to sulfide, because sulfide is a well-known hole scavenger in QDSSC (the dark green arrow shown in Figure 6.2c).[25] The S^{2-} induced redshift of CdSe QDs was assigned the formation of $CdSe_xS_{1-x}$ outer layer.[25] This is unlikely in the current system because we use multiple shell ($CdSe/CdS_{3ML}ZnCdS_{2ML}ZnS_{2ML}$) QDs, in which the CdSe core is well protected away (~ 2.33 nm) from the QD surface. In principle, sulfide can bind to QD ZnS surface (with surface Zn^{2+}) and increases the effective size of QDs. According to an effective mass calculation, the 1S exciton energy decreases by ~ 0.3 meV with one additional ZnS monolayer on the QD studied here, much smaller than the observed 14 meV shifting.[28] Red-shifted QD absorption peaks can also result from strong coupling between QD hole levels and adsorbed ligand molecular orbitals.[29] This is also unlikely here because the interaction of the core-confined hole with adsorbate level is significantly reduced in these core/multishell QDs.

Instead, we propose that the observed spectral shifting and emission quenching here is an indication of charging of QDs in the sulfide electrolyte. Besides the quantized conduction (valance) band electron (hole) states, QDs also have surface states within the band gap. It has been shown that those QD surface states are redox active in electrochemical cells,[30-33] in the presence of chemical reductants[34,35] or in contact with n-doped semiconductor substrates.[36-38] Sulfide ions can bind strongly to QD surface Cd^{2+} or Zn^{2+} and have strong reducing ability (-0.45 V *vs*. NHE). The potential is not high enough to reduce the conduction band 1S electron level of QDs used here (estimated to be -0.66 V *vs*. NHE[37]), which can be confirmed by the retention of 1S exciton feature in the static absorption spectra (as shown in Figure 6.2a). However, this potential is sufficient for reducing redox-active surface states within the band gap, forming charged QDs with surface "spectator" electrons (as shown in Figure 6.2c dark red arrow).[39] These surface charges generate an electric field in the QD which perturbs the excitonic electron/hole wavefuctions and their optical transitions through Stark effect.[39-42] Charged QDs with red-shifted emission spectra (compared to their neutral counterparts) have been reported.[35,36,40] For example, a ~ 35 meV red-shifted emission has been observed for CdSe/ZnS QDs on ITO with 2-3 estimated excess electrons.[36]

For systems with closely spaced broad transitions, such as QDs where valance band levels are densely spaced relative to the transition linewidth, the electric field will shift and mix the overlapping states and the Stark effect induced spectral change can be adequately represented by the second derivative of the absorption spectrum.[42-44] Indeed, as shown in Figure 6.2b (pink line), the 2nd derivative of the QD absorption spectrum (prior to charging by S^{2-}) shows qualitative agreement with the absorption difference spectrum between the QD-S^{2-} and QD samples. Furthermore, Stark effect

induced QD spectral change has also been observed in excited QDs.[44] The TA difference spectrum of QDs at 0 ps after 400 nm excitation (pulse width ~ 100 fs) is shown in Figure 6.2b (dark green line), which shows derivative features similar to the 2nd derivative of the absorption spectrum and the absorption difference spectrum of charged QDs (QD-S^{2-} minus QD). At this early delay time, the electric-field of hot electron-hole pairs, generated at high energy levels above the conduction and valence band edges, modifies the optical transitions at lower energies through the Stark effect, giving rise to the derivative like features in the TA spectrum.

The effect of an external point charge on QDs optical and electronic properties has been calculated before.[39-41] In addition to modulating exciton transition energy, Wang also shows that the surface localized spectator electron in charged QDs can also pull the hole wave function toward it, which reduces the electron-hole spatial overlap inside the QD, reducing the oscillator strengths of excitonic transitions.[41] This could explain the slightly larger negative features in the QD-S^{2-}-QD absorption difference spectrum than the 2nd derivative of the QD absorption spectrum. Because of the heterogeneity of QD charging degree and charging sites, a more quantitative modeling of the effect of charging on QD absorption and emission spectra are difficult at the present.[40,41] Despite these complexities, the qualitative agreement of the three spectra shown in Figure 6.2b strongly supports that the shift in the absorption spectrum of QD-S^{2-} can be attributed to QD charging.

The 1S exciton bleach recovery and PL decay kinetics of QD and QD-S^{2-} are compared in Figure 6.3b. For better comparison with PL decay, the 1S beach recovery kinetics from TA measurement have been inverted and normalized. For QD sample, TA and PL decay kinetics agrees well with each other, showing an intrinsic half-life

time of ~ 15 ns. For QD-S^{2-}, both TA and PL kinetics show a much faster decay than the QD sample, indicating charging induced exciton quenching in the QD-S^{2-} sample. The TA and PL kinetics agree with each other in the first ~ 2 ns by which time the majority (~ 64 %) of the excited state population has decayed. After that, PL decay kinetics shows a faster decay than the 1S exciton bleach recovery.

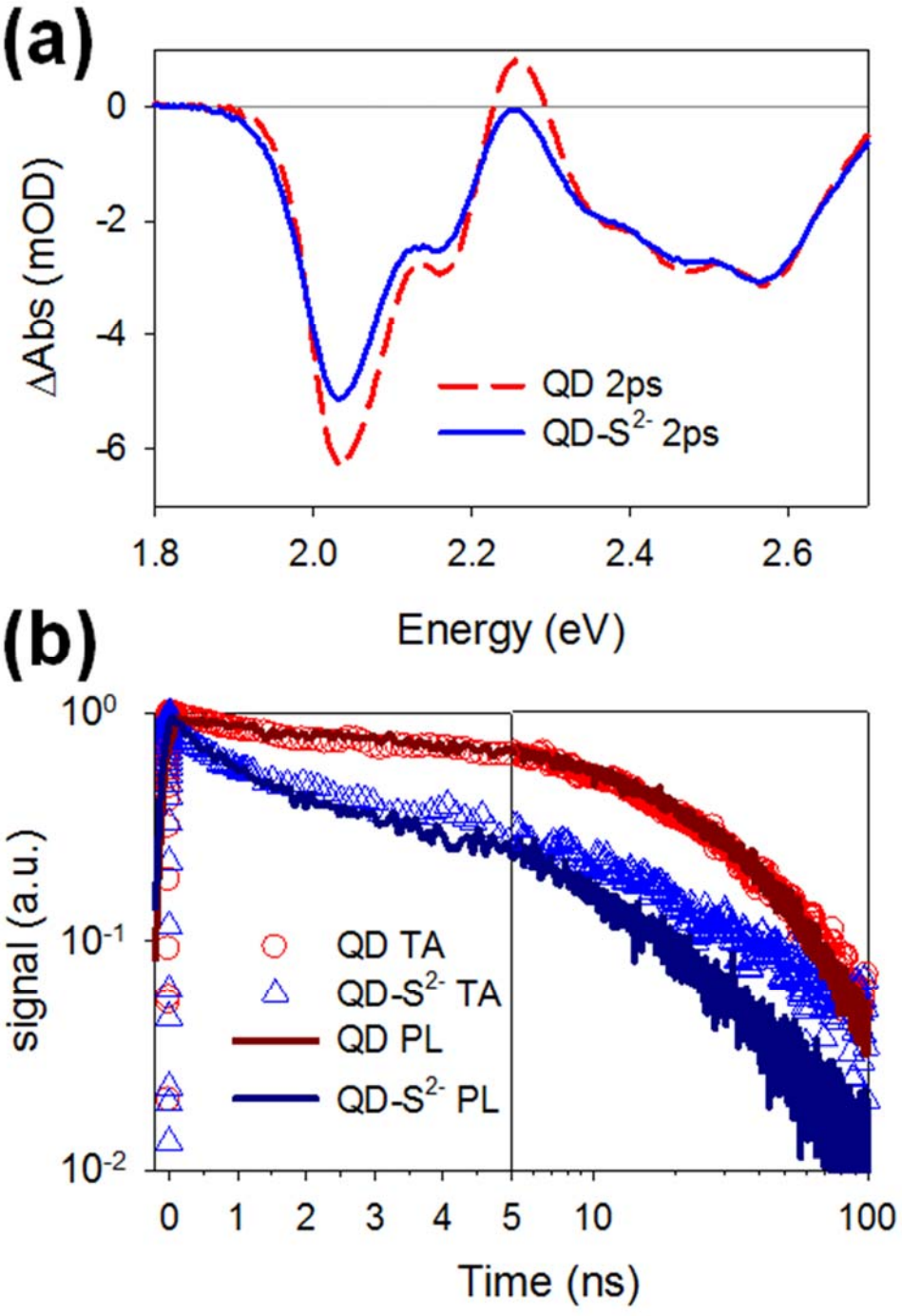

Figure 6.3 (a) TA spectra of QDs (red dashed line) and QD-S^{2-} (blue solid line) at 2 ps after 400 nm excitation. (b) TA kinetics at 1S exciton bleach (TA, open symbols) and ensemble-averaged photoluminescence decay (PL, solid lines) of QD and QD-S^{2-} solutions. The TA kinetics have been inverted and normalized for better comparison with the PL kinetics. The horizontal axis is in linear scale in the left panel (0-5 ns) and in logarithmic scale in the right panel (5-100 ns).

It has been reported that excitons dynamics in charged QDs are significantly altered due to the presence of Auger recombination pathway, in which the electron-hole pair can recombine nonradiatively by giving its energy to the extra charges. To probe this effect as well as the expected hole transfer to S^{2-}, we studied QD-S^{2-} by both transient absorption (TA) spectroscopy and photoluminescence decay (PL).[37] The TA spectra of both QD and QD-S^{2-} after 400 nm (3.1 eV) excitation are shown in Figure 6.3a (at 2 ps) and Figure 6.4 (0-100 ns). These spectra were taken in QD and QD-S^{2-} solutions of the same QD concentration under identical excitation conditions therefore with the same amount of absorbed photons. The measurements were carried out at low excitation intensity (20 $\mu J/cm^2$) to ensure that most excited QDs are in single exciton state, which can be confirmed by the negligible amplitude of fast bleach recovery component in the TA spectra of QD samples.[45] At 2 ps, the initially created hot electrons (holes) have relaxed to the conduction (valance) band edge, giving rise to the state-filling induced bleach signal at the 1S exciton position (~ 2.04 eV) and signals at higher energy positions due to the presence of the 1S exciton. Compared with QD, QD-S^{2-} shows red-shifted and broadened TA spectra which is due to charging induced Stark effect and consistent with steady state measurements above.

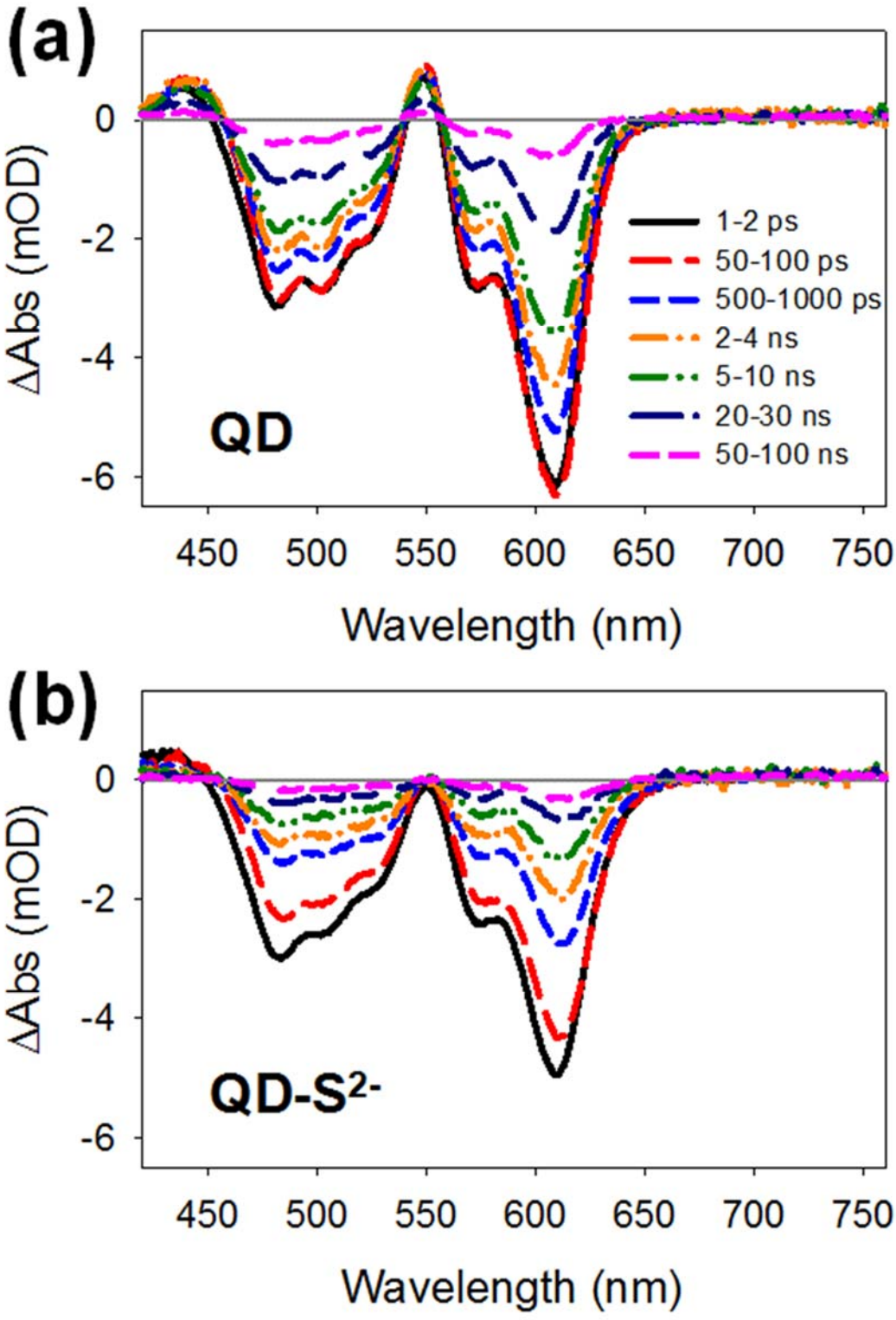

Figure 6.4 TA spectra of QD (a) and QD-S^{2-} (b) under 400 nm excitation at indicated delay time intervals. The TA spectra at 0-1 ns and 1-100 ns were obtained from femtosecond and nanosecond transient absorption spectrometers, respectively.

Because the 1S exciton bleach signal in CdSe QDs is dominated by the state filling of conduction band $1S_e$ level with negligible contribution from the holes, its kinetics reflects the 1S electron depopulation process.[44,46] The decay rate of the 1S electron TA signal is $k_{TA} = k_{ET} + k_{e\text{-}h}$, where k_{ET} is the electron trapping/transfer rate for QDs and $k_{e\text{-}h}$ is the 1S electron-hole recombination rate. On the other hand, because the PL intensity is proportional to the concentration of 1S exciton (1S electron and 1S hole), both electron and hole depopulation processes can lead to PL decay. Therefore, the PL decay kinetics is given by $k_{FL} = k_{ET} + k_{e\text{-}h} + k_{HT} = k_{TA} + k_{HT}$, where k_{HT} is the hole transfer or trapping rate. As shown in Figure 6.3b, the good agreement between TA and PL kinetics of the QD sample indicates negligible hole trapping process for these QD, which is reasonable because the multishell type I structure confines the hole in the CdSe core away from the surface. For QD-S^{2-}, the similar TA and PL kinetics in the first 2 ns suggests that their faster decay compared to free QDs is not caused by the hole transfer/trapping process and can only be attributed to faster electron-hole recombination, electron transfer or trapping. Because S^{2-} is a hole acceptor, it should not speed up the electron transfer process. Adsorption of S^{2-} is also unlikely to enhance electron trapping rate in this system because of the presence of multiple ZnS shells. Therefore, the most likely reason for the faster TA and PL kinetics for QD-S^{2-} in the first 2 ns is a faster electron-hole recombination process ($k_{e\text{-}h}$). It includes the intrinsic decay of uncharged QDs and the additional decay pathways induced by the presence of S^{2-}. Assuming the former remains unchanged, the enhanced electron-hole recombination can be attributed to Auger recombination in charged QDs, as indicated by the green arrow in Figure 6.2c. This assignment is in agreement with shortened PL lifetime reported in charged QDs prepared by a variety of charging approaches.[30,32,35-38,47,48] Instead of slow electron-

hole radiative decay in neutral QDs, photoexcited electron-hole pairs in charged QDs can recombine nonradiatively with a faster rate by exciting the surface spectator electrons through a Auger recombination process. From the TA decay kinetics of QD-S^{2-} which reflects the electron relaxation process in charged QDs, a half-life time of ~ 1.2 ns can be estimated for the Auger recombination process, much shorter than the intrinsic half-life time (~ 15 ns) for QDs. This value is similar to the Auger recombination lifetimes of similar core/multishell QDs on n-ITO (~ 3 ns)[38] and on n-ATO (~ 5 ns)[37], where these QDs are charged by fermi-level equilibration with n-type substrates.

A faster PL decay than bleach recovery ($k_{FL} > k_{TA}$) can be clearly observed for QD-S^{2-} after ~ 2 ns, indicating the onset of the hole removal process. Hole removal in charged QDs can occur through direct hole transfer to surface sulfide or mediated through surface electrons. These pathways cannot be differentiated based on the TA or PL measurement alone.

6.2.2 Charge Transfer from QD to TiO_2 w/o S^{2-} Electrolytes

In QDSSCs, the competition between interfacial ET and intraparticle exciton relaxation determines the electron injection efficiency from photoexcited QDs to semiconductor metal oxide films and thus the device efficiency. To demonstrate the effect of electrolyte charging on electron injection efficiency in QDSSCs, we compare ET processes from these CdSe core/shell QDs to TiO_2 films with and without the presence of S^{2-} electrolytes. ZrO_2 films are chosen as a reference for non-injecting substrate since ET from QDs to ZrO_2 is not expected.

As shown in Figure 6.5b and d, QDs on TiO_2 shows a faster decay than those on ZrO_2, confirming ET from QDs to TiO_2. In the presence of S^{2-} electrolyte, QDs on both ZrO_2 and TiO_2 films have much shorter lifetimes due to electrolyte charging induced fast Auger recombination in QD. These PL decay kinetics can be well fitted by a biexponential function (as shown in black line), from which a half-life time $\langle\tau_{1/2}\rangle$ can be determined listed in Table 6.1. From the half-life time of QDs on TiO_2 and ZrO_2, the average ET rates k_{ET} from QDs to TiO_2 can be determined to be 0.086 ns^{-1} (without S^{2-}) and 0.163 ns^{-1} (with S^{2-}), respectively, using $k_{ET} = 1/\langle\tau_{1/2}\rangle_{TiO2} - 1/\langle\tau_{1/2}\rangle_{ZrO2}$. Together with the QD intrinsic decay rate $k_R = 1/\langle\tau_{1/2}\rangle_{ZrO2}$, the electron injection efficiency can be estimated by, $\eta_{inj} = k_{ET}/(k_{ET} + k_R)$. The electron injection efficiency is 45.6 % for QDs on TiO_2 films without S^{2-} electrolyte solution. In the presence of S^{2-} solution, the electron injection efficiency decreased to 25.1%, due to electrolyte charging induced fast Auger recombination in QDs which competes efficiently with interfacial ET process.

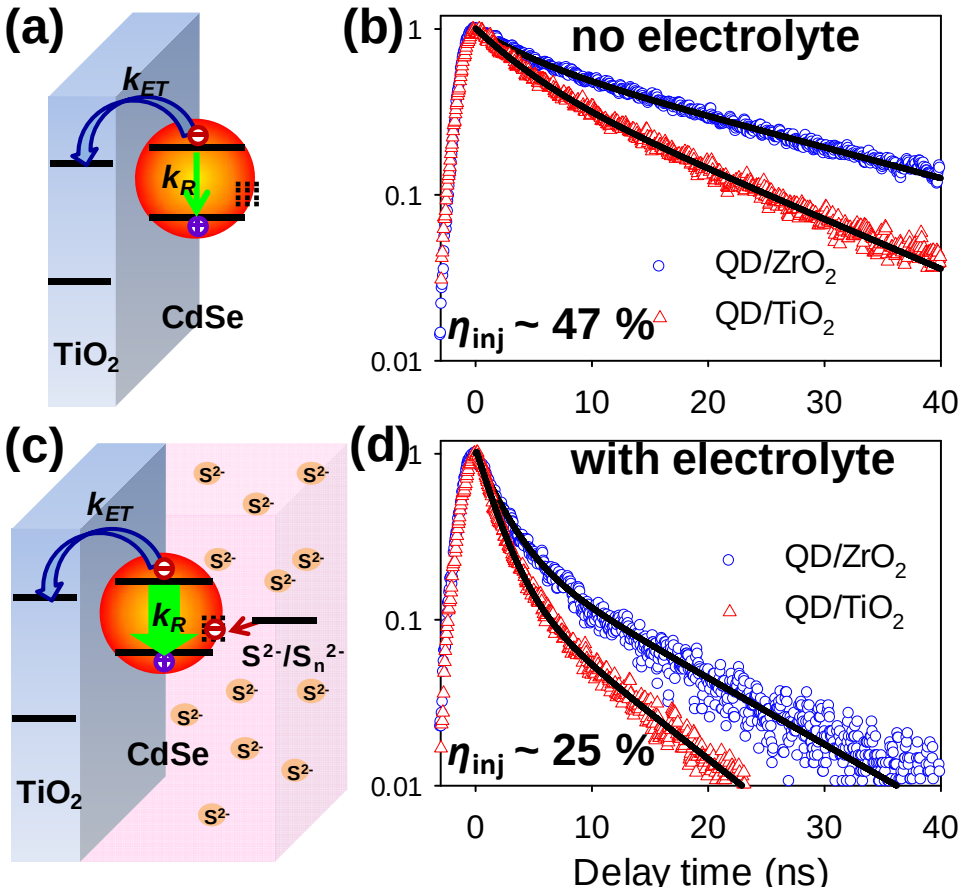

Figure 6.5 (left) Schematic representations of interfacial electron transfer and competing pathways at CdSe QD/TiO_2 interface in the absence (a) and presence (c) of redox electrolytes. (right) PL decay of QDs on ZrO_2 (blue circles) and TiO_2 (red triangles) films without (b) and with (d) S^{2-} electrolyte**.**

There have been many reports of QDSSCs based on TiO_2 nanocrystalline thin films sensitized by core-only CdSe QDs.[17,22-24,49] Interfacial ET times from CdSe QDs to TiO_2 in the absence of redox electrolytes are typically several to hundreds of ps.[18,20,22,50] Considering the relatively long intrinsic exciton lifetime in such QDs measured in solutions or on insulating films (1-10s ns),[24,28,50] efficient carrier injection and high absorbed-photon-to-charge-efficiency (APCE) values in QDSSCs were expected but often not observed (< ~ 45% reported by most groups).[17,18,22,24,49,51] These QDs should also be charged in working devices due to the presence of sulfide

and other redox electrolytes. The Auger recombination rate in charged core-only CdSe QDs should be faster than multishell QDs studied here, since the former usually have more surface trapping sites and the spectator electrons interact more strongly with the excitons. Based on the previously reported biexciton lifetime in core-only CdSe QDs(10s of ps)[45] and the measured Auger recombination lifetime in charged CdSe core/multishell QDs, the Auger recombination time between tens to hundreds of ps can be reasonably assumed for charged core-only CdSe QDs. This exciton Auger recombination lifetime is comparable with ET time to TiO_2, which would lead to low electron injection efficiency in these QDSSCs (Figure 6.5c). It is likely that the reduced electron injection efficiency caused by QD charging and reported interfacial charge recombination loss,[11,17,25,52] are two of the main reason for the observed low APCE values and power conversion efficiencies in CdSe QDSSCs. It is interesting to note that compared to single component CdSe/TiO_2 QDSSCs, similar devices with ZnS or CdTe overlayer coating on CdSe,[49,51] CdS and CdSe co-sensitization,[11,53] or multilayer CdSe[54] have exhibited much higher APCE values. Besides the reported retardation of charge recombination process, a reduction in Auger recombination rate in charged QDs may also be in part responsible for the improved efficiency. These multilayer structures decrease the interaction of excitons with the surface spectator electrons located at QD-electrolyte interface, thus reducing Auger recombination rate in charged QDs and enhancing the electron injection efficiency.

Table 6.1 Biexponential Fitting Parameters to the PL Decay for QDs on ZrO_2 and TiO_2

	τ_1 /ns (A_1)	τ_2 /ns (A_2)	$<\tau_{1/2}>$/ns
QD/ZrO_2	4.42 (0.31)	23.49 (0.69)	9.75

QD/TiO_2	3.93 (0.45)	14.57 (0.55)	5.30
QD/ZrO_2-S^{2-}	2.01 (0.74)	10.01 (0.26)	2.11
QD/TiO_2-S^{2-}	1.70 (0.81)	7.97 (0.19)	1.58

6.2.3 Single Quantum Dot Exciton Quenching Dynamics.

To prepare samples for single QD studies, QDs with NaOH (sample 1) and QDs with S^{2-} (all chemicals of same concentrations as above) at different mixing times: 1 min (sample 2), 5 mins (sample 3), and 20 mins (sample 4) were quickly diluted to ~ 10 pM and then spin-coated on glass cover slips. About fifty single particles from each sample were studied.

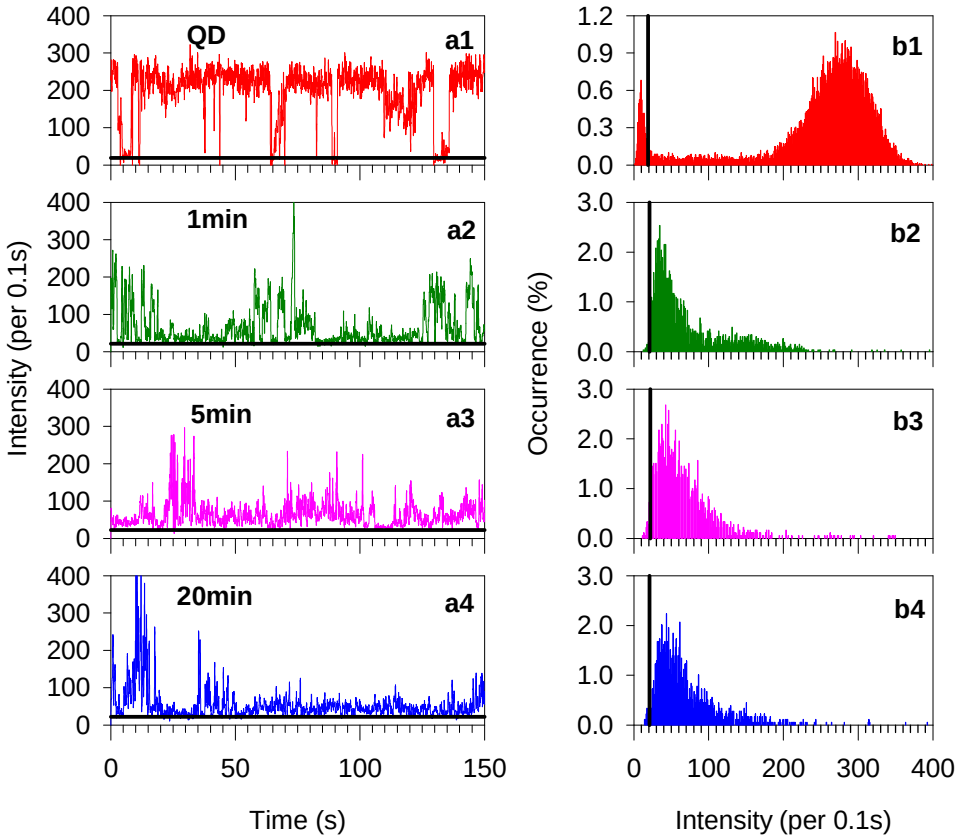

Figure 6.6 Typical photoluminescence intensity trajectories (ai) and PL intensity histograms (with a one photon bin) (bi) of representative single QDs from 1, 2, 3, 4 sample (i=1-4 for samples 1- 4, respectively). Black lines in ai) and bi) indicate the threshold separating the on- and off- states.

Typical single QD PL intensity from samples 1-4 are shown in Figure 6.6 panels a1-4, respectively. For all single QDs, the lifetime and intensity fluctuations are positively correlated, consistent with the reported single QD blinking dynamics.[55-57] We attribute all points with intensity within two standard deviations of the background level to off-states and all points with higher intensities to non-off-states. The thresholds separating non-off and off-states are indicated by the black lines in Figure 6.6ai. Histograms of single QD PL intensity of samples 1-4 are plotted in Figure 6.6 panels b1-4. The PL intensity histogram of the QD from sample 1 (uncharged QD) has two distinct peaks separated by the threshold: on-state emission centered around 300 counts/0.1s and an off-state around 10 counts/0.1s (near the background emission level). In charged QDs (samples 2-4), the off state population is greatly reduced and instead of on state as in free QD, the emission intensity of the non-off state in charged QDs shifts below 250 counts/0.1s and the intensity decreases with the mixing time. This non-off state with lower intensity has been generally observed in charged QDs and can be denoted as “gray state”.

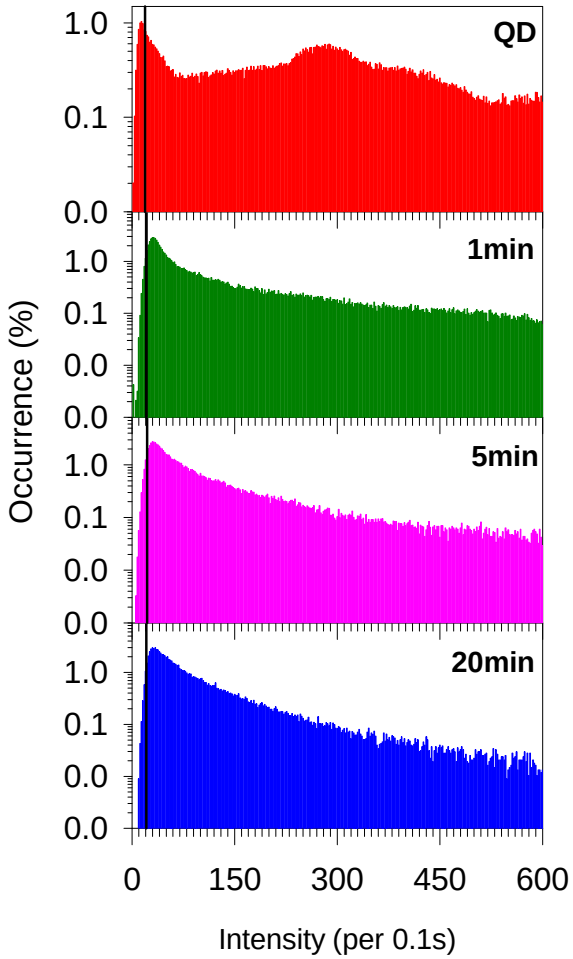

Figure 6.7 Total histograms of fluorescence intensity (with a one photon bin). Black lines indicate the threshold emission intensity separating the on- and off- states.

Similar single QD PL intensity distributions were observed in other QDs, from which the total histograms of intensity are constructed. The total emission intensity histograms of 50 single QDs for samples 1 – 4 are shown in Figure 6.7. The occurrence probability is plotted in logarithmic scale to clearly show the change in the high emission intensity region, in which the amplitudes are small for QDs from samples 2-4. In free QDs (red), the non-off-state emission level spreads out from 80 to 600 counts per 0.1s with a small peak centered at around 300 counts per 0.1s. The broad distribution in emission intensity is attributed to variation of quantum yields

among QDs. In charged QDs (samples 2-4), the emission intensity distribution shifts to lower value with increasing charging time.

By comparing the distributions of emission intensity between free QDs and charged QDs (Figure 6.7), we found that the probability for QDs in off-state is greatly suppressed in charged QDs. Also, with increasing charging time, the occurrence of off-state emission is even smaller. It is well-known that the off-states in QDs can be attributed to the positively charged state generated by electron trapping in the surface trap states on QDs. In this charged state, the fast Auger relaxation process dominates over the fluorescence emission process. The emission of QDs can be resumed when the trapped electron recombines with the positive charge inside QDs. Under the presence of S^{2-}, the QD is negatively charged by electrons injection to surface trapped states. As a result, the occurrence of off-states, which is a result of positively charged QDs, can be suppressed due to the increased probability of the positive charge being neutralized by the surface trapped electrons.

To quantify the occurrence and duration of off-states and on/gray states in charged QDs, we calculate the probability densities *P(t)* of QDs at on/gray or off states for a duration time of *t*:

$$P_i(t) = \frac{N_i(t)}{N_{i,total}} \times \frac{1}{\Delta t_{avg}} \ (i = \text{on or off}) \quad (6.1)$$

Here, *N(t)* is the number of "on/gray" or "off" events with duration time of *t*, N_{total} is the total number of "on/gray" or "off" events, and Δt_{avg} is the average of the time intervals to the preceding and subsequent events.

As shown in Figure 6.7, both $P_{on/gray}(t)$ and $P_{off}(t)$ for single QDs from samples **1**-4 show power law distributions at short time but deviate from this at longer time, similar to results reported for free QDs and QD-electron acceptor complexes.

These *P(t)* distributions can be fit by a truncated power law:

$$P_i(t) = B_i t^{-m_i} \exp(-\Gamma_i t) \quad (i = \text{on or off}) \quad (6.2)$$

where B is the amplitude, m the power law exponent, and Γ the saturation rate. The fitting parameters are listed in Table 6.2. Compared to the free QDs, the charged QDs in samples 2-4 have both bigger Γ_{gray} and Γ_{off}. The bigger Γ_{gray} indicates that the gray states have a shorter duration time compared with the on states in neutral QDs, which is because that the presence of trapped electrons opens up the additional non-radiative Auger recombination channel for charged QDs. On the other hand, bigger Γ_{off} shows that the excessive electrons in charged QDs can suppress the off-states, which is believed to be due to the regeneration of a positive charged state to neutral state, by surface electrons recombining with the hole in the core of QDs. With longer charging time, QDs are charged with more electrons which results in an even larger Γ_{off}.

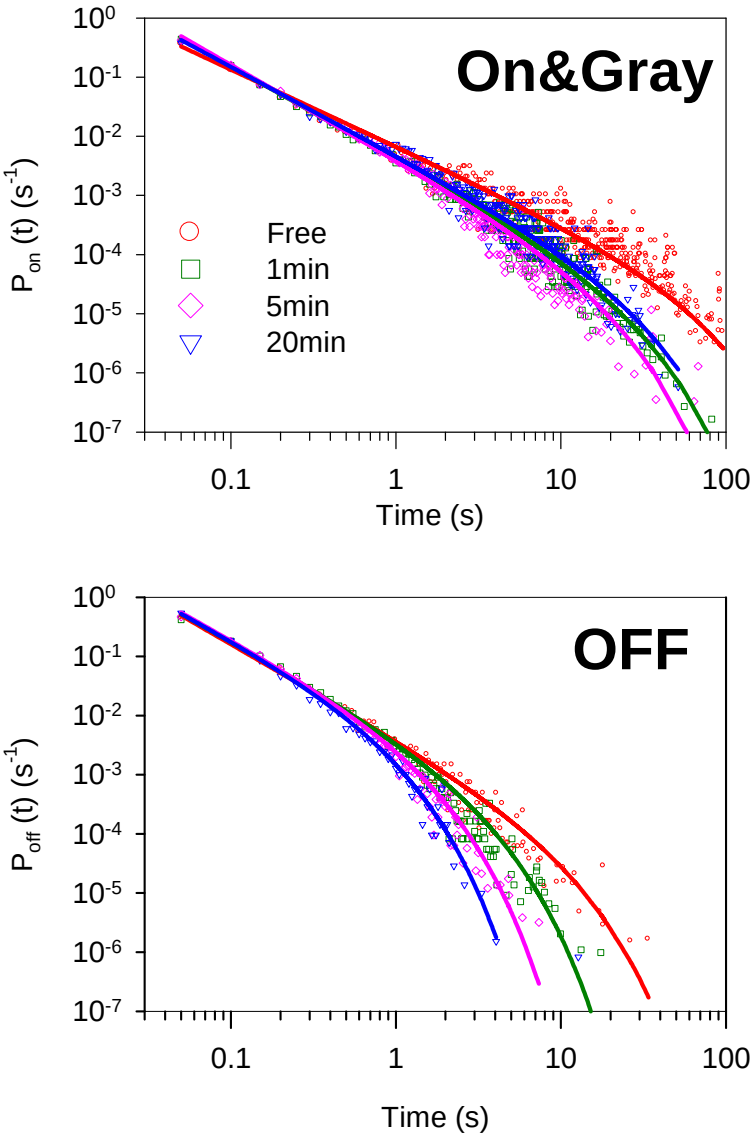

Figure 6.8 Probability density distributions of (a) on states (P_{on}) and (b) off states (P_{off}) as a function of on (off) time intervals, constructed from free QDs in sample 1 (red circle); Probability density distributions of (a) gray states (P_{gray}) and (b) off states (P_{off}) of charged QDs in sample 2 (green square), sample 3 (pink diamond) and sample 4 (blue triangle). The solid lines are the best fits according to equation (6.5).

Table 6.2 Fitting parameters of $P_{on/gray}$ *(t)* and P_{off} *(t)* for all single QDs from samples 1-4.

Sample#	$\mathbf{m_{on}}$	$\mathbf{1/\Gamma_{on}}$	$\mathbf{m_{off}}$	$\mathbf{1/\Gamma_{off}}$
1	1.30±0.03	50±5	1.60±0.02	7.66±0.54
2	1.56±0.05	20±2	1.56±0.05	2.32±0.11
3	1.60±0.04	14±1	1.52±0.02	1.06±0.04
4	1.50±0.03	21±1	1.48±0.02	0.66±0.02

As we can see from the intensity analysis, the emission level of charged QDs are typically low, which makes the lifetime fitting difficult due to the limited number of photons. Thus, instead of generating lifetime trajectories by fitting the fluorescence decay curves within a 2s bin as we used to do, we built up a fluorescence decay profile for each single particle using all the photons detected in each intensity trajectory trace. Typical decay curves from samples 1-4 are plotted in Figure 6.9. It can be concluded that, with the increase of charging time, the decay lifetime decreases, indicating an increased quenching rate. This observation is consistent with what we have found in ensemble averaged measurements, suggesting that with reaction time increases, the QDs become more charged.

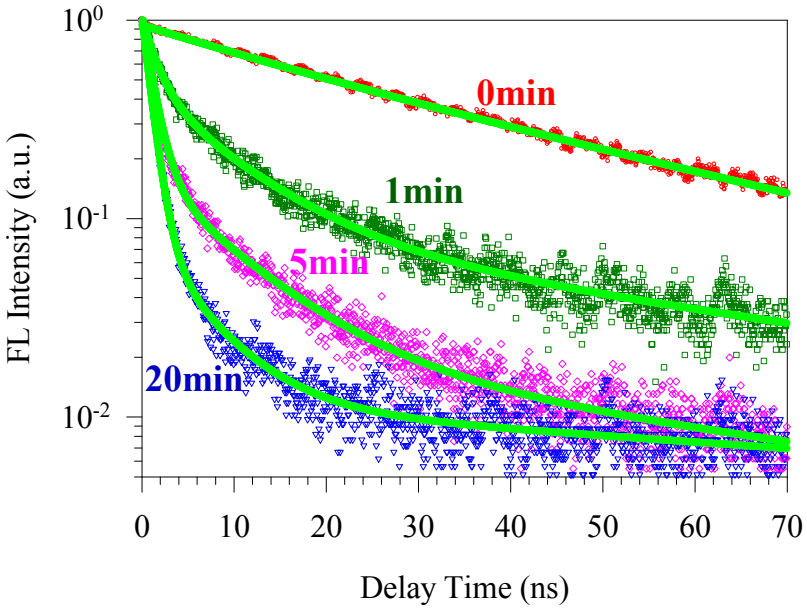

Figure 6.9 Fluorescence decay profiles of representative single QDs from sample 1 (red circle), 2 (dark green square), 3 (pink diamond), and 4 (blue triangle). The fitting curves are also plotted for each decay profile using green solid lines.

The decay profiles in Figure 6.9 are fitted using a least-square fit method, i.e. the deviation between data and fitting is minimized to determine the parameters in the fitting function. For free QDs (sample 1), a two-exponential function is used to account for the two rate components from both on-states and off-states (equation 6.3). The chi-square is close to 1 (Table 6.3), which indicates that the two-exponential function is a suitable function to describe the decay profile. For charged QDs (samples 2-4), a three-exponential function is used to fit the decay kinetics (equation 6.4), which also provide a good description according to the chi-square values (Table 6.3).

$$I = a_1 * \exp(-r_1 t) + a_2 * \exp(-r_2 t) \quad (6.3)$$

$$I = a_1 * \exp(-r_1 t) + a_2 * \exp(-r_2 t) + a_3 * \exp(-r_3 t) \quad (6.4)$$

where I is the normalized fluorescence intensity in arbitrary unit, r_i and a_i are the rate components and corresponding amplitude.

The average rate is calculated using the weighted rate method:

$$r = \sum_i a_i r_i \quad (6.5)$$

Table 6.3 Fitting parameters of decay profiles in Figure 6.9

Sample#	Rate (ns^{-1})	error(ns^{-1})	chi-square
1	0.031	0.001	0.996
2	0.381	0.008	0.992
3	0.761	0.007	0.996
4	0.983	0.006	0.998

The average rate of each sample and error in the average rate are all listed in Table 6.3. It can be seen that the average decay rate for free QD is 0.03 ns^{-1}, which is consistent with what we observed in previous work.[58-66] For charged QDs, the rate increases from 0.38 ns^{-1}, 0.76 ns^{-1}, to 0.98 ns^{-1} as the charging time increases. This trend is consistent with the observation in our ensemble measurements (Figure 6.1 b) and can be attributed to the increase in charging degree with longer charging time.

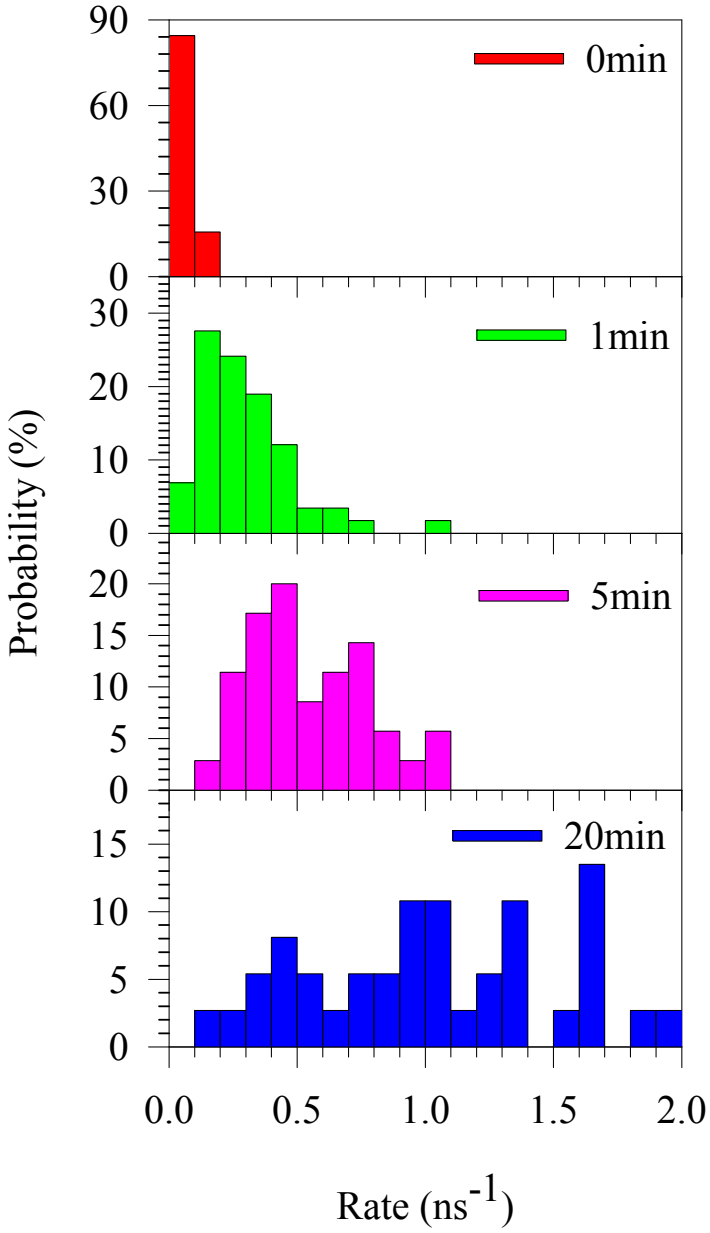

Figure 6.10 Histograms of average decay rates of sample 1 (red), 2 (green), 3 (pink), and 4 (blue). The bin is 0.1 ns^{-1}.

The same method was applied to fit all the single particles in all four samples and average rates are obtained. Histograms of the averages in the four samples are plotted in Figure 6.10. The free QDs show a narrow distribution with a peak at 0.1 ns^{-1}, which is quantitatively consistent with our previous measurement on similar QDs.[58-66] For the three charged QD samples, the distributions shift to the bigger rate region, with

peaks at 0.2 ns^{-1}, 0.5 ns^{-1}, and 1.0 ns^{-1}, respectively. The increase in these averages rate can be attributed to the increased charging degree as the reaction time become longer from sample 2 to 4. Besides the rates increasing, the width of the rate distributions from sample 1 to 4 also increases. This indicates that the static heterogeneity between single particles becomes bigger as the charging increases, which can be due to the different charging degree and charging sites in different QDs. This increased static heterogeneity in charged QDs is consistent with our previous QD-ATO study, reflecting the heterogeneous nature of the surface trap states in QDs.

6.3 Summary

In conclusion, with steady-state and time-resolved absorption and emission spectroscopic techniques, we show CdSe core/shell QDs are charged in the presence of sulfide electrolytes, which leads to shortened exciton lifetime due to fast Auger recombination process (~ 1.2 ns) in charged QDs. When the charging induced Auger recombination time is comparable with interfacial ET time, the efficiency of charge separation decreases, degrading the performance of QD-based photovoltaic and photocatalytic devices. We believe that this is a key efficiency reducing factor that has often been overlooked in these QD based devices. This charging effect should be present for all colloidal QDs and nanostructures in redox active media, including QDSSCs with redox electrolytes and QD-based photocatalytic solutions with sacrificial electron donors, as long as the chemical potentials of the redox couples are located above the surface trap states in QDs. Our findings also demonstrate a fundamental difference between QDs and molecular dyes in redox reactions: i.e. charging of QDs by the redox active mid-gap states.

From the single QD study, we conclude that, the off-states in charged QDs are suppressed due to the efficient recombination between trapped electrons donated by S^{2-} and the positive charge inside QDs. A distribution in the average decay rates was observed in different charged samples. This distribution is attributed to the different changing degree among charged QDs. It is also found that the distribution becomes broader as charging time increases, which is a result of the different charging degree and charging sites in different QDs.

Reference

(1) Kamat, P. V.; Tvrdy, K.; Baker, D. R.; Radich, J. G. *Chemical Reviews* **2010**, *110*, 6664.

(2) Nozik, A. J.; Beard, M. C.; Luther, J. M.; Law, M.; Ellingson, R. J.; Johnson, J. C. *Chem. Rev.* **2010**, *110*, 6873.

(3) Debnath, R.; Bakr, O.; Sargent, E. H. *Energy Environ. Sci.* **2011**, *4*, 4870.

(4) Kamat, P. V. *Acc. Chem. Res.* **2012**, *45*, 1906.

(5) Sambur, J. B.; Novet, T.; Parkinson, B. A. *Science* **2010**, *330*, 63.

(6) Semonin, O. E.; Luther, J. M.; Choi, S.; Chen, H.-Y.; Gao, J.; Nozik, A. J.; Beard, M. C. *Science* **2011**, *334*, 1530.

(7) Tisdale, W. A.; Williams, K. J.; Timp, B. A.; Norris, D. J.; Aydil, E. S.; Zhu, X.-Y. *Science* **2010**, *328*, 1543.

(8) O'Regan, B.; Gratzel, M. *Nature* **1991**, *353*, 737.

(9) Bach, U.; Lupo, D.; Comte, P.; Moser, J. E.; Weissortel, F.; Salbeck, J.; Spreitzer, H.; Gratzel, M. *Nature* **1998**, *395*, 583.

(10) Santra, P. K.; Kamat, P. V. *J. Am. Chem. Soc.* **2012**, *134*, 2508.

(11) Yu, X.-Y.; Liao, J.-Y.; Qiu, K.-Q.; Kuang, D.-B.; Su, C.-Y. *ACS Nano* **2011**, *5*, 9494.

(12) Yella, A.; Lee, H.-W.; Tsao, H. N.; Yi, C.; Chandiran, A. K.; Nazeeruddin, M. K.; Diau, E. W.-G.; Yeh, C.-Y.; Zakeeruddin, S. M.; Grätzel, M. *Science* **2011**, *334*, 629.

(13) Bessho, T.; Zakeeruddin, S. M.; Yeh, C.-Y.; Diau, E. W.-G.; Grätzel, M. *Angew. Chem. Int. Ed.* **2010**, *49*, 6646.

(14) Chen, C.-Y.; Wang, M.; Li, J.-Y.; Pootrakulchote, N.; Alibabaei, L.; Ngoc-le, C.-h.; Decoppet, J.-D.; Tsai, J.-H.; Grätzel, C.; Wu, C.-G.; Zakeeruddin, S. M.; Grätzel, M. *ACS Nano* **2009**, *3*, 3103.

(15) Hodes, G. *The Journal of Physical Chemistry C* **2008**, *112*, 17778.

(16) Mora-Seró, I. n.; Giménez, S.; Fabregat-Santiago, F.; Gómez, R.; Shen, Q.; Toyoda, T.; Bisquert, J. *Acc. Chem. Res.* **2009**, *42*, 1848.

(17) Lee, H. J.; Yum, J.-H.; Leventis, H. C.; Zakeeruddin, S. M.; Haque, S. A.; Chen, P.; Seok, S. I.; Grätzel, M.; Nazeeruddin, M. K. *J. Phys. Chem. C* **2008**, *112*, 11600.

(18) Tvrdy, K.; Frantsuzov, P. A.; Kamat, P. V. *Proc. Natl. Acad. Sci.* **2011**, *108*, 29.

(19) Žídek, K.; Zheng, K.; Ponseca, C. S.; Messing, M. E.; Wallenberg, L. R.; Chábera, P.; Abdellah, M.; Sundström, V.; Pullerits, T. *J. Am. Chem. Soc.* **2012**, *134*, 12110.

(20) Watson, D. F. *J. Phys. Chem. Lett.* **2010**, *1*, 2299.

(21) Guijarro, N. s.; Lana-Villarreal, T.; Shen, Q.; Toyoda, T.; Gómez, R. *J. Phys. Chem. C* **2010**, *114*, 21928.

(22) Robel, I.; Subramanian, V.; Kuno, M.; Kamat, P. V. *J. Am. Chem. Soc.* **2006**, *128*, 2385.

(23) Tachibana, Y.; Akiyama, H. Y.; Ohtsuka, Y.; Torimoto, T.; Kuwabata, S. *Chem. Lett.* **2007**, *36*, 88.

(24) Kongkanand, A.; Tvrdy, K.; Takechi, K.; Kuno, M.; Kamat, P. V. *J. Am. Chem. Soc.* **2008**, *130*, 4007.

(25) Chakrapani, V.; Baker, D.; Kamat, P. V. *J. Am. Chem. Soc.* **2011**, *133*, 9607.

(26) Sambur, J. B.; Parkinson, B. A. *J. Am. Chem. Soc.* **2010**, *132*, 2130.

(27) Lee, H. J.; Chen, P.; Moon, S.-J.; Sauvage, F. d. r.; Sivula, K.; Bessho, T.; Gamelin, D. R.; Comte, P.; Zakeeruddin, S. M.; Seok, S. I.; Grätzel, M.; Nazeeruddin, M. K. *Langmuir* **2009**, *25*, 7602.

(28) Zhu, H.; Song, N.; Lian, T. *J. Am. Chem. Soc.* **2010**, *132*, 15038.

(29) Frederick, M. T.; Amin, V. A.; Cass, L. C.; Weiss, E. A. *Nano Lett.* **2011**, *11*, 5455.

(30) Galland, C.; Ghosh, Y.; Steinbruck, A.; Sykora, M.; Hollingsworth, J. A.; Klimov, V. I.; Htoon, H. *Nature* **2011**, *479*, 203.

(31) Qin, W.; Shah, R. A.; Guyot-Sionnest, P. *ACS Nano* **2011**, *6*, 912.

(32) Qin, W.; Guyot-Sionnest, P. *ACS Nano* **2012**, *6*, 9125.

(33) Weaver, A. L.; Gamelin, D. R. *J. Am. Chem. Soc.* **2012**, *134*, 6819.

(34) Rinehart, J. D.; Weaver, A. L.; Gamelin, D. R. *J. Am. Chem. Soc.* **2012**, *134*, 16175.

(35) Bang, J.; Chon, B.; Won, N.; Nam, J.; Joo, T.; Kim, S. *J. Phys. Chem. C* **2009**, *113*, 6320.

(36) Yalcin, S. E.; Yang, B.; Labastide, J. A.; Barnes, M. D. *J. Phys. Chem. C* **2012**, *116*, 15847.

(37) Song, N.; Zhu, H.; Liu, Z.; Huang, Z.; Wu, D.; Lian, T. *ACS Nano* **2013**, *7*, 1599.

(38) Jin, S.; Song, N.; Lian, T. *Acs Nano* **2010**, *4*, 1545.

(39) Franceschetti, A.; Zunger, A. *Phys. Rev. B* **2000**, *62*, R16287.

(40) Early, K. T.; Sudeep, P. K.; Emrick, T.; Barnes, M. D. *Nano Lett.* **2010**, *10*, 1754.

(41) Wang, L. W. *J. Phys. Chem. B* **2001**, *105*, 2360.

(42) Sacra, A.; Norris, D. J.; Murray, C. B.; Bawendi, M. G. *J. Chem. Phys.* **1995**, *103*, 5236.

(43) Norris, D. J.; Sacra, A.; Murray, C. B.; Bawendi, M. G. *Physical Review Letters* **1994**, *72*, 2612.

(44) Klimov, V. I. *J. Phys. Chem. B* **2000**, *104*, 6112.

(45) Klimov, V. I.; Mikhailovsky, A. A.; McBranch, D. W.; Leatherdale, C. A.; Bawendi, M. G. *Science* **2000**, *287*, 1011.

(46) Klimov, V. I. *Annu. Rev. Phys. Chem.* **2007**, *58*, 635.

(47) Yalcin, S. E.; Labastide, J. A.; Sowle, D. L.; Barnes, M. D. *Nano Lett.* **2011**, *11*, 4425.

(48) Jha, P. P.; Guyot-Sionnest, P. *Acs Nano* **2009**, *3*, 1011.

(49) Lee, H.; Wang, M.; Chen, P.; Gamelin, D. R.; Zakeeruddin, S. M.; Grätzel, M.; Nazeeruddin, M. K. *Nano Lett.* **2009**, *9*, 4221.

(50) Robel, I.; Kuno, M.; Kamat, P. V. *J. Am. Chem. Soc.* **2007**, *129*, 4136.

(51) Shen, Q.; Kobayashi, J.; Diguna, L. J.; Toyoda, T. *J. Appl. Phys.* **2008**, *103*, 084304.

(52) Barea, E. M.; Shalom, M.; Giménez, S.; Hod, I.; Mora-Seró, I. n.; Zaban, A.; Bisquert, J. *J. Am. Chem. Soc.* **2010**, *132*, 6834.

(53) Lee, Y.-L.; Lo, Y.-S. *Adv. Funct. Mater.* **2009**, *19*, 604.

(54) Shalom, M.; Buhbut, S.; Tirosh, S.; Zaban, A. *J. Phys. Chem. Lett.* **2012**, 2436.

(55) Issac, A.; Jin, S.; Lian, T. *J. Am. Chem. Soc.* **2008**, *130*, 11280.

(56) Jin, S.; Hsiang, J.-C.; Zhu, H.; Song, N.; Dickson, R. M.; Lian, T. *Chemical Science* **2010**, *1*, 519.

(57) Song, N.; Zhu, H.; Jin, S.; Zhan, W.; Lian, T. *ACS Nano* **2011**, *5*, 613.

(58) Issac, A.; Jin, S. Y.; Lian, T. Q. *J Am Chem Soc* **2008**, *130*, 11280.

(59) Jin, S. Y.; Hsiang, J. C.; Zhu, H. M.; Song, N. H.; Dickson, R. M.; Lian, T. Q. *Chem Sci* **2010**, *1*, 519.

(60) Jin, S. Y.; Lian, T. Q. *Nano Lett* **2009**, *9*, 2448.

(61) Jin, S. Y.; Lian, T. Q. *Sci China Chem* **2011**, *54*, 1898.

(62) Jin, S. Y.; Snoeberger, R. C.; Issac, A.; Stockwell, D.; Batista, V. S.; Lian, T. Q. *J Phys Chem B* **2010**, *114*, 14309.

(63) Jin, S. Y.; Song, N. H.; Lian, T. Q. *Acs Nano* **2010**, *4*, 1545.

(64) Song, N. H.; Zhu, H. M.; Jin, S. Y.; Lian, T. Q. *Acs Nano* **2011**, *5*, 8750.

(65) Song, N. H.; Zhu, H. M.; Jin, S. Y.; Zhan, W.; Lian, T. Q. *Acs Nano* **2011**, *5*, 613.

(66) Song, N. H.; Zhu, H. M.; Liu, Z.; Huang, Z. Q.; Wu, D.; Lian, T. Q. *Acs Nano* **2013**, *7*, 1599.

Chapter 7 Summary and Diresctions

QDs have shown great advantages in photocatalytic/voltaic devices and optical imaging/display applications, where their performances are governed by their excited-state dynamics (i.e. intrinsic relaxation and interfacial energy/charge transfer) and their emission behaviors (i.e. on/off probability and duration). Ensemble averaged spectroscopic measurements could provide useful information, however, the photophysical properties of each individually particles are lost due to the ensemble averaging, which prevents the understanding and manipulation on a higher level. In this dissertation, we show the unique advantages of time-resolved single particle fluorescence spectroscopy technique, which tracks the excited state dynamics and emission properties simultaneously on a single particle level. They reveal dynamics phenomena of single QDs in the charge transfer and emission process (the rate distribution, heterogeneity, blinking, and correlation).

In QD-C_{60} and QD-PTZ complex studies, by combining the ensemble averaged transient absorption and fluorescence decay measurements, the interfacial charge transfer mechanism (electron transfer for QD-C60 and hole transfer for QD-PTZ) and the transfer rates are determined. With single particle fluorescence technique, the rate of each individual QD-adsorbate complex can be measured, from which the rate distribution and fluctuation can be constructed. The distributions of rate and the standard deviations can be well modeled assuming a Poisson distribution of adsorbate molecules on QD surface. We believe this distribution is applicable to other self-assembled QD nanostructures, and it is the origin of distributions of the averages and fluctuations of their interfacial dynamic properties. Besides the charge transfer rates, the effect of electron/hole transfer process on QD blinking behaviors was also

investigated. Compared with QD-electron acceptor complex where electron transfer shortens the long-on state and increases the off state probability, the hole acceptors do not significantly alter the on- and off- state probability. Instead, it increases the probability of weakly emissive grey states, due to hole transfer (to create a negatively charged QDs) and hole filling (to neutralize the positively charged QDs) processes.

For QDs on n-doped Sb:SnO_2 and QDs in S^{2-} redox electrolytes, by combining transient absorption and fluorescence decay kinetics, we observed the expected electron (QDs on Sb:SnO_2) and hole (QDs in S^{2-}) transfer processes from QDs. An additional fast quenching process was observed for these QDs compared with QDs on undoped SnO_2 or QDs in water. Considering the redox active surface states in QDs and reduction environment (n-type substrate and S^{2-} electrolyte), we believe these QDs are charged and this faster exciton quenching process can be attributed to fast Auger recombination in charged QDs due to electron injection from the reductive environment to QDs surface states. QDs on SnO_2 and ATO films show similar on and off time probability densities in blinking dynamics but different heterogeneity nature in exciton decay rates. For QDs on SnO_2, we observed comparable contributions of static and dynamic heterogeneity to the total distribution of exciton quenching rates. On ATO surfaces, the static heterogeneity is greatly increased compared to QDs on SnO_2, indicating a large heterogeneity of Auger recombination rates in charged QDs, which is likely caused by a distribution of the number of charges and/or charging sites on the QD surface. For QDs in the S^{2-} solution, the off-states in charged QDs are suppressed due to the hole removal (from surface trapped electron or S^{2-}) process which can neutralize the positively charged QDs. With increasing charging time, the exciton quenching rate becomes faster and distribution becomes broader, due to increased charging degree and charging sites in different QDs.

Thus far, the single semiconductor nanoparticle studies still mostly focus on the traditional spherical QDs and few studies have worked on the semiconductor nano-heterostructures which combine several components in a rational manner and functionalize them synergistically. By combining the single particle fluorescence spectroscopy and spatial resolution technique such as atomic force microscope, these techniques have the potential to further reveal the structure-property relationship in nanosystems and devices.

On the other hand, current single QD studies are still aiming on fundamental questions, and are mostly conducted under simplified experimental conditions compared with real devices. Further complications may arise in more complex environments under the device operation conditions. Therefore, research should move forward to apply the single particle spectroscopy to the real photovoltaic/catalyst devices and optical imaging system under working conditions.